LASER PHOTOFRAGMENTATION AND HETEROGENEOUS CHEMILUMINESCENCE FOR NITRO-BASED EXPLOSIVE DETECTION

By

MARIA PAMELA PINEDA MONTEROLA

A DISSERTATION PRESENTED TO THE GRADUATE SCHOOL
OF THE UNIVERSITY OF FLORIDA IN PARTIAL FULFILLMENT
OF THE REQUIREMENTS FOR THE DEGREE OF
DOCTOR OF PHILOSOPHY

UNIVERSITY OF FLORIDA

2007

Gratefully dedicated to my family and to the loving memories of my father

ACKNOWLEDGMENTS

I would like to thank many people for all their help in completing this dissertation and in my journey through graduate school. My main adviser, Prof. James D. Winefordner, has been a wonderful mentor and inspiration. I greatly admire his dedication to education and research. I would like to acknowledge Dr. Nicoló Omenetto for his valuable research guidance. He never ceases to amaze me with his creative ideas, and his passion for science is really contagious. I am very grateful to Dr. Benjamin W. Smith, a.k.a. as the Mac Gyver of our lab, for all his advice in instrument design and his cool ways in troubleshooting. I would like to extend my appreciation to Dr. Igor Gornushkin for many intellectual conversations about spectroscopy and life.

I would like to thank my committee members, Dr. William Harrison, Dr. David Hahn and Dr. Michael Scott for their valuable comments and suggestions in the completion of this research dissertation.

I would like to recognize the US Army as a main source of research funding.

A special thanks to Dr. John Birks of University of Colorado for providing us the gas-liquid exchange module and Dr. Mike Shepard of US Naval Surface Warfare Center for providing us the with explosive samples. I would also like to acknowledge Duran and Tan's research groups for allowing me to use their micro balance and spectrofluorometer. All the UV-Vis measurements were conducted in the laboratory of Dr. Kathryn Williams.

I would like to express my deep gratitude to all support staff in chemistry, including the machine and electronic shops for all of their contribution in instrument development. It has been a blessing to have Ms. Lori Clark from the Graduate Student Coordinator's Office and Ms. Jeanne Karably from the Analytical Chemistry Division with their unwavering patience and assistance.

My five years at the University of Florida would not have been so enjoyable if it were not for the wonderful people of Omenetto-Smith-Winefordner group. I would like thank Ron Whiddon, Nick Taylor, Benoit Lauly and Jonathan Merten for being ready to help with anything in the lab; with lasers, lifting, gas refilling and so on. I would like to recognize Jonathan Merten again for his editorial assistance. A special thanks to Dr. Joy Guingab, Mariela Rodriguez, Dr. Xi-hong Wu, Akua Oppong-Anane and Lydia Edwards for friendship. Those fun times and great memories will always be treasured and cherished.

Heartfelt thanks goes to my friends who made my stay here at Gainesville pleasant these five years. I am very grateful to Ms. Anne Moore for being so kind to me and for being my second mom here in Gainesville. I would like to extend my gratitude to Merilla Stefan for her camaraderie, Alexandr Oblezov for being so reliable at all times, especially during my second year here at UF, Chen Liu and Ozlem Demir for their companionship and for setting examples of hard work and perseverance. I am so blessed to have a very good support group from my fellow Filipino graduate students. My heartfelt gratitude goes to Jhoanna Mendoza, Dr. Suzette Pabit, Dr. Jemy Gutierrez, Machel Malay, Joey Orajay, Attorney Tesi Lou Guanzon, and Ai-ai Cojungco. They helped make Gainesville a second home for me.

Most of all, I would like to thank my family for their incredible support and love. I would like to acknowledge my brothers, Conrad, Chris and Carlo. My brothers and I shared wonderful memories of playing basketball, chess, and play stations which instilled in me the art of being a ‘warrior’ in any game of life. I am forever grateful to my mother for her incredible strength and unconditional love. I am also forever in debt with my father’s legacy, of being so humble, kind, and handsome.

TABLE OF CONTENTS

page

ACKNOWLEDGMENTS 4

LIST OF TABLES 9

LIST OF FIGURES 10

LIST OF ABBREVIATIONS 13

ABSTRACT 15

CHAPTER

1 INTRODUCTION 17

Background and Significance 17
Chemistry and History of Explosives 17
Significance of Explosive Detection 20
Review of Methods for Explosive Detection 22
Challenges on Explosive Detection 27
Scope of Research Dissertation 27

2 PHOTOFRAGMENTATION PATHWAYS OF NITRO COMPOUNDS 38

Introduction 38
Basic Theory of Photofragmentation 38
Basic Theory of REMPI-TOFMS and LIF 40
PF Mechanism of Explosives based on PF-REMPI-TOF and PF-LIF 42
Experimental Section 46
Reagents and Chemicals 46
Apparatus and Methodology 47
Results and Discussion 49
Detection of NO_2 Fragments 49
Photofragmentation of NO_2 51
Conclusion 53

3 NO_2 DETECTION BY CHEMILUMINESCENCE 65

Introduction 65
Basic Theory of Chemiluminescence 65
Luminol-NO_2 Chemiluminescence 67
Review of CL Methods for NO_2 detection 68
Experimental Section 70
Reagents and Chemicals 70
Apparatus and Methodology 70

Results and Discussion 73
Chemical Parameters 73
Physical Parameters 75
Performance of Luminol-CL Detector 76
Performance of Luminol/H_2O_2 CL Detector 77
Luminol CL Detector Compared to Other CL Set-ups 77
Conclusion 78

4 CONVERSION OF NO TO NO_2 98

Introduction 98
Experimental Section 99
Reagents and Chemicals 99
Apparatus and Methodology 99
Results and Discussion 100
Conclusion 100

5 LASER PHOTOFRAGMENTATION AND CHEMILUMINESCENCE FOR NITRO-BASED EXPLOSIVE DETECTION 103

Introduction 103
Experimental Section 105
Reagents and Chemicals 105
Apparatus and Methodology 106
Results and Discussion 107
Relative PF Efficiency of Nitro-aromatic Compounds 107
NO_2 Photolysis with Luminol-CL Detector 108
Analytical Capability of PF-CL Detector 108
Conclusion 111

6 DIRECT DETECTION OF EXPLOSIVE IN SOIL 126

Introduction 126
Environmental Hazards of Explosive Contaminated Soil 126
Review of Explosive Detection in Soil 127
Experimental Section 128
Chemical and Reagents 128
Apparatus and Methodology 129
Results and Discussion 130
Conclusion 131

7 CONCLUSIONS AND FUTURE WORKS 136

Summary and Conclusions 136
Future Research Directions 137

LIST OF REFERENCES 142

BIOGRAPHICAL SKETCH 148

LIST OF TABLES

Table		page
1-1	Physical and chemical properties of nitrocompounds used in the study.	31
1-2	Physical and chemical properties of some nitro-based explosives.	32
1-3	Summary of the performance of various explosive detectors reviewed in this study.	34
2-1	Colorimetric analysis of NO_2 fragments after photofragmentation of some nitro-based explosives	63
3-1	Summary of the LOD obtained from different luminol-NO_2 CL set-ups.	97
5-1	Comparative table showing summary of the performance of various explosive detectors based on PF-FD technique	113
5-2	Determination of PF efficiency of nitro-aromatic compounds	118
5-3	Analytical figures of merit of PF-luminol CL detector for some nitro-based explosives	125
6-1	Explosives concentration in the contaminated soil	134

LIST OF FIGURES

Figure		page
1-1	Classification of explosives based on composition and performance.	29
1-2	Structural formulas and names of nitrocompounds used in the study.	30
1-3	Chart showing some of the technologies presently available and under development for the detection of trace explosives.	33
2-1	The fate of electronically excited species (AB*) formed after absorption of light, ($h\upsilon$).	54
2-2	Schematic representation of the photodissociation of a triatomic molecule (ABC).	55
2-3	Various molecule ionization processes through photon absorption.	56
2-4	Schematic of REMPI apparatus.	57
2-5	Schematic of PF-LIF apparatus.	58
2-6	Photofragmentation set-up. A) schematic of PF-NO_2 fragment collection set-up B) actual picture of the PF cell	59
2-7	Nitrogen dioxide detection by colorimetric method.	60
2-8	Schematic of time-resolved absorbance experimental set-up.	61
2-10	Results obtained with fast time resolved experiments.	64
3-1	Schematic diagram for static Chemiluminescence (CL) device.	79
3-2	Schematic diagram for continuous Chemiluminescence (CL) device:	80
3-3	Luminol oxidation mechanism.	81
3-4	Luminol-CL detector set-up.	82
3-5	Schematic of spectrofluorometer used for acquiring luminol-NO_2 CL emission spectra.	83
3-6	Chemiluminescence Set-up	84
3-7	Luminol/H_2O_2-CL detector.	85
3-8	Dilution set-up.	86
3-9	Effect of KOH concentration .	87

3-10 Effect of luminol concentration on CL signal.....88

3-11 Effect of adding various type of alcohols on CL signal.....89

3-12 Effect of p-iodophenol concentration on CL signal.....90

3-13 Luminol-NO_2 Emission Spectra. 91

3-14 Effect of gas sample flow rate on CL signal.....92

3-15 Effect of the orientation of luminol-NO_2 mist with respect to the PMT window on signal response. 93

3-16 Effect of the storage time of luminol solution on CL signal.....94

3-17 Calibration curve of NO_2 using Luminol-CL set-up.....95

3-18 Calibration curve of NO_2 using Luminol/H_2O_2-CL set-up. 96

4-1 Experimental set-up used for evaluating the efficiency of CrO_3 oxidation unit. 101

4-2 CL spectra. 102

5-1 Photofragmentation-Chemiluminescence detector. 115

5-2 Photofragmentation set-up used for NO_2 photolysis. 116

5-3 Chemiluminescence signals obtained for nitro-aromatic compounds at varying laser energy.....117

5-4 Chemiluminescence signals obtained before and after PF of NO_2. 119

5-5 Effect of varying laser energy on the CL signal of $NO_{x(x=1,2)}$ fragments obtained after photofragmentation of A) solid and B) vapor phase of PETN. 120

5-6 Effect of varying total number of laser pulses on the CL signal of $NO_{x(x=1,2)}$ fragments obtained after PF of solid and vapor phase of PETN.....121

5-7 Effect of varying total number of laser pulses on the mass of PETN ablated and on the CL signal of $NOx_{(x=1,2)}$ fragments obtained after PF of solid PETN.....122

5-8 Effect of varying laser energy on the mass of PETN ablated and on the CL signal of $NO_{x(x=1,2)}$ fragments obtained after PF of solid PETN. 123

5-9 Calibration curves of PETN, RDX, and TNT. 124

6-1 Cross section of the CL cell. 132

6-2 Calibration curve for PETN contaminated soil.....133

6-3 CL Spectra after PF of A) empty sample holder B) pure $NaNO_2$ C) pure $NaNO_3$. 135

7-1 Alternative scheme for detecting peroxide-based explosives. 141

LIST OF ABBREVIATIONS

Chemical Compounds

3-APA*	3-aminophthalate
BuOH	butanol
DMNB	2,3 dimethyldinitrobutane
2,4 DNT	2,4 dinitrotoluene
DNB	dinitrobenzene
EGDN	ethylene glycol dinitrate
EtOH	ethanol
HMX	High Melting eXplosive
MeOH	methanol
Luminol	5-amino-2,3-dihydro-1,4-phthalazine dione
NO_2	nitrogen dioxide
NO	nitrogen oxide
4 NT	4-nitrotoluene
$NO_{x(x=1,2)}$	$NO + NO_2$
PETN	Pentaerythridoltetranitrate
RDX	Research Department eXplosive
TEA	triethanolamine
TNT	trinitrobenzene
TNT	trinitrotoluene

Techniques

CE	Capillary Electrophoresis
CI-MS	Chemical Ionization-Mass Spectrometry
CL	Chemiluminescence
CRS	Cavity Ringdown Spectroscopy
DIAL	Differential Absorption LIDAR
DIRL	Differential Reflection LIDAR
ECD	Electron Capture Detection
EI	Electron Ionization
FL	Fluorescence
FNA	Fast Neutron Analysis
GC	Gas Chromatography
GC-TEA	Gas Chromatography-Thermal Energy Analyzer
HPLC	High Performance Liquid Chromatography
IMS	Ion Mobilty Spectrometry
IR	Infrared Spectroscopy
LIBS	Laser Induced Breakdown Spectroscopy
LIDAR	Laser Light Detection and Ranging
PD	photodissociation
PF-FD	Photofragmentation-Fragment Detection
PF	photofragmentation
PF-LIF	Photofragmentation-Laser Induced Fluorescence

Techniques (continued)

PF-REMPI	PF-Resonance Enhanced Multi-photon Ionization
PL	Photoluminescence
TNA	Thermal Neutron Analysis
TOFMS	Time-of-Flight Mass Spectrometry

Units of Measure

mC	milli Coulomb
ppm	parts in 10^{6}
ppb	parts in 10^{9}
pptr	parts in 10^{12}
ppmv	parts in 10^{6} vapor
ppbv	parts in 10^{9} vapor
pptv	parts in 10^{12} vapor
SLPM	standard liter per minute

Miscellaneous

ArF	Argon Fluoride laser
BDE	Bond Dissociation Energy
EEG	Electroencephalogram
HE	high explosives
ΔHs	heat of sublimation
LE	low explosives
LOD	Limit of Detection
MEMS	micro electrochemical systems
NIST	National Institute of Standards and Technology
NDF	neutral density filter
PD	photodiode
PMT	photo multiplier tube
SAW	surface acoustic wave
(S/N)	signal-to-noise ratio

Abstract of Dissertation Presented to the Graduate School
of the University of Florida in Partial Fulfillment of the
Requirements for the Degree of Doctor of Philosophy

LASER PHOTOFRAGMENTATION AND HETEROGENEOUS CHEMILUMINESCENCE FOR NITRO-BASED EXPLOSIVE DETECTION

By

Maria Pamela Pineda Monterola

August 2007

Chair: James D. Winefordner
Major: Chemistry

The purpose of this research was to develop a simple, fast, reliable, sensitive and potentially portable explosive detection device employing laser photofragmentation (PF) followed by heterogeneous chemiluminescence (CL) detection. The PF process involves the release of $NO_{x(x=1,2)}$ moieties from explosive compounds such as TNT, RDX, and PETN through a stepwise excitation-dissociation process using a 193 nm ArF laser. The $NO_{x(x=1,2)}$ produced upon PF is subsequently detected by its CL reaction with basic luminol solution .The intensity of the CL signal was detected by thermoelectrically cooled photomultiplier tube with high quantum efficiency and negligible dark current counts.

The research work was divided into four stages: (1) discerning the PF pathways of nitro-based explosives (2) luminol-CL method development and optimization for improving NO_2 sensitivity (3) construction of CrO_3 oxidizer for NO to NO_2 conversion (4) evaluation of the device in detecting nitro-based explosives in various media including air and soil matrix.

In the first stage of the research, the following PF pathways were verified using classical colorimetric analysis and a fast time resolved absorbance method.

$$R{-}NO_2 + h\nu \rightarrow R + NO_2; \quad h\nu = 193 \text{ nm} \qquad (1)$$

$$NO_2 + h\nu \rightarrow NO + O^*; \quad h\nu = 193 \text{ nm} \qquad (2)$$

The second stage involved the development and optimization of NO_2 detection using luminol CL. In this system, a stream of NO_2 gas passed through a concentric nebulizer and was used to aspirate a spray of luminol solution. The aspiration process maximized NO_2/luminol contact area enhancing the CL signal. The current system was able to improve the detection limit through optimization of all the feasible physical and chemical parameters involved in the CL reaction between luminol and NO_2. Detection limit (LOD) of 19 ppt NO_2 at (S/N) = 3 was reported. The optimal reagent solution from the viewpoint of sensitivity of the response to NO_2 (maximum signal/signal noise ratio) is 5 x 10^{-3} M luminol + 0.01 M p-iodophenol + 0.2 M KOH. A Luminol/H_2O_2 CL set-up was also explored where a bundle of porous polypropylene fibers was used to bring the NO_2 into contact with luminol solution. A LOD of 178 ppt NO_2 at (S/N) = 3 was obtained.

In the third stage, a CrO_3 oxidizer was constructed for NO to NO_2 conversion. Photolysis of nitro compounds produced NO (reaction 2) which is not detectable by luminol-CL system. To further increase the sensitivity of the device for NO_2 fragments, NO must be converted back to NO_2.

Finally, the fourth stage was integration of PF and CL units into an explosive detection device via a CrO_3 oxidizer. The system was able to detect energetic materials in real time at ambient conditions. Detection limits of 3.4 ppbv for PETN, 1.7 ppbv for RDX, and 34.5 ppbv for TNT were obtained. It was also demonstrated that the presence of PETN residue within the range of 61 to 186 ng/cm^2 can be detected at a given signal to background ratio of 10 using a few micro joules of laser energy. The technique also demonstrated its potential for direct analysis of trace explosive in soil. LOD range of 0.5 to 4.3 ppm for PETN was established, an analytical capability comparable to currently available techniques.

CHAPTER 1
INTRODUCTION

Background and Significance

Chemistry and History of Explosives

A chemical explosive is a compound or a mixture of compounds which, when ignited by heat, impact, friction, or shock, undergoes very rapid and self propagating decomposition that results in formation of more stable material, the liberation of heat, development of a sudden pressure effect, and production of loud noise and a flash which is called explosion.[1]

Explosives have been classified based on their composition and rates of decomposition (Figure 1-1). Low explosives (LE) were prepared by mixing solid oxidizers and fuels, a process that has remained virtually unchanged for centuries. Propellants and pyrotechnics are included in this category. Propellants are used in guns and rockets. Most rocket propellants are composites based on a rubber binder, ammonium perchlorate oxidizer, and a powdered aluminum fuel; or composites based on a nitrate ester (e.g., nitrocellulose or nitramines) or nitroglycerine. On the other hand, pyrotechnics include illuminating and signaling flares. Pyrotechnics are composed of organic oxidizer and metal powder in a binder. Illuminating flares contain sodium nitrate ($NaNO_3$), magnesium (Mg), and a binder while signaling flares contain barium (Ba), strontium (Sr), or other metal nitrates. High explosives (HE) were prepared using mixtures of mononuclear energetic material such as trinitrotoluene (TNT), in which each molecule contain both the oxidizing and the fuel components. Since, HE act as their own oxidant as well as fuel, their total energy is much lower than that of LE. However, the rate at which the combustion energy is released in HE is relatively faster when compared to the release rate of LE. The speed of HE reactions gives them a greater power than LE. HE detonate at velocity of km s^{-1} while LE rapidly burn or deflagrate at relatively low rate range of cm s^{-1}.

HE are further classified as primary and secondary based on their susceptibility to initiation. Primary explosives such as lead azide and lead stryphrate are highly susceptible to initiation. Ther are also referred to as initiating explosives because they can be used to ignite secondary explosives. Secondary explosives, which include nitroaromatics (e.g., TNT), nitramines (e.g., RDX) and nitrate ester (e.g., PETN), are formulated to detonate only under specific circumstances. Secondary explosives are often used as main charge or bolstering explosives.[2]

PETN, RDX, TNT, NT, and 2,4 NT were the model compounds used in this study. Their structural formulas as well as the summary of their physical and chemical properties are shown in Figure 1-2 and Table 1-1, respectively. Other common explosives are also listed on Table 1-2.

Trinitrotoluene (TNT) was first synthesized in 1893 by a German chemist Joseph Wilbrand.[3] The synthesis is performed in two steps. First, toluene is nitrated with a mixture of sulfuric and nitric acid to produce mono and dinitrotoluence. Next, the mixture of mono and dinitrotoluence is further nitrated with a mixture of nitric acid and oleum, a more potent nitration reagent.

TNT is a pale crystalline aromatic hydrocarbon that was originally used as a yellow dye. Its potential as an explosive was not appreciated for several years mainly because of it does not detonate easily. In order to detonate, TNT must be confined in a casting or shell and subjected to severe pressures and/or temperatures (936^{o}F), such as from a blasting cap or detonator. In fact, US army tests on pure TNT show that when struck by a rifle bullet, TNT failed to detonate 96% of the time and when dropped from an altitude of 4000 feet onto concrete, a TNT filled bomb failed to explode 92% of the time.[3]

TNT was first used on a wide scale during World War I. The importance of TNT as a military explosive is based upon its safety in manufacturing, loading, transportation, and storage. As of today, TNT is mainly used as military munitions, quarrying activities, and civilian mining. TNT is a constituent of many explosives such as amatol, pentolite, tetrytol, torpex, tritonal, piciatol, and edratol. [2]

Research Department eXplosive (RDX), or also commonly known as cyclonite or hexogen was first prepared in 1899 by German chemist Hans Henning.[4] Its explosive properties were not discovered until 1920. In 1940s, RDX was produced by the Bachmann process which reacts hexamine with nitric acid, ammonium nitrate, glacial acetic acid, and acetic anhydride. The crude product is filtered and recrystallized to form RDX.

RDX is a white crystalline nitramine compound. It deflagrates rather than explodes and only detonates with a detonator. There are many interpretations of its acronyms including Royal Demolition eXplosive, Research Department (Composition) X, and Research Department eXplosive. The latter is mostly likely correct. In the UK, new military explosives were given an identification number preceded by the letters 'RD' indicating 'Research Department Number'. For some reason, no number was given to this explosive. Instead the letter 'X' was appended to indicate 'unknown' with the intention of adding the a number letter. Although a number was issued, the term 'RDX' stuck. [4]

RDX was widely used during World War II as a main component of the first plastic explosive. RDX has been used in several terrorist related explosions in India over the years such as the serial bomb blast in Mumbai of March 8, 1993 in which more than 300 people were killed and about 1500 injured. Again, on July 11 of 2006, where a series of powerful explosions took place in seven suburban Mumbai's Western Railway train line, killing 209 people and injuring

over 700. RDX is a main constituent of many explosives such as Torpex, Tertrytol, Cyclotol, Composition A, A_5, B, C, H_6 and C_4.[2]

Pentaerythritol tetranitrate (PETN) was first synthesized in 1891 by Tollens and Wiegand.[5] PETN's preparation involves the nitration of pentaerythritol with a mixture of concentrated nitric and sulfuric acid.

PETN is a white crystalline compound belonging to the same chemical family as nitroglycerin-i.e., the nitrate esters. RDX is less sensitive than nitroglycerin but is easily detonated. It is the least stable of secondary explosive.

In 1912, after being patented by German government, the production of PETN started. PETN was used by the German Army in World War I.[5] It is used in detonating fuses (Primacord) and in a mixture, called Pentolite, with an equal amount of TNT in grenades and projectiles. During World War II, the Rocket Launcher (commonly known as a Bazooka) charged, with 8 ounce of pentolite, could penetrate up to five inches of armor. PETN is a main constituent of many explosives such as Datasheet and Semtrex, a Czech-made explosive that has been used commonly in many terrorist bombings.[2] PETN is also used as vasodilator or a heart stimulant. The medicine for heart disease, "Lentonitrat", is pure PETN. [5]

Significance of Explosive Detection

The field detection of explosives is an extremely relevant analytical issue in law enforcement and environmental applications.

With the increasing use of explosives by terrorist groups and individuals, law enforcement and security agents are faced with the problem of detecting hidden explosives in luggage, mail, vehicles, aircraft, on travelers and so on. Counter surveillance activities also include the detection of trace explosives during investigation of bombing scenes. Post explosion analysis is a

great importance for such investigations, particularly for drawing connections between cases and suspects.

The September 11th disaster on the twin towers was one of the most terrible attacks worldwide. It was a temporary high point of numerous horrible attacks the recent years. Very often, nitro-based explosives are involved in these attacks including the detonation of 250 g plastic explosive to bring down Pan American Flight 103 in Scotland in 1998 and the bombings at the World Trade Center in 1993, Oklahoma City in 1995, Moscow in 1999 and 2002 and many more.[6] To protect society against such attacks, early detection of explosive is needed.

Explosive analysis is also necessary in order to address environmental and/or health related concerns. Explosive materials exhibit some toxicity, and ingestion or inhalation of explosive materials may cause a significant health problems. Sites where analysis may be required include military test ranges and industrial facilities where explosive materials are manufactured in order to ensure the safety of the workers and nearby residents. In additions, sites may have become contaminated by improper storage and disposal of explosive materials, and analysis may be required as part of environmental clean-up.

The detection of landmines is an urgent worldwide problem that requires specific and effective field detection methods. There are at least 125 million unexploded landmines buried in 70 countries around the world.[7] Detection of landmines is essential to prevent the leaking of undetonated explosives into water and soil. The inherent difficulty in mine clearance is complicated by the great variety of materials in use. Most modern landmines contain only a small amount of metal, so that traditional detection techniques based on metal detectors are less useful.

Review of Methods for Explosive Detection

Extensive efforts have been devoted to the development of effective and innovative explosive detection systems. There are various techniques currently available and under development. Explosive detection techniques can be broadly classified into two categories: bulk detection and trace detection. In bulk detection, a macroscopic mass of explosive material is detected directly, usually by viewing images by X-ray scanners or similar equipment. In trace detection, the explosive is detected by chemical identification of microscopic residues of explosive compound. In trace explosive detection, the explosive residue can be in either or both of two forms: vapor and particulate. Vapor detection examines the vapor emanating from the concealed explosive samples and particulate detection examines the microscopic residues of explosives that would be present on individuals or contaminated materials.

X-ray detection is a well established conventional system where X-ray energy is measured after passing through an object. This bulk explosive detection approach is capable of differentiating substances according to their densities and atomic numbers. Commercial X-ray detection systems used for airport baggage inspection have a throughput rate of up to 800 bags per hour.[7] No quantitative data on sensitivity and false alarm rate have been published for this method. Other types of bulk explosive detectors are nuclear inducing techniques which used neutrons instead of photons. Among of these methods are Thermal Neutron Analysis (TNA) and Fast Neutron Analysis (FNA).

Figure 1-3 illustrates the classification of explosive trace detectors based on the operating principle of the method. Commonly used explosive detectors can be broadly classified as: (1) separation-based techniques, (2) mass sensors, (3) electrochemical sensors, (4) biosensors and (5) optical sensors (6) photofragmentation-fragment detection approaches.

Separation-based techniques include High Performance liquid Chromatography (HPLC), Capillary Electrophoresis (CE) [8; 9] and Gas Chromatography (GC) combined with Time-of-Flight Mass Spectrometry (GC-TOFMS)[10], Electron Capture Detector (GC-ECD)[11] or Thermal Energy Analyzer (GC-TEA)[12]. GC can also be coupled with Ion Mobility Mass spectrometry (GC-IMS) [13-18].

GC-ECD has an advantage in quantitative explosive analysis in soil due to its compatibility with acetonitrile, a preferred solvent for extracting explosive residues from soil. ECD is based on the high electron affinity of nitro moieties present in the molecules of explosive which readily capture electrons produced by a radioactive ^{63}Ni source. The decrease in a signal due to the consumption of free electrons is proportional to the analyte concentration.

In IMS, explosive vapors are converted to ions at atmospheric pressure and these ions are characterized by their gas phase mobility in a weak electric field. Currently, the most widely deployed explosives screening technology at airports is IMS, including the Ionscan 400 and Sabre 2000 which detect trace explosive collected from the contaminated surface of baggage or paper tickets by either vacuum or wiping.[14] Recently, a new IMS injection port inlet has been developed which collects the explosive sample using solid phase micro extraction.[1] Solid phase micro extraction is a simple adsorption and desorption technique for concentrating volatile compounds from air.

GC can also be coupled with chemiluminescence detector which is also known as TEA analyzer. Pyrolysis of explosives produces NO fragments that are consequently reacted with ozone (O_3) to produce electronically excited NO_2 (NO_2*). The NO_2* decays back to its ground state with emission of chemiluminescence light in the near-infrared region. The emitted light is

detected by a photomultiplier (PMT). The light intensity is proportional to the NO concentration and hence, to the explosive concentration.

A mass sensor was used as the GC detector in the EST-4200 Ultimate Vapor Tracer, a hand held instrument used in selected airports here in the U.S. It can also be an explosive detector by itself when combined in an array, which is often referred to as "electronic noses". Mass sensors include surface acoustic wave (SAW) detectors, normally coated with different semi-selective polymeric layers and micro electromechanical systems (MEMS), including micro cantilever detectors. Mass sensors typically adsorb the chemicals of interest into the surface and the device detects the change in mass. The detection can be through changes in acoustic waves propagating along the surface, as in the case of SAW, or by actual bending or a change in shape of the device as mass is accumulated as in the case of MEMS.

Electrochemical sensors (ECD) detect signal changes in an electrical current being passed through electrodes that interact with the target chemicals. The fact that nitro-based explosives can be reduced into amines makes them an ideal candidate for electrochemical detection. Electrochemical sensors can be classified as potentiometric (measure of voltage), amperometric (measure of current) and conductometric (measure of conductivity).

Biological explosive detectors, including specially trained dogs are considered the most successful and widespread system for explosive detection at airports and public areas. In addition to canines, other animal species have been proposed as alternative methods of biological explosive detection. A research project in Tanzania trains African Giant Pouched rats to detect landmines. Reports indicate that rats maybe capable of detecting similarly low level of explosive odor compared to dogs.[19] Bees are also being studied as a biological explosive detection system. It has been demonstrated that bees have a sense of smell comparable to dogs and are capable of

detecting explosives odors at concentrations lower than most instruments.[20] The bees can be imaged or traced to the source, or more commonly, used to survey areas by examining the chemical residues brought back to hives. Advantages include that they can be trained quickly and will not set off any mines. Limitations include the bees do not fly at night, in heavy rain, or in cold weather (below 40^{o}F). [20]

The immunosensor is a class of explosive biosensors and involves the use of antibodies as the biosensing element. Reaction takes place between a target analyte and a specific antibody. The basis of assay is the change in fluorescence emission intensity of a fluorescently labeled TNT analogue pre-bound to an anti-TNT antibody. The change in intensity occurs due to competitive displacement of the labeled TNT by the TNT from the samples.

Optical techniques under investigation include absorption based detection. This is the simplest method among different spectrometric methods. Several kinds of color change chemical sensors have developed for rapid onsite detection of explosives. On the other hand, photoluminescence (PL) detection is based on monitoring the luminescence of an electron rich semi-conducting polymeric film on exposure to the analyte in a flowing air stream. The PL is quenched on exposure to nitroaromatic compounds by electron transfer.

In Laser Induced Breakdown Spectroscopy (LIBS), a short laser pulse is focused on the sample. Laser energy heats, vaporizes, atomizes, and ionizes the sample material, generating a small plasma plume. As the plasma decays or cools down (approximately 1 μs after the laser pulse), excited atoms and ions in the plasma emit a secondary light, which is collected and spectrally resolved by the spectrophotometer, then analyzed by a light detector. As a result, the multi-elemental composition of the sample can be determined. For explosive detection, different

H, O, and N emission intensity ratios were studied to identify the analyte as organic explosive, organic non-explosive or non-organic sample.

The Terahertz (THz) explosive sensor is based on differential absorption. The given item or region is illuminated by THz radiation containing at least two distinct frequencies. The frequencies of radiation depend on the THz spectra of the targeted explosives and are chosen so as to maximize the contrast between the presence and absence of explosives. THz spectroscopy has not only the capability to detect the presence of explosive but can also determined the specific type of explosive as different explosives have unique THz specific finger prints.

Raman spectroscopy can also be used for detecting explosive vapor by monitoring the NO_2 stretching modes between 1300 and 1370 cm^{-1}. This method is based on the inelastic light scattering effect due to interaction of light with a sample. This technique is hampered by the weak Raman signal.

Stand-off technologies under development include Laser Light Detection and Ranging (LIDAR), differential absorption LIDAR (DIAL), and differential reflection LIDAR (DIRL) for imaging and LIBS as well.

Cavity ringdown spectroscopy (CRS) is a suitable direct technique for vapor detection that passes a high intensity pulse tunable laser beam through highly reflective mirrors, which form the cavity. The intensity of the time dependent decay of the light leaking through the mirror is measured.

The Photofragmentation-Fragment Detection (PF-FD) approach is based on detecting NO_2 moieties after photofragmentation of explosive compounds. Photofragmentation is usually done by pyrolysis or UV laser irradiation. $NO_{x(x = 1,2)}$ fragments are then detected by TOFMS, fluorescence, or TEA analyzer.

Table 1-3 summarizes the results obtained with different types of explosive detectors except for PF-FD approach which will be discussed comprehensively in succeeding chapters.

Challenges on Explosive Detection

There are several obstacles to fast and easy vapor explosive detection. The vapor pressures of explosives are low (Table 1-1 and 1-2). The equilibrium vapor pressure of most explosive at ambient temperature ranges between 10^{-4} to 10^{-9} torr and corresponds to equilibrium vapor concentrations in the region of 10 μg/L down to 10 ng/L.[20] This vapor concentration is measured for pure samples at equilibrium in a closed container. However, in the field, the environment will not be a closed system and may contain possible interferents. In addition, the deliberate concealment (e.g. hard top case, suicide bombers, etc.) of the explosive influences the detection. As a rough 'rule of thumb', a method that is suitable for direct explosive vapor detection should be able to detect concentrations down to less than 1 ng/L (ppb level).[20]

The limited sample size available for analysis is not only a critical problem with explosive vapor but also with contaminated soil samples as well. Current methods used for detection of explosive in soil such as GC-ECD and HPLC are inadequate due to their slow detection time and tedious sample preparation.

Scope of Research Dissertation

There is no single explosive detector that promises speed, selectivity, and sensitivity all together. Although each of the methods mentioned above exhibits one or more inherent advantages and disadvantages, their common feature is a high degree of complexity which hinders their potential to be miniature mass-deployable devices. IMS are the only commercialized handheld trace explosive detectors usually employed in airports. IMS instruments are quite expensive and use a radioactive source (^{63} Ni), which is not environmental

friendly. Because of these limitations, there is a pressing need for improved instrumental technique for trace explosive detection.

The focus of this dissertation is on the development of a simple, fast, reliable, sensitive and potentially portable explosive detection device employing laser photofragmentation followed by chemiluminescence.

In Chapter 2, generation of NO_2 fragments and its further dissociation into NO and O* was confirmed after photolysis of nitro-containing explosives by a 193 nm ArF laser using classical colorimetric analysis and a fast time-resolved absorption experiment, respectively. In Chapter 3, NO_2 sensitivity was improved using luminol-chemiluminescence technique. In Chapter 4, an oxidation unit was constructed and evaluated for NO to NO_2 conversion. Chapter 5 involved the integration and evaluation of the photofragmentation and chemiluminescence units as a single device for detecting nitro-based explosives. In Chapter 6, the capability of the system to directly detect an explosive in soil was evaluated. General conclusions and recommendations for future directions are described in Chapter 7.

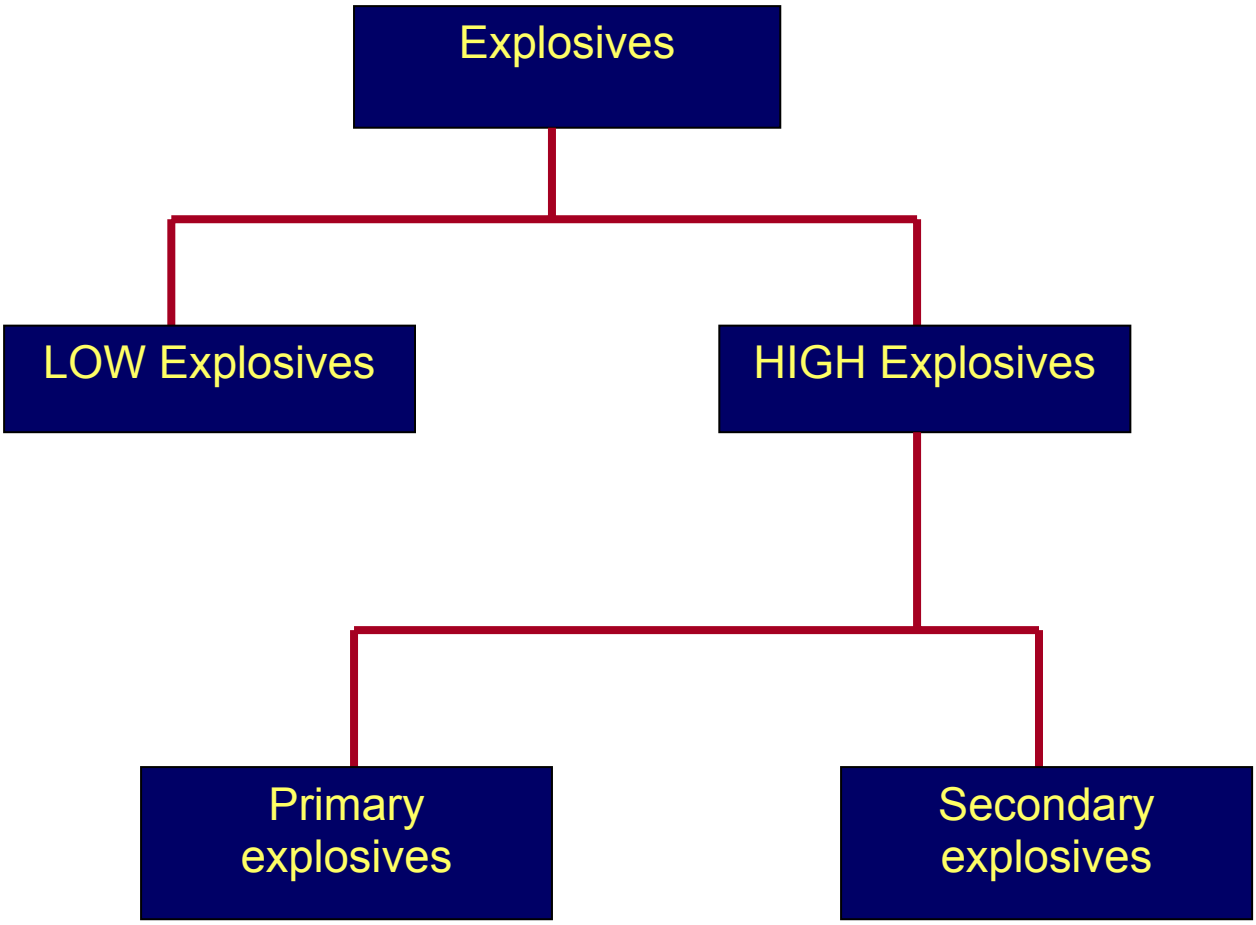

Figure 1-1. Classification of explosives based on composition and performance.

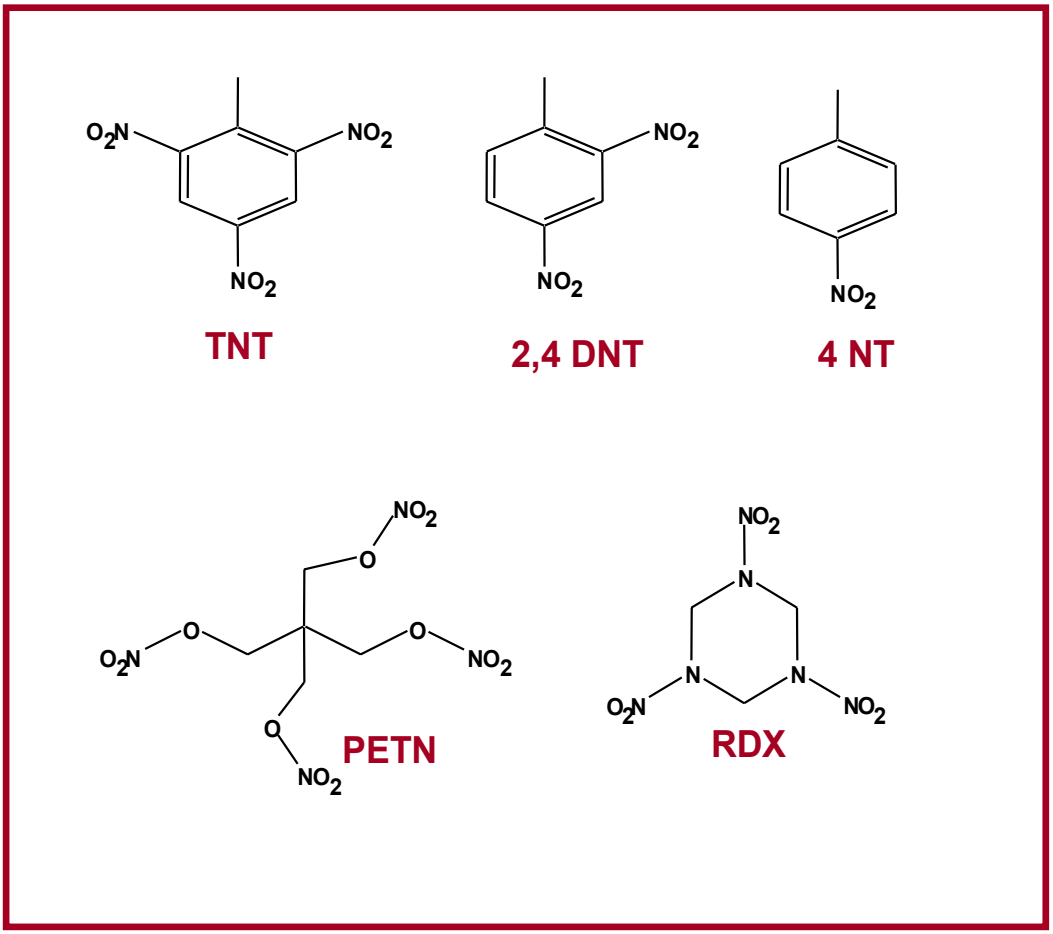

Figure 1-2. Structural formulas and names of nitrocompounds used in the study.

Table 1-1. Physical and chemical properties of nitrocompounds used in the study.

Properties	TNT	RDX	PETN
Chemical Formula	$C_6H_2(NO_2)_3CH_3$	$C_3H_6N_6O_6$	$C_5H_8N_4O_{12}$
IUPAC name	2-methyl-1,3,5-trinitrotoluence	1,3,5-trinitro-1,3,5-triazacyclohexane	1,3-dinitro-2,2-bis(nitramethyl) propane
Molar mass (g/mol)	227.131	222.117	316.140
Appearance	yellow needles	white crystalline solid	white crystalline solid
Density (g/cm^3 at 20^oC)	1.65	1.82	1.77
Melting point (^oC)	80.4	205.5	141.3
Boiling point (^oC)	Decomposes at 295	Ignites at 234	Decomposes at 190
Solubility in water at 20^oC (mg/L)	130	40	43
Solubility in	ether,benzene,acetone, pyridine	Acetone, acetronitrile	benzene, sparingly solouble in alcohol,ether and acetone
Vapor pressure at 25^oC (torr)	5.8×10^{-6} (7.7 ppb)	4.6×10^{-9} (6 ppt)	1.4×10^{-8} (18 ppt)
Shock sensitivity	insensitive	low	medium
Friction sensitivity	insensitive	low	medium
Explosive velocity (m/s)	6900	8750	8400
RF Factor*	1.00	1.60	1.66

* RF factor is a measurement of an explosive's power for military demolition purposes. TNT equivalent is a measure of the energy released from the detonation of a nuclear weapon or a given quantity of fissionable material, in terms of the amount of TNT which could release the same amount of energy when exploded.

Table 1-2. Physical and chemical properties of some nitro-based explosives.

Explosive class	Explosive/ Symbol	Formula	Molar mass (amu)	Vapor pressure at 25°C (torr)
Acid salt	Ammonium nitrate	NH_4NO_3	80.04	5.0×10^{-6}
Aliphatic nitro	nitromethane	CH_3NO_2	61.04	2.8×10^{1}
	2,3-Dimethyl-dinitrobutane/ DMNB	$C_6H_{12}N_2O_4$	176.17	2.1×10^{-3}
Aromatic nitro	2-Nitrotoluene/ *o*-MNT	$C_7H_7NO_2$	137.14	1.5×10^{-1}
	4-Nitrotoluene/ *p*-MNT	$C_7H_7NO_2$	137.14	4.1×10^{-2}
	2,4-Dinitrotoluene/ DNT	$C_7H_6N_2O_4$	182.14	2.1×10^{-4}
	2,4,6Trinitrophenol/ Picric acid	$C_6H_3N_3O_7$	229.11	5.8×10^{-9}
Nitrate ester	Ethylene glycol dinitrate/EGDN	$C_2H_4N_2O_4$	152.06	2.8×10^{-2}
	Trinitroglycerin/ NG	$C_4H_5N_3O_9$	227.09	2.4×10^{-5}
Nitramine	Tetranitro-*N*-methylamine/Tetryl	$C_7H_5N_5O_8$	287.15	5.7×10^{-9}
	Tetranitro-tetrazacyclooctane/ HMX	$C_4H_8N_8O_8$	296.16	1.6×10^{-13}
	Hexanitro-hexaaisowurzitane/ CL20	$C_6H_6N_{12}O_{12}$	438.19	N/A

N/A not available.

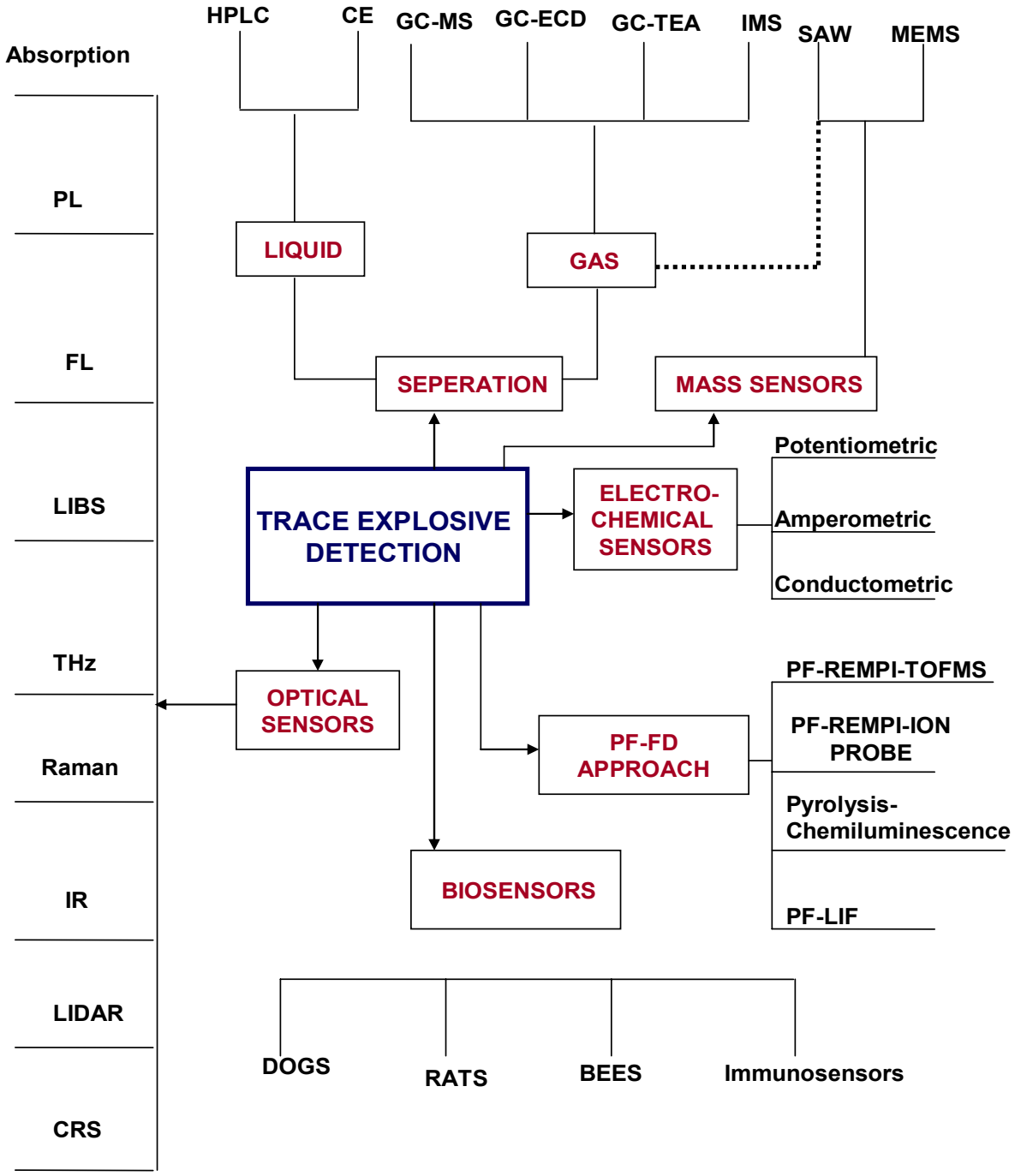

Figure 1-3. Chart showing some of the technologies presently available and under development for the detection of trace explosives.

Table 1-3.Comparative table showing summary of the performance of various explosive detectors reviewed in this study.

Transducer	Field of Application	Explosive Detected	Limit of detection	Comments	References
HPLC-UV Absorption, 254 nm	Aquifer samples	TNT	0.10 ng/mL	time consuming and tedious sample preparation	21
		RDX	0.10 ng/mL		
CE	collected in the vicinity of military installation Laboratory liquid samples	TNT, TNB	60, 160 µg/L	time consuming and tedious sample preparation, costly	9
		tetryl	200 µg/L		
GC-Laser Ionization Time-of-Flight-MS	laboratory vapor sample	NB	17-24 ppb; (S/N=2)	bulky	10
		2,4-DNT	~40 ppb; (S/N=2)		
GC ECD	soil sample	4-NT	10 µg/kg	time consuming and tedious sample preparation costly; not environmental friendly	11
		2,4-NT,TNT	1 µg/kg		
		RDX	3 µg/kg		
		HMX	25 µg/kg		
		PETN,NG	10-40 µg/kg		

Table 1-3. (Continued).

Transducer	Field of Application	Explosive Detected	Limit of detection	Comments	References
GC-TEA	laboratory vapor sample	4-NT	137 µg/L	Poor performance for explosive vapor detection, bulky,	12
		2,4-NT	18.2 µg/L		
		TNT	22.7 µg/L		
Electrospray-IMS	laboratory vapor sample	TNT	15 µg/L	IMS in general has a higher % of false positive and negative responses; low mass spectroscopic resolution; uses radio active source which is not environment friendly	13
		RDX	20 µg/L		
		HMX	86 µg/L		
		EGDN	190 µg/L		
GC-IMS (multi-capillary chromatographic column)	laboratory liquid sample	PETN	8 ng/L		15
		TNT	14 ng/L		
		2,4-DNT	16 ng/L		
Corona discharge-IMS	laboratory solid sample	PETN	8×10^{-11} g		16
		TNT	7×10^{-11} g		
		RDX	3×10^{-10} g		

Table 1-3. (Continued).

Transducer	Field of Application	Explosive Detected	Limit of detection	Comments	References
MEMS	laboratory vapor sample	PETN,RDX,TNT	low femto gram level 520 ppt	Limited applications due to noisy chemical background	22,23
Electrochemical Electrochemical Electrochemical	soil sample marine water soil extract and ground water	RDX TNT RDX TNT 2,4-DNT ,4-NT	0.12 ppm 25 ppb 60 ppb 0.11 ppm 0.15 ppm	In general, electro-chemical sensors suffer from limited sensitivity and mobile electrolyte. Also, electrodes can be easily fouled	24,25,26
Canines	airports, public places seawater	almost all	approximately low pptr level	subject to fatigue and behavioral variations	20,27
Immunosensors		TNT	250 ppt	Limited application,anti-bodies are not re-usable, unreliability	28
Absorption	laboratory samples of contaminated finger prints	DNT DNB	N/A	Applicable only for qualitative analysis	29
PL based	air and sea water	TNT picric acid	4 ppb TNT in air,1.5 ppt TNT in sea water, 6 ppb picric acid in sea water	bulky, relatively low sensitivity	30

Table 1-3.(Continued).

Transducer	Field of Application	Explosive Detected	Limit of detection	Comments	References
FL based	laboratory samples	TNB,TNT,DNB, tetryl,2,4-DNT	1 ppm for all of these explosives		31
FL based	Water samples	DNP DNT, NB	1 x 10^{-6} mol/L 40 ppb 17-24 ppb		32
LIBS	Laboratory samples	HMX,PETN,HMX, TNT,C4,M43	not available	qualitative analysis	33
Tetrahertz	Laboratory solid samples	RDX	not available	qualitative analysis	34,35
Raman	Laboratory vapor sample	2,4-DNT	5 ppb	qualitative analysis	36
Optic probe Raman	Laboratory samples of contaminated finger prints	RDX, PETN	µg range	qualitative analysis	37
IR	Laboratory vapor sample	TNT,RDX,PETN	not available	qualitative analysis	38
Mid-IR CRS	Laboratory vapor sample	TNT	75 ng/L	bulky	39

CHAPTER 2
PHOTOFRAGMENTATION PATHWAYS OF NITRO COMPOUNDS

Introduction

This chapter begins with the discussion of the basic theory of photofragmentation (PF) followed by a review of previous works elucidating the PF pathways of nitro compounds using Resonance Enhanced Multi-photon Ionization Time-of-Flight Mass spectrometry (REMPI-TOFMS) and Laser Induced Fluorescence (LIF). Generation of NO_2 fragments and their further dissociation into NO and O* was confirmed after photolysis of nitro-containing explosives by 193 nm ArF laser using classical colorimetric method and fast time-resolved absorption experiment, respectively.

Basic Theory of Photofragmentation

Photochemical processes can be classified based on the fate of electronically excited species formed after absorption of light. As shown in Figure 2-1, when a molecule (AB) has absorbed a quantum of radiation, (*hv*), it becomes 'energy rich or excited' in the process. There are several pathways by which an electronically species (AB*) may lose its energy. Some of these pathways are through chemical reaction of the reactive fragments formed, isomerization or ionization processes.[40] The process whereby the excited state species is split into simpler fragments is called photofragmentation (PF) or photodissociation (PD).

There are two important PF rules that may be stated as follows:

(1) Only the light absorbed by a system is effective in producing a PF in a molecule. This is also known as the Grottus-Draper Law. [41]
(2) Each photon absorbed activates one molecule in the primary excitation step of a photochemical sequence. [41]

Over the past four decades, various theoretical models and experimental techniques have been developed to advance the understanding of molecular dissociation induced by photon excitation. For instance, theoretically constructed potential energy curves or surfaces for PF of

diatomic or polyatomic molecules have been widely used to predict or explain the experimental phenomena.[42] As an example, consider the following PF for a hypothetical molecule ABC.

$$ABC + h\nu \rightarrow AB + C \qquad (2\text{-}1)$$

In Figure 2-2, the ground and excited state potential energy surface are termed G and E, respectively while R is the internuclear distance between atom C and the AB moiety and *hv* is the energy of the laser photon. The ground state potential energy surface is bound and evolves at long AB─C internuclear distances to an asymptotic energy which corresponds to the energy difference of the separated AB and C fragments. The energy difference between the ground state of the ABC molecule and the ground state energy of the two AB and C fragments is the bond dissociation energy (D_E). Following the absorption of a photon (of energy hυ), the ground state molecule is, in this case, excited to a repulsive excited state, (E). Depending on the repulsive character of the excited state, the molecule will dissociate promptly or more slowly, into the fragments AB and C. The excess energy, which is the difference between the energy of the photon and the bond dissociation energy, may be distributed among all available degrees of freedom of the nascent fragments (translational and internal). The release of kinetic energy causes the AB and C fragments to move away from the point in space where they were generated. The proportion of the excess energy released as kinetic energy and the masses of the AB and C fragments determine their recoil speeds. The residual excess energy is divided over the other degrees of freedom of the fragments and may, for instance, lead to rotational, vibrational, and/or electronic excitation of the fragments. By considering the law of conservation of energy, an expression for the partitioning of energy can be written as follows:

$$\Delta E_{ex} = h\upsilon + E^{p}_{int} - D_{o(AB-C)} = E_E + E_T + E_V + E_R \qquad (2\text{-}2)$$

where available or residual energy (ΔE_{ex}) consists of the photon energy ($h\upsilon$) plus the internal energy of the parent molecule (E^{p}_{int}) minus the energy $D_{o(AB-C)}$ required to break the B─C bond. This residual energy is partitioned into the electronic (E_E), translational (E_T), vibrational (E_V) and rotational (E_R) degrees of freedom of the fragments.[42]

Basic Theory of REMPI-TOFMS and LIF

Propellants and explosives contain molecules with characteristic functional groups, namely the NO_2 moiety bonded to carbon, (─C─NO_2 for nitrocompounds), oxygen, (─C─O─NO_2 for nitric ester) or nitrogen ((─C─N─NO_2 for nitramines). This functional group is weakly bound to the main skeletal portion of the parent molecule by approximately 40 to 60 kcal/mole depending upon the specific molecule.[43] It is this moiety that is responsible for the weak and structureless absorption observed in the UV region near 230 nm.[44]

Resonance Enhanced Multi-photon Ionization (REMPI) technique typically involves a resonant single or multiple photon absorption to an electronically excited intermediate state followed by another photon which ionizes the atom or molecule. An ion and a free electron will result if the photons have imparted enough energy to exceed the ionization threshold energy of the system. Typically, small molecules composed of light atoms will have ionization energies around 10-15 eV, corresponding to the absorption of three UV photons from the ground state of the neutral molecule.[45] The cross section of the ionization process is greatly enhanced if there is a real excited state resonant at the energy of one or two absorbed photons (Figure 2-3).[45]

Multi-photon fragmentation and ionization can occur by two distinct mechanisms. First, molecules absorb photons, exciting them to a dissociative state below the ionization limit. If the laser pulse duration is much shorter than the lifetime of dissociative state, then the up pumping rate may be so high that ionization occurs before dissociation. The ions may absorb additional photons before fragmenting. This process is ionization followed by dissociation (ID) or ladder

climbing.[45] However, if the laser pulse duration is longer than the dissociative state lifetime, then the laser intensity is sufficiently high, these fragments may absorb additional photons to further dissociate or ionize. This process is dissociation followed by ionization (DI) or ladder switching. Thermally labile compounds, which include many nitro compounds, fragment primarily by the DI route while many aromatic compounds fragment by ID route alone.[45]

A schematic of a typical REMPI apparatus is presented in Figure 2-4. A gas phase sample is introduced into the apparatus, typically in the form of a molecular beam. A high power, pulsed laser is used to induce multi-photon absorption, resulting in fragmentation and ionization.[46] The resulting ions are then detected by Time-of –Flight-Mass Spectrometry (TOF-MS).

Laser Induced Fluorescence (LIF) is simply the optical emission from molecules that have been excited to higher levels by absorption of laser radiation. LIF has been used to study the electronic structures of the molecules and to make quantitative measurements of their concentrations.[46]

LIF for explosive detection is usually combined with photofragmentation in order to dissociate a target molecule and subsequently detect the fluorescence of the generated fragments. This is done because the fluorescence of most explosives is weak while the fluorescence intensity of $NO_{(X=1, 2)}$ fragments produced after photolysis is strong.[47]

Figure 2-5 shows a schematic of a PF-LIF experimental system. A UV laser is used to dissociate and induce fluorescence in the sample. A photomultiplier (PMT) detects the LIF signal which can be averaged and recorded on a digital oscilloscope. The laser wavelength can also be scanned to collect LIF spectra. These spectra can be used to identify the wavelength of the highest intensity LIF signal.

PF Mechanism of Explosives based on PF-REMPI-TOF and PF-LIF

In 1983, Butler, et al. [48] studied the dissociation of nitromethane (CH_3NO_2) at 193 nm using LIF and molecular beam photofragment translational energy spectroscopy which is similar to REMPI-TOFMS except for the addition of an electron ionization (EI) source at the entrance of TOF analyzer. The primary photodissociation process is shown to be cleavage of the C─N bond to yield CH_3 and NO_2 radicals with quantum yield almost equal to unity. The translational energy distribution for this chemical process indicates that there are two distinct mechanisms by which CH_3 and NO_2 radicals are produced. The dominant (major) mechanism produces CH_3 and NO_2 in its electronically excited ($\tilde{\mathbf{A}}\ ^2B_2$) state. The electronically excited NO_2 has sufficient internal energy to further dissociate to NO and O* as follows:

$$NO_2\ (\tilde{\mathbf{A}}\ ^2B_2) \rightarrow NO\ (X^2\Pi) + O\ (^1D) \qquad (2\text{-}3)$$

In the minor mechanism, the NO_2 fragment is produced in the excited ($\mathbf{B}\ ^2B_2$) state, which has a large cross section for absorbing another photon. The subsequent absorption of an additional 193 nm photon results in further photodissociation of NO_2 into NO and O* as shown below.

$$NO_2\ (\mathbf{B}\ ^2B_2) + h\upsilon \rightarrow NO\ (A^2\Sigma^+); \qquad h\upsilon = 193\ \text{nm} \qquad (2\text{-}4)$$

Almost at the same time, Blais [49] obtained the same results as Butler et al. and determined that about 30% of the NO_2 produced from primary photodissociation participates in the second absorption. Fragments from photodissociation were observed at m/z values of 15, 16, and 30 corresponding to CH_3, O, and NO. A very small signal at m/z = 46 (NO_2) was measured. The NO_2^+ signal was significantly lower than that of NO^+ signal, presumably due to extensive fragmentation of vibrationally excited NO_2 molecules in the ionizer.

In 1984, Renlund [50] reported the decomposition of nitromethane (CH_3NO_2), nitrobenzene ($C_6H_5NO_2$), and n-propylnitrate ($CH_3(CH_2)_2ONO_2$). The emission of C*, CH*, and NO_2* was monitored from 380 to 650 nm. Of particular note is the behavior of the NO_2 yield as a function

of laser fluence. In the case of nitromethane and n-propylnitrate, the NO_2 yield varies linearly with fluence until it saturates; however, saturation was not observed with nitrobenzene, but instead the NO_2 yield increases more sharply with higher fluence conditions. It was concluded then that by increasing the rate of energy deposition, the yield of NO_2 can be accelerated suggesting that the primary dissociation of nitrobenzene into C_6H_5 and NO_2 may change as a function of laser intensity.

In 1989, Capellos et al. [51] used PF-LIF technique to study the photodecomposition of RDX vapor at 428K using KrF laser with 248 nm and 15 ns pulse radiation. They observed prompt emission at 305-320 nm and at 380-420 nm following photolysis of RDX. Based on the spectra recorded, they attributed the UV emission to electronically excited OH ($^2\Sigma^+$) and the structureless visible emission centered at 608 nm to electronically excited NO_2 ($^2B_2$). Monitoring the signal intensity as a function of laser fluence revealed that NO_2 ($^2B_2$) was formed by a one-photon process while OH ($^2\Sigma^+$) was formed by a two-photon process. The production of NO_2 ($^2B_2$) was claimed to result primarily from the N─N bond scission of electronically excited RDX and OH ($^2\Sigma^+$) possibly via dissociation of vibrationally excited nitrous acid (HONO) which is generated by a H atom rearrangement in RDX, followed by five member ring formation and HONO elimination.

In 1993, Galloway et al. [52] used PF-REMPI-TOFMS in studying the pathways and kinetic energy disposal of the photodissociation of nitrobenzene. At several photolysis wavelengths between 220 and 320 nm, the following photodissociation pathways for nitrobenzene were observed:

$$C_6H_5NO_2 \rightarrow C_6H_5 + NO_2 \qquad (2\text{-}5)$$

$$C_6H_5NO_2 \rightarrow C_6H_5NO + O \qquad (2\text{-}6)$$

$$C_6H_5NO_2 \rightarrow C_6H_5O + NO \quad (2\text{-}7)$$

$$C_6H_5NO_2 \rightarrow C_5H_5 + CO + NO \quad (2\text{-}8)$$

The relative yield of the pathways producing NO_2 and NO varies strongly with the photolysis wavelength. The production of NO_2 exceeds that of NO by about 50% for the 280 nm photolysis, but increases to almost six fold excess in 222 nm dissociation.

Lemire et al.[53; 54](1993), Marshall et al. [55](1994), and Ledingham et al. [56](1995) used the same technique and all confirmed the characteristic fingerprint at m/z = 30 (NO^+) for nitrobenzene; 2,4 DNB; TNT; EGDN; PETN; RDX; and Semtrex sample at λ = 226 nm.

Simeonsson et al. [57](1994) repeat the same experiment using a 193 nm laser instead. The same mass spectra were obtained except for a higher signal intensity at m/z =30 (NO), which can be attributed to the higher pulse energy of an argon fluoride (ArF) laser (λ = 193 nm) compared to a dye laser (λ = 266 nm).

In 1996, Moyang et al. [58] studied the photodissociation of nitrocellulose by means of electron impact ionization ion trap mass spectrometer (EI-MS). In this article, nitrocellulose was irradiated at 532, 355, and 266 nm and with a tunable dye laser operating in the range of 310-330 nm. The first mass spectrum obtained with 532 nm laser light only showed mass peaks corresponding to background gases: water, nitrogen and oxygen. However, irradiation with 355 nm light produced three major peaks at m/z = 19, 30, and 48, corresponding to protonated water (H_3O^+), nitric oxide (NO^+), and hydrated nitric oxide complex ($NO{\cdot}H_2O^+$). When 266 nm laser light was used, the intensities of the mass peaks occurring at m/z 30 and 48 increased approximately four times in comparison with the same peaks observed using 355 nm light. The wavelength dependence of removing the NO_2 moieties from its parent molecule (or denitration) in the 310-330 nm range has been measured, and the NO yield normalized by laser intensity

showed a linear decrease of NO yield with increasing laser wavelength. All of these results suggest the simple trend that shorter wavelength UV light induces more denitration. The weight loss rate of sample due to denitration induced by 266 nm laser light was measured to be 4.0±0.4 μg J^{-1}. This value represents a 5.8% photon-to-nitro group conversion efficiency. A laser intensity threshold about 6 mJ cm^{-2} was observed; above which thermal decomposition occurs (detonation of sample occurs).

Research on photofragmentation of nitro-containing compounds within the last 20 years did not experimentally confirm the detection of NO_2 fragments which is fundamentally essential in supporting the primary photodissociation of nitro compounds as shown below:

$$R{-}NO_2 \rightarrow R + NO_2 \qquad (2\text{-}9)$$

PF-REMPI-EI-TOFMS during 1980's claimed that NO_2^+ was not detected due to extensive fragmentation of NO_2 molecules in the ionizer while PF-REMPI-TOFMS during the 1990's attributed the absence of NO_2^+ signal due to the absence of a real excited state resonant with the energy of two absorbed photons to ionize NO_2 to NO_2^+. However, NO_2 fragments were detected by its prompt fluorescence emission. Detecting NO_2 using this method is not that reliable since the NO_2* emission is irradiated over a large spectral region (from visible to near IR) where other excited fragments are also expected to emit.

The work presented in this dissertation was able to detect directly NO_2 fragments from explosives after their photolysis with an ArF laser by a classical colorimetric method. Furthermore, the photodissociation of NO_2 fragments into NO and O* was confirmed using a time resolved absorption experiment.

Experimental Section

Reagents and Chemicals

Explosive samples. Five percent (v/v) solutions of PETN, RDX, and TNT in acetone were provided by Naval Surface Warfare Center (MD, USA). Acetone was allowed to evaporate at room temperature to obtain the crystalline samples. Solid reagent grade chemicals (99% purity) of 4-NT and 2,4 NT were used and purchased from Sigma Aldrich (St. Louis, MO).

Colorimetric experiment. All chemicals used were analytical reagents from Fischer Scientific Inc. (Hampton, NJ) unless otherwise stated. Deionized water from Millipore Milli-Q deionizing system was used for preparing all the reagent solutions.

Triethanolamine (TEA) solution was prepared by dissolving 15 g of TEA in 1 L of water.

Standard Nitrite solution was prepared by dissolving 0.2 g dried $NaNO_2$ (105^oC for 1 hour) in 100 mL of water. Exactly one mL of this solution was diluted using TEA solution to get 4 μg/mL of nitrite which serves as a stock solution.

Neutral red solution was prepared by dissolving 0.1 g of neutral red (Basic red 5 C.I. 50040) in 1 L of water containing 2.5 mL of 4.25 M H_2SO_4. The dye solution was stable for thirty days.

1 % (wt./v) Sodium hypophosphite(NaH_2PO_2) was prepared by dissolving 1 g of NaH_2PO_2 in 100 mL of water.

1 % (wt./v) Potassium bromide (KBr) was prepared by dissolving 1 g of KBr in 100 mL of water.

Time-resolved absorption experiment. Copper powder (325 mesh) was purchased from Alfa Products (Danvers, MA) and reacted with 98 %(v/v) nitric acid (HNO_3).

Apparatus and Methodology

Photofragmentation-NO_2 fragment collection. Figure 2-6A shows the photofragmentation (PF) set-up used for NO_2 fragment collection. The set-up consists of the PF cell containing the explosive sample, an argon fluoride (ArF) laser to photolyze the sample, and a delivery gas system to purge all the photofragmented products into the glass bubbler containing TEA solution. The PF cell (Figure 2-6B) is made of cylindrical stainless steel with an O.D. of 1.93 cm and a length of 4.85 cm. Both ends of the PF cell were enclosed with quartz window (D = 1.80 cm) to allow passage of UV radiation into the cell. The delivery gas system was coupled into the PF cell through solenoid valves (Asco Inc., NJ) that were attached to both sides of the cell. A tank containing ninety nine percent pure N_2 gas was attached to the entrance of solenoid valve I while the exhaust end of solenoid valve II connects the PF cell to the gas bubbler. The gas flow rate was controlled by a mass flow controller manufactured by Alicat Instrument Inc. (Tucson, AZ).

In these experiments, solid explosive sample was deposited and tightly packed into a small aluminum cylindrical cup (O.D. = 1.9 mm; Depth = 4.5 mm). The sample was then securely placed into the circular quartz disk having its center drilled and hollowed to exactly fit the sample holder. This circular disk serves as the backside window panel of the PF cell.

An argon fluoride (ArF) excimer laser (GAM Laser Inc., Orlando, FL) was used to generate the photolysis wavelength of 193 nm. Each experimental run used 80 000 laser pulses with an average energy of 8 mJ/pulse. The pulse length and the repetition rate are 15 ns and 50 Hz, respectively. The beam diameter is 3.1 mm. It should be noted that PF is distinct from Laser-Induced Breakdown Spectroscopy (LIBS). The laser flux employed in PF is always sufficiently low to avoid laser induced breakdown of the sample medium or the creation of plasma.

The ArF laser ablated and photolyzed the explosive sample while N_2 gas (0.5 SLPM flowrate) which serves as the carrier gas is continuously introduced to purge the photofragmented products into the bubbler containing 10 mL of TEA solution. The TEA solution trapped the NO_2 fragments into the bulk solution by converting them to nitrite ions (NO_2^-) as shown by the following equation:

$$N(HOCH_2CH_2)_3 + \mathbf{2NO_2} + 2OH^- \rightarrow \mathbf{2NO_2^-} + {}^-O^+N(OHCH_2CH_2)_3 + H_2O \quad (2\text{-}10)$$

Colorimetric analysis. The nitrite ions in TEA solution were then analyzed using colorimetric method by mixing exactly 2 mL of aliquot solution of TEA into 25 mL standard flask containing 2 mL of 0.01 % neutral red, 1 mL of 4.25 M H_2SO_4, and 1 mL KBr. This was followed by addition of 1 mL of 1 % NaH_2PO_2 and mixed thoroughly. The mixed solution was then diluted to mark and the absorbance was measured at 530 nm against distilled water.

Preparation of the Calibration Graph. Aliquots of the standard stock solution of NO_2^- containing 0 to 85 µg of nitrite were added to a series of 25 mL standard flask containing the same reagents used for preparing the samples. Absorbance was measured at 530 nm against distilled water. The calibration graph obtained was linear but with a negative slope.

Nature of Species Responsible for Color. A known excess amount of neutral red on treatment with nitrite solution undergoes diazotization in acidic medium (Figure 2-7A). KBr acts as a catalyst for this reaction On treatment with NaH_2PO_2, the diazonium salt undergoes deamination and causes a decrease in absorbance proportional to the concentration of added nitrite ions. The absorption spectrum of unreacted neutral red is shown on Figure 2-7B.

PF-time resolved absorption experiment. Figure 2-8 shows the PF set-up used for confirming the further dissociation of NO_2 fragments into NO and O* upon absorption of a photon with 193 nm wavelength. The set-up consists of the PF cell containing the NO_2 gas

sample, an ArF laser to photolyze the sample, and a detection system to monitor the change in the profile of the laser pulse before and after photolysis. Neutral density filters were added to attenuate the laser pulse energy and to prevent the saturation of the ET-2030 photodiode detector (Electro-Optics Technology, Traverse City, MI). The set-up is capable of monitoring the intensity versus time profile of the laser pulse after photofragmentation of NO_2 gas.

Nitrogen dioxide gas was produced by reacting pulverized Cu with concentrated nitric acid in a sealed 250 mL Erlenmeyer flask (reaction 11). The NO_2 gas generated from this reaction was collected using a gas syringe and injected into a quartz cell (Diameter = 2.0 cm; Length = 10.0 cm) through its rubber septum cover.

$$Cu_{(s)} + 4HNO_{3\,(aq.)} \rightarrow Cu(NO_3)_{2(s)} + 2\,H_2O_{\,(l)} + 2NO_{2(g)} \qquad (2\text{-}11)$$

The ArF laser beam was focused into the cell and used to photolyze the NO_2 gas sample. The photodiode detector is triggered by the PMT system to collect the signal from the laser. The intensity versus time profile of the laser pulse was monitored and plotted by fast oscilloscope (HP54542C Oscilloscope, Hewlett Packard, Pab Ator, California). The ArF laser was calibrated using an MPE 2500 power meter from Spiricon Power Products Inc., Logan, Utah.

Results and Discussion

Detection of NO_2 Fragments

The calibration graph (Figure 2-9) for NO_2 fragment detection was obtained by plotting absorbance values at 530 nm against the mass of nitrite in µg. Linear dynamic response was found within the range of 0 to 85 µg NO_2^-. The calibration plot is a straight line; with correlation coefficient(R) value of -0.98506 and obeying the following equation:

$$A_{(dye)} = -0.00753(m) + 0.65734 \qquad (2\text{-}12)$$

where A is the absorbance and m is the amount of nitrite in µg. The limit of detection (LOD) was 0.78 µg (0.02 mmol) nitrite. LOD is defined by the following equation:

$$LOD = (k \cdot s_{blk}) / m \qquad (2\text{-}13)$$

where k is the confidence factor which is equal to 3, s_{blk} is the standard deviation of the blank and m is the slope of the line or the calibration sensitivity.

The precision of the method has been established at 19 μg nitrite which gave a relative standard deviation (RSD) of 5.66% where n = 10.

The amount of NO_2 fragments detected for each solid explosive sample is shown in Table 2-1, which experimentally shows the primary photodissociation of explosives after photolysis at 193 nm. The amount of the sample ablated was determined from another experimental run where there is no flow of carrier gas. The aluminum cup sample holder was weighed before and after photofragmentation using a microbalance. The fraction of NO_2 detected was calculated by the following equation:

$$\text{Fraction of } NO_2 \text{ detected} = \frac{\text{moles of } NO_2^- \text{ detected in TEA solution}}{NO_2^- \text{ moles ablated}} \qquad (2\text{-}14)$$

The fraction of NO_2 detected for all the explosive samples was approximately the same with the exception of RDX. RDX' significantly higher fraction of detected NO_2 might be due to its PF mechanism as elucidated by Capellos et al.[51] Nitramines have a characteristic dissociation pathway which involve HONO elimination from a parent molecule. HONO produced during photolysis can be readily trapped and absorbed in a basic TEA solution, subsequently increasing the fraction of NO_2 detected.

The validity of the colorimetric analysis has been established using NO_2 gas standards having concentrations of 5 and 10 ppm. The NO_2 gas was purged into the same bubbler containing 10 mL TEA solution at flow rate of 0.3 SLPM. Exactly two mL of this solution was

analyzed for nitrite content following the procedure described under the calibration graph. The following equation was used to convert the μg NO_2^- determined into ppm concentration.

$$NO_{2\,(ppm)} = (mD)/(40.9VMAS) \qquad (2\text{-}15)$$

where m is the mass of nitrite ions in μg, D is the dilution factor, V is the volume of the gas in L collected at standard temperature and pressure, M is the molar mass of NO_2 in g/mol, A is the fraction of $NO_{2(g)}$ absorbed by TEA solution , and S is the fraction of NO_2 gas converted to NO_2^- ions. The numerical values of A and S are 0.95 and 0.85, respectively.[59] Based on this equation, NO_2 concentrations of 6.1±0.0 and 11.9±0.4 ppm were obtained after analyzing 5 and 10 ppm NO_2 standards, respectively.

From these sets of data, the direct confirmation of NO_2 fragments was established after photolysis of explosives at 193 nm. Relatively low fraction of NO_2 detected for each sample indicates the further photodissociation of NO_2 into NO and O* upon absorption of an additional photon.

Photofragmentation of NO_2

Nitrogen dioxide exposed to tropospheric UV radiation photodissociate at $\lambda \leq 420$ nm to give NO and O*.[60]

$$NO_2 + h\upsilon \rightarrow NO + O^*; \quad h\upsilon \leq 420 \text{ nm} \qquad (2\text{-}16)$$

A fast time resolved absorption experiment has been used to verify the photodissociation of NO_2 at 193 nm. Light from ArF excimer laser was used to decompose NO_2 at ambient conditions. The laser pulse has a duration of 10 ns and delivered output energy of 10 mJ/pulse at a repetition rate of 20 Hz. The oscilloscope was set to obtain the average of 32 pulses for each run of the experiment under closed batch system. The NO_2 concentration diluted in air was approximately around 120 ppm or about 3% in terms of the partial pressure of NO_2 gas with

respect to the atmospheric pressure. The concentration of NO_2 was calculated using the following equation:

$$\% NO_2 (P^o_{NO_2}/P_{atm}) = \frac{A R T C}{0.434\sigma LPN} \times 100\% \quad (2\text{-}17)$$

where A is the initial absorbance (0.7), R is the universal gas constant (0.08206 L-atm/mol-K), T is the room temperature (298K), C is the conversion factor (1000 cm^3/L), σ is the absorption cross section of NO_2 at 193 nm (2.0 x 10^{-19} cm^2)[61], L is the length of the PF cell (10 cm), N is Avogadro's number (6.02 x 10^{23} molecules/mole).

Figure 2-10A shows the profile of the ArF laser pulse before and after the photolysis of NO_2 gas sample. Plot A represents the actual profile of the laser pulse. Plot B represents the profile of the laser pulse after passing it through an empty PF cell and an added neutral density filter. Plot C represents the profile of the laser pulse after passing it through the PF cell containing NO_2 gas sample. From these sets of data, the time-resolved absorbance plots were obtained (Figure 2-10B). If the absorption of light is uniform during the entire duration of the pulse and the detector responds linearly to light, then the plot of time-resolved absorbance versus time will show a constant value for the entire duration of the pulse. This is exactly the case after adding a neutral density filter which is shown by the $A_1(t)$ plot. On the other hand, if the first part of the pulse induces a dissociation process and the fragments produced do not absorb, the shape of the pulse will be distorted since now the second part of the pulse will show no absorption. The overall result would be a non-constant behavior of the time-resolved absorbance plot during the entire duration of the pulse as shown by the $A_2(t)$ plot.

Conclusion

The following PF pathways were confirmed using classical colorimetric analysis and fast time resolved absorbance.

$$R{-}NO_2 + h\upsilon \rightarrow R + NO_2; \quad h\upsilon = 193 \text{ nm} \qquad (2\text{-}18)$$

$$NO_2 + h\upsilon \rightarrow NO + O^*; \quad h\upsilon = 193 \text{ nm} \qquad (2\text{-}19)$$

Confirmation of $NO_{x(x = 1,2)}$ generation after photolysis of nitro-based explosives was the basis for developing an explosive detector based on PF-Fragment detection scheme

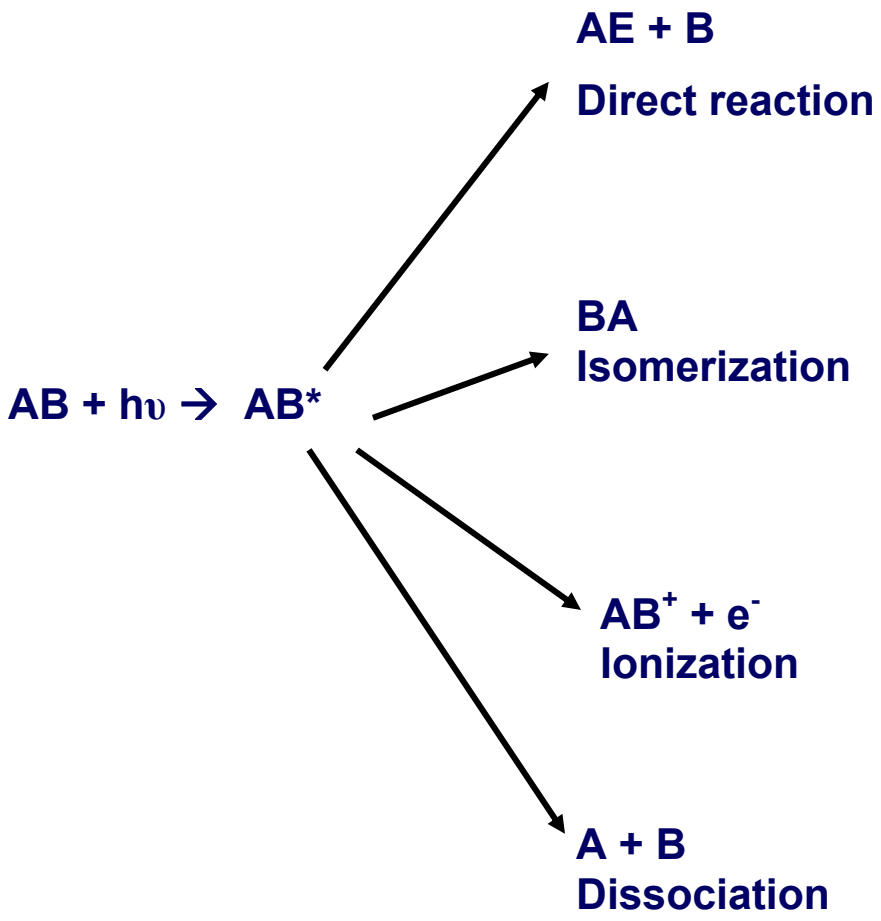

Figure 2-1. The fate of electronically excited species (AB*) formed after absorption of light, ($h\upsilon$).

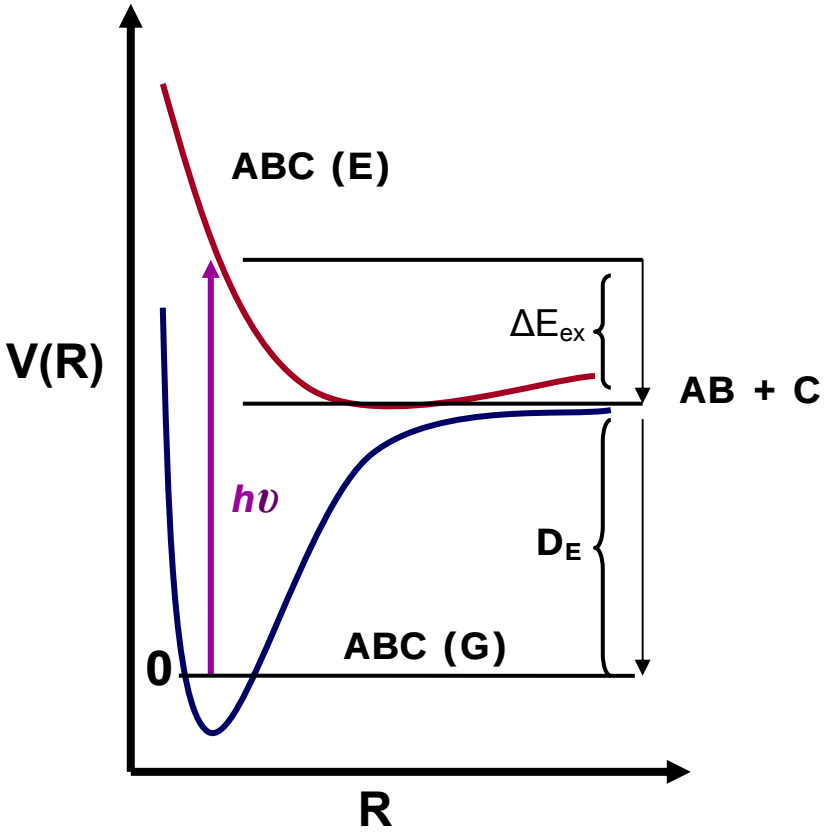

Figure 2-2. Schematic representation of the photodissociation of a triatomic molecule (ABC). R is the distance between C and the AB diatomic fragment, DE is the bond dissociation energy and hυ is the energy of the photon. Through absorption of a photon, the molecule is excited to a repulsive state via which it dissociates. The excess energy (ΔEex) is the energy difference between the photon energy and bond dissociation energy.

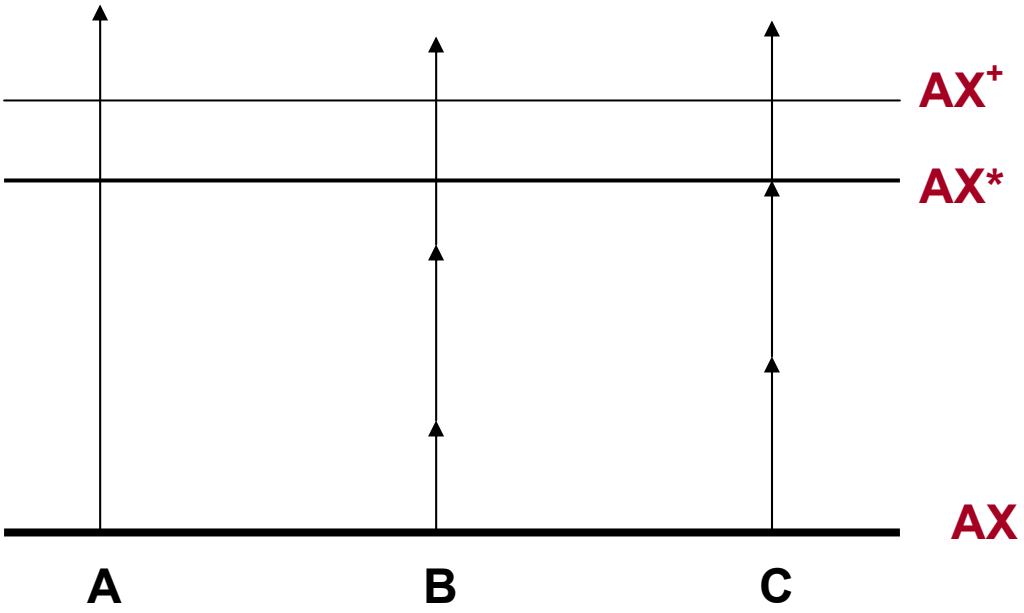

Figure 2-3. Various molecule ionization processes through photon absorption. A) Ionization via direct one-photon aborption B) non-resonant multi-photon ionization and (c) resonance enhanced multi-photon ionization (REMPI). Process C) is an example (2 + 1) REMPI scheme; two photons are required to excite the molecule AX to a resonant excited intermediate state AX* and one more to ionize AX*.

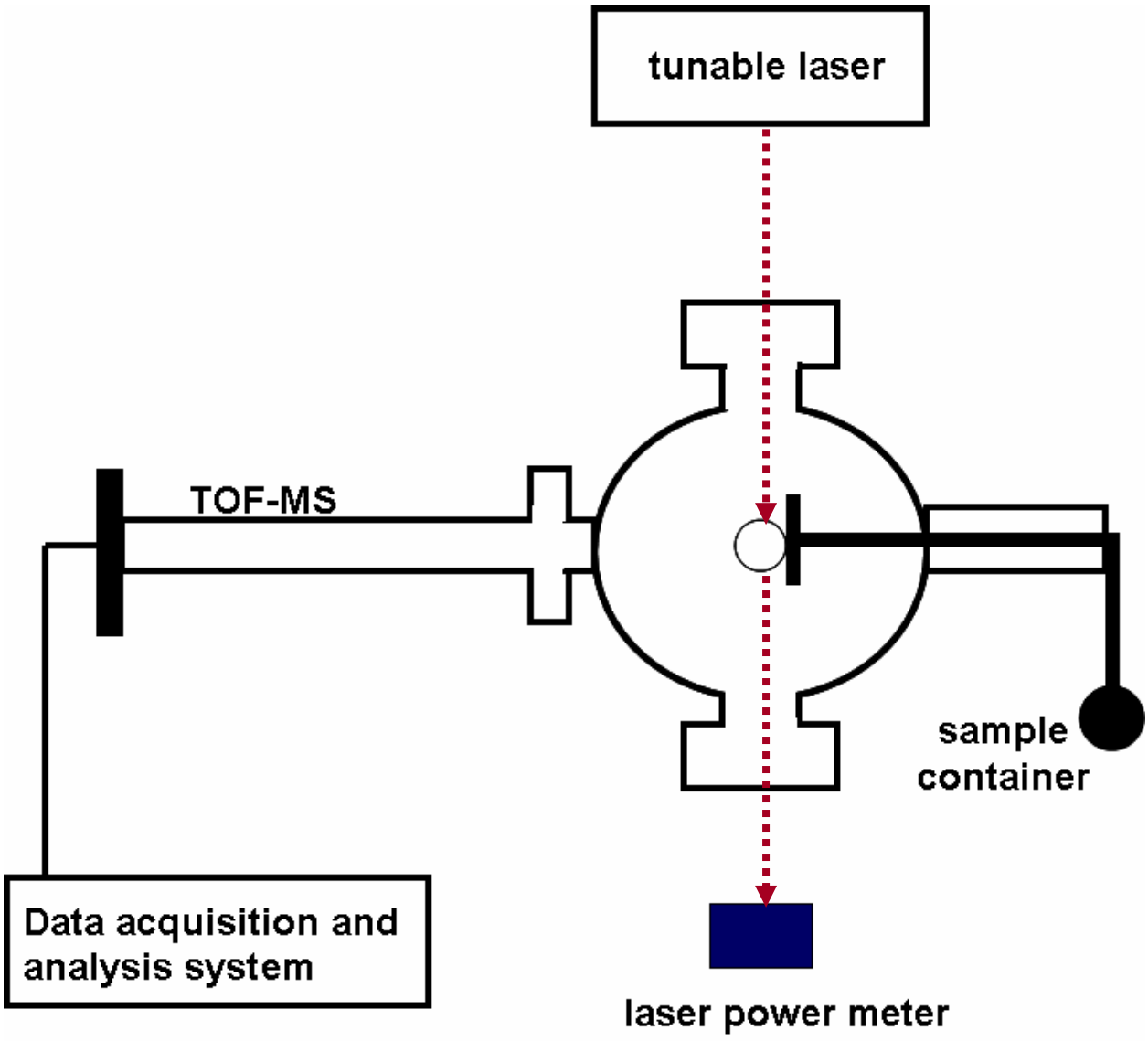

Figure 2-4. Schematic of REMPI apparatus.

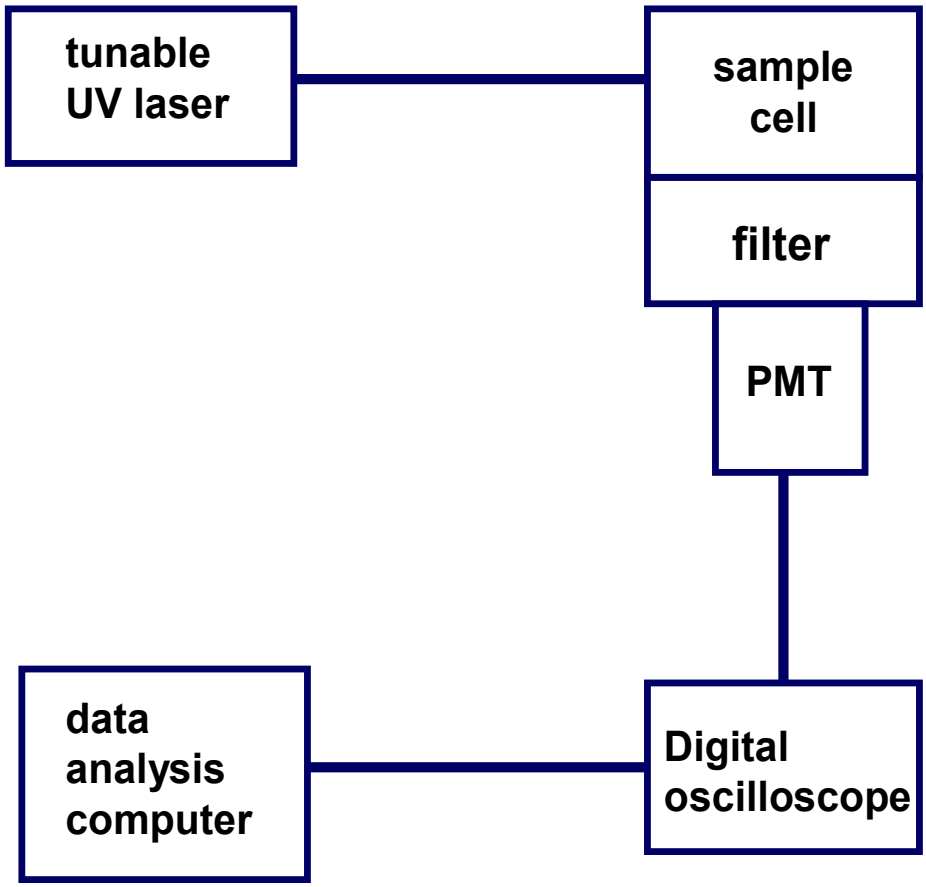

Figure 2-5. Schematic of PF-LIF apparatus.

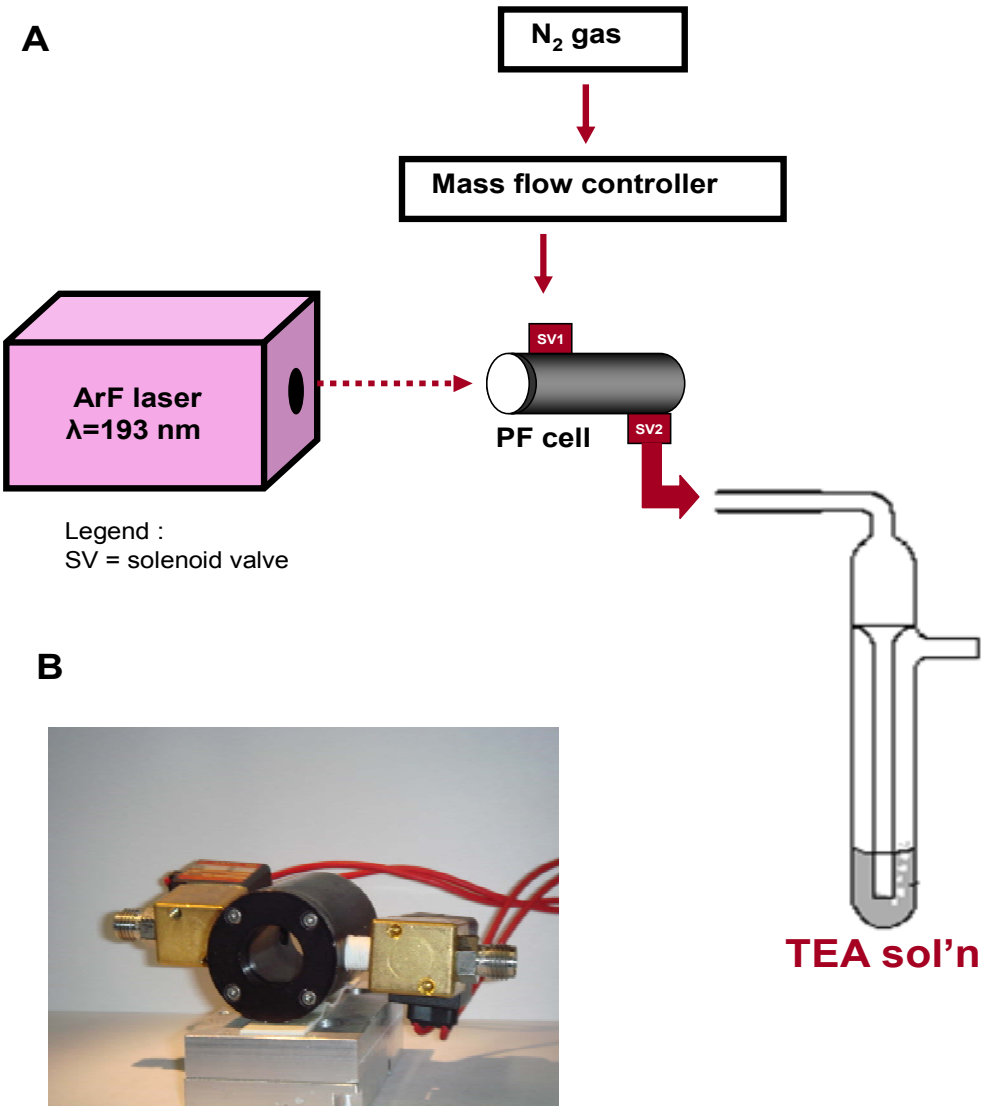

Figure 2-6. Photofragmentation set-up. A) schematic of PF-NO_2 fragment collection set-up B) actual picture of the PF cell

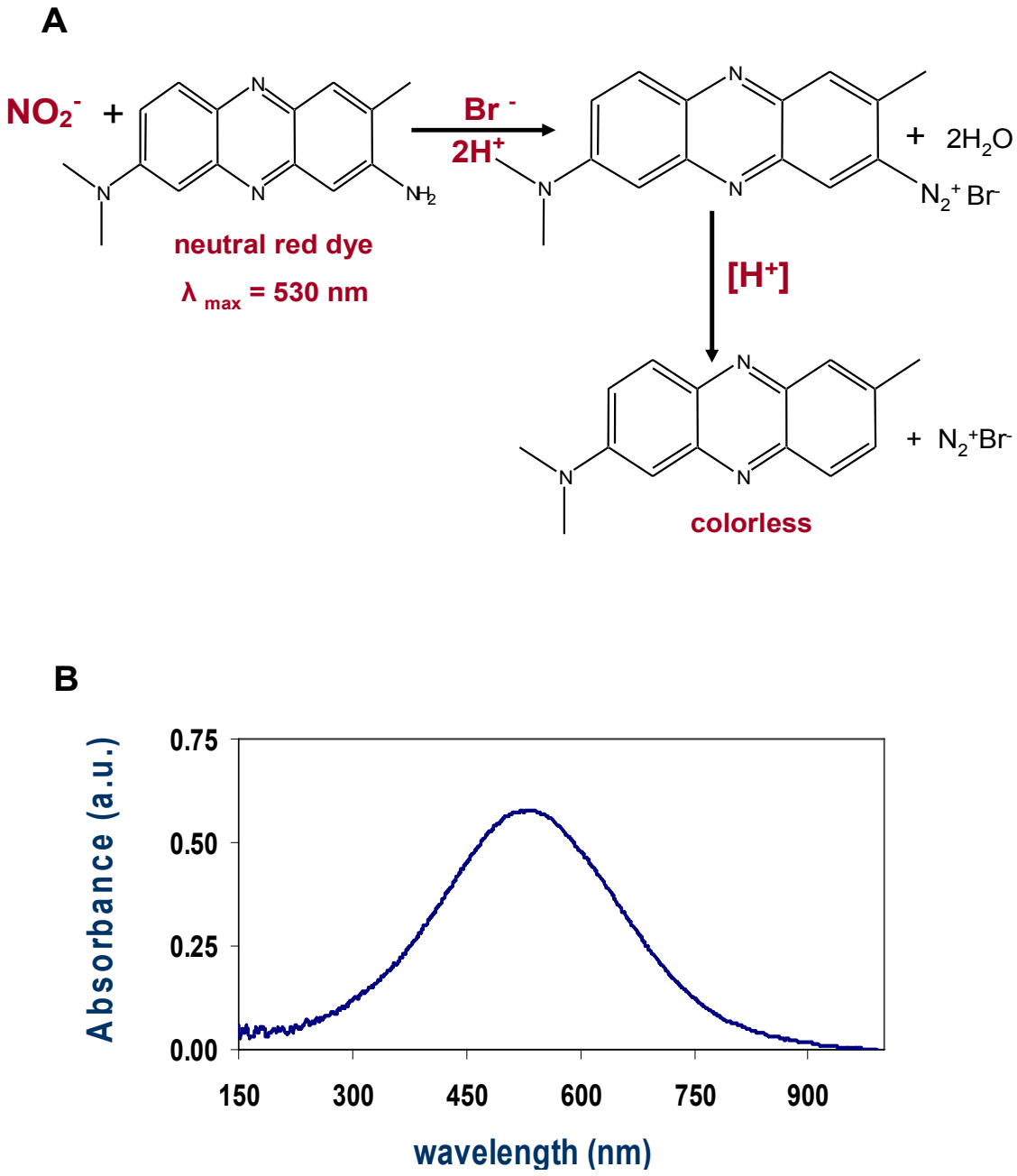

Figure 2-7. Nitrogen dioxide detection by colorimetric method. A) species responsible for color B) absorption spectrum of neutral red dye.

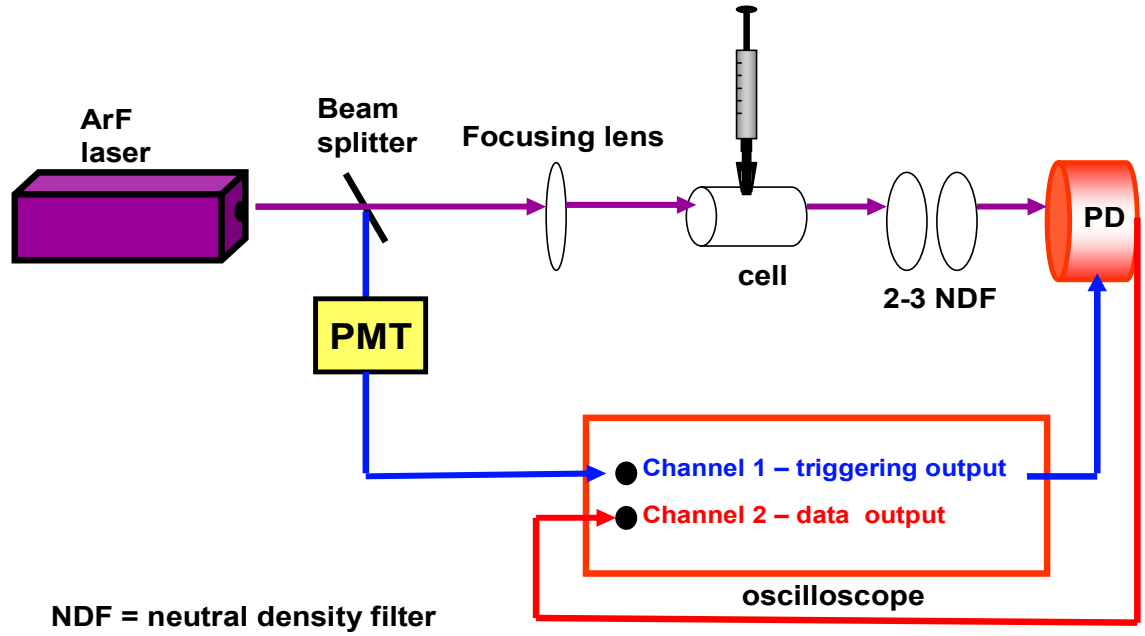

Figure 2-8. Schematic of time-resolved absorbance experimental set-up.

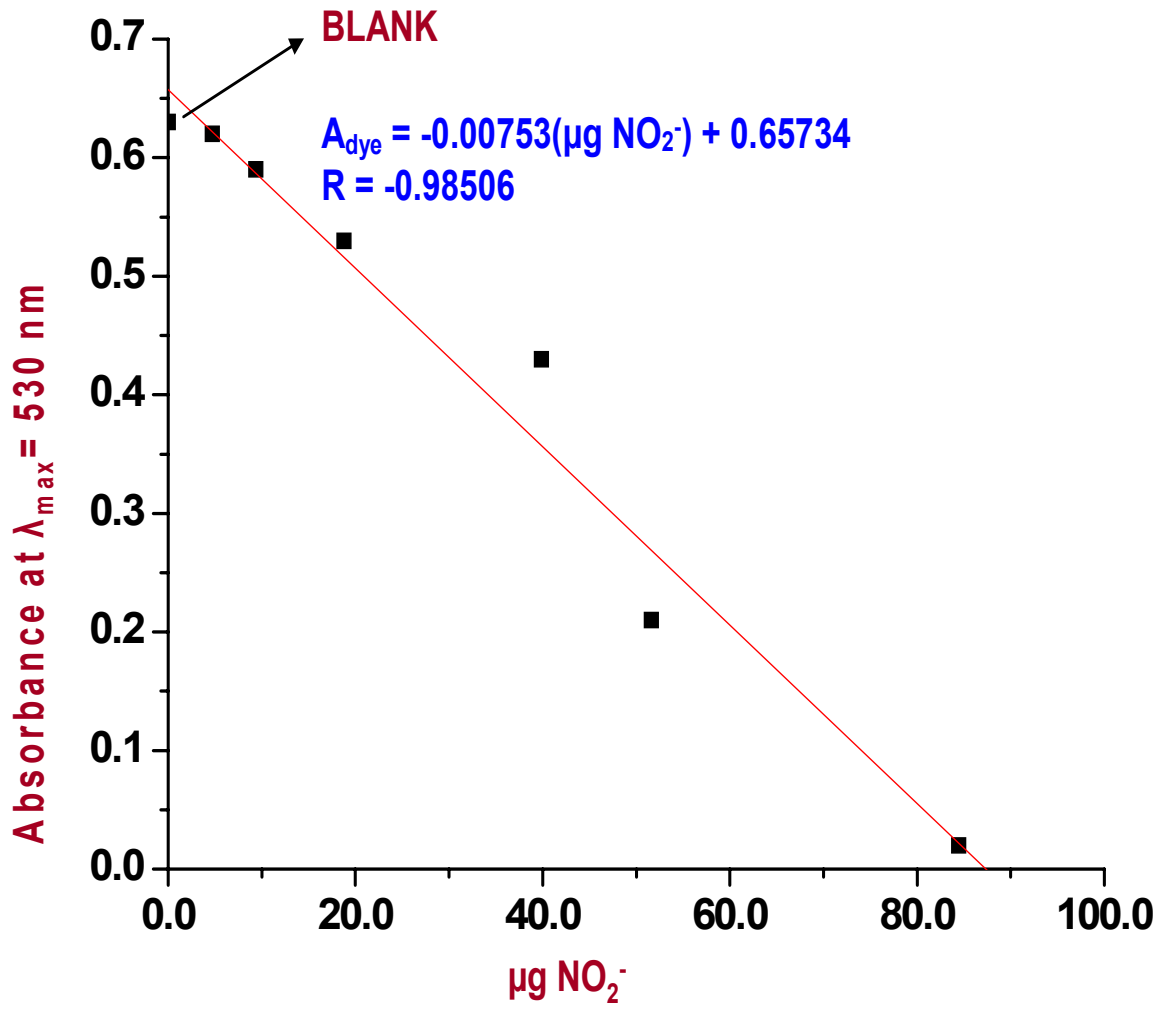

Figure 2-9. NO_2^- calibration curve.

Table 2-1. Colorimetric analysis of NO_2 fragments after photofragmentation of some nitro-based explosives.

Explosive sample	Actual NO_2 ablated(µmol)[a]	NO_2 detected (µmol)[b]	% NO_2 detected
4 nitrotoluene	1.04±0.22	0.140±0.008	13.5±1.4
2,4 nitrotoluene	1.24±0.05	0.190±0.011	15.3±3.8
trinitrotoluene	0.78±0.06	0.150±0.008	19.2±5.8
PETN	7.96±0.10	1.000±0.056	12.6±0.7
RDX	2.46±0.22	1.69±0.096	68.7±7.3

[a] based on the ablated mass of the explosive sample obtained by weighing the sample before and after photofragmentation using microbalance
[b] amount of NO_2 detected using colorimetric method

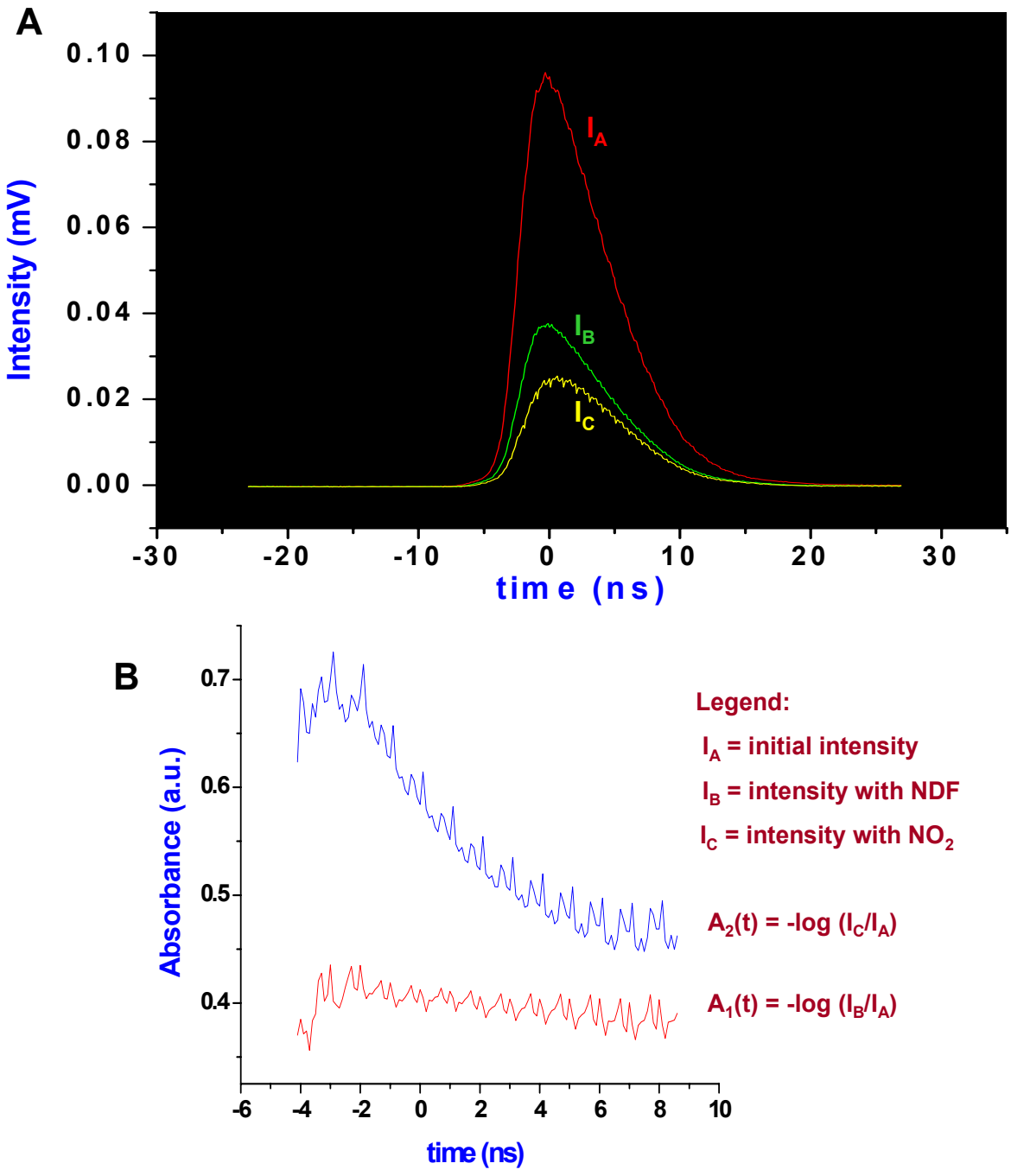

Figure 2-10. Results obtained with fast time resolved experiments. A) profile of ArF laser pulse before and after NO_2 photofragmentation B) time resolved absorbance plots for NO_2 photofragmentation.

CHAPTER 3
NO_2 DETECTION BY CHEMILUMINESCENCE

Introduction

Highly sensitive detection of nitrogen dioxide gas (NO_2) is essential not only for air monitoring purposes, but also for developing explosive detection. Common explosives can be detected based on their characteristic functional group, specifically the NO_2 moieties that can be photofragmented from the parent molecule using a UV laser. This chapter begins with a discussion of the theory of chemiluminescence, followed by a review of previous NO_2 detection systems, and finally, an evaluation and assessment of a newly developed instrument based on luminol chemiluminescenece (CL) for the analysis of NO_2 fragments from explosives.

Basic Theory of Chemiluminescence

Chemiluminescence (CL) is defined as the production of electromagnetic radiation (UV, Vis, or IR) as a result of a chemical reaction.[62] A significant fraction of reaction intermediates or products are produced in excited electronic states and emit light on returning to the ground state. The following reactions are three common sequences used to produce CL:

$$A + B \rightarrow I + I^*; \quad I^* \rightarrow I + h\nu \rightarrow P \qquad (3\text{-}1)$$

$$A + B \rightarrow P + P^*; \quad P^* \rightarrow P + h\nu \qquad (3\text{-}2)$$

$$I^* \text{ (or } P^*) + F \rightarrow I \text{ (or P)} + F \rightarrow F + h\nu \qquad (3\text{-}3)$$

where A, B are reactants, I is an intermediate, P is the product, and F is a fluorescence acceptor. Reactions 1 and 2 illustrate that the luminescing species can be an intermediate or a product in a reaction. Reaction 3 represents sensitized CL in which the excited species produced transfers its energy to an efficient fluorophore acceptor which then fluoresces.[63]

The CL quantum efficiency ($Ø_{CL}$) is defined as:

$$(Ø_{CL}) = (\text{number of photons emitted/number of photons reacted}) \qquad (3\text{-}4)$$

It can be represented as the product of two efficiencies or

$$(\Phi_{CL}) = \Phi_{ex}\, \Phi_{L} \qquad (3\text{-}5)$$

where Φ_{ex} is the efficiency of the production of excited species (the fraction of reacting molecules that produces an excited molecule) and Φ_{L} is the luminescence efficiency (or the fluorescence quantum efficiency) of the luminescing species.[63]

For CL to occur, three general conditions must be met. First, there must be sufficient energy to produce an excited state. Thus, the reaction must be exothermic such that

$$-\Delta G > (hc/\lambda_{ex}) \geq (2.86 \times 10^{4}) / \lambda_{ex} \qquad (3\text{-}6)$$

where ΔG is the free energy change (kcal mol^{-1}) of the reaction and λ_{ex} is the upper wavelength limit in nm for excitation of the luminescing species. For CL emission in the visible region, $-\Delta G$ must be 40 to 70 kcal mol^{-1}.[62] Second, there must be a favorable pathway to produce the excited state. Third, photon emission must be a favorable deactivation process for the excited product in relation to other competitive non-radiative process.[62]

CL has the potential for being the basis of chemical analysis. Chemiluminescence detection is based on measuring the emission of photons from the excited molecules. Often, it is possible to arrange reaction conditions such that the luminescence signal is related to the analyte concentration.

The analytical performance of CL techniques is governed primarily by the chemistry of the reaction utilized and the luminescence characteristics of the emitting species. Careful control of the reaction conditions is mandatory. By chemical parameter optimization, the analytical advantages of CL including high sensitivity, low detection limits, and wide linear ranges can be maximized and achieved with very simple equipment. These attributes also result from the fact that no light source is required, significantly eliminating the background noise from the source.

CL is up to 100 000 times more sensitive than absorption spectroscopy and at often 1000 times more sensitive than fluorometry.[64]

One attractive feature of CL technique is the simplicity of the instrumentation. All that is required is a reaction cell, a detector, and a signal processor-readout system. The emitted light intensity is measured by means of a photomultiplier (PMT). Because only one emitter is normally present in the reaction medium, no monochromator is required to discriminate among different wavelengths.

There are two ways of measuring CL, namely: (1) static mode and (2) continuous flowing stream mode.[63] In the static mode, (also known as batch or discrete sampling), the CL reagents and the analyte are mixed rapidly and the CL intensity versus time profile is measured (Figure 3-1). The initial increase in intensity is due to the finite time for mixing of reagents or an induction period in the reaction. The decay of the signal is caused by the consumption of the reagents and changes in the CL quantum efficiency with time. The analytical signal can be taken as the peak signal or the signal after some fixed delay time from the point of mixing, (the integral of the signal over some period) or the signal (area) of the entire peak.

In the continuous flow mode, the CL reagents and the analyte are continually pumped and combined at tees and sent to a flow cell or mixed and observed in an integral reactor flow cell as shown in Figure 3-2. When the cell is totally filled with the reaction mixture, a maximum CL signal is obtained. Then, the system will equilibrate reaching a steady state signal. The signal represents the output integrated over the residence time of the reaction mixture in the cell.

Luminol-NO_2 Chemiluminescence

While there are many chemical reactions that are chemiluminescent, the oxidation of luminol ($C_8H_7N_3O_2$, which is also known as 5-amino-2,3-dihydro-1,4-phthalazinedione) is one of the most commonly known. Luminol was first synthesized in 1893, and its ability to yield a

chemiluminescent reaction in basic solution in the presence of an oxidant such as hydrogen peroxide was first reported in 1928 by H.O. Albrecht.[65]

The luminol CL system consists of water, base (sodium or potassium hydroxide), oxidant, catalyst, and luminol. A variety of oxidants including permanganate, hypochlorite, hydrogen peroxide, and nitrogen dioxide have been used in the luminol reaction. Typical catalysts include peroxidase, hemin, and transition metal ions (Co^{2+}, Cu^{2+}, Fe^{3+} etc.).[66]

The CL reaction used for NO_2 detection is based on the same principle. NO_2 is detected by an increase in CL intensity that results when NO_2 reacts with an alkaline solution of luminol. The CL reaction is as follows:

$$2C_8H_7N_3O_2 + 4OH^- + 2NO_2 \rightarrow 2C_8H_5O_4 + 3N_{2(g)} + 4H_2O + h\nu \qquad (3\text{-}7)$$

The CL spectrum has maximum emission intensity at 425 nm with an approximately 100 nm bandwidth.[67] Despite intensive studies, the mechanism of luminol oxidation in water has not been fully elucidated. However, the general outline of the reaction has been agreed upon and is shown in Figure 3-3. Base oxidizes the luminol leaving negative charges on nitrogen atoms which move onto the carbonyl oxygen to form what is known as enolate anion. The oxidizing agent next performs a cyclic addition to the two carbonyl carbons which leads to formation of 3-aminophthalate (3-APA*).[68] White et al. have shown that the CL spectrum of luminol matches the fluorescence spectrum of the 3-aminophthalate anion and, hence, identifying it as the emitting species.[69] Since then, several other investigators have confirmed the identity of the emitter. [70-72]

Review of CL Methods for NO_2 detection

The detection of nitrogen dioxide gas (NO_2) by means of chemiluminescent reaction with luminol in aqueous solution has been the subject of considerable interest and development .The first prototype detector employing this approach was developed in 1980's by Maeda et al.[73] by

directly reacting the $NO_{2(g)}$ at the surface of continuously flowing luminol solution. The intensity of luminescent radiation emitted by the reaction was monitored by photomultiplier (PMT) detector. This system was very sensitive to movements of the compartment and had relatively slow time response. An alternate design for chemiluminescent detection of $NO_{2(g)}$ was subsequently presented by Wendel et al.[66;74], who allowed a stream of $NO_{2(g)}$ to pass over filter paper drenched with basic luminol solution. The CL reaction occurs on the surface of the filter paper which is adjacent to the PMT window. A fabric wick has also been used instead of filter paper to make a compact commercial NO_2 detector (Luminox LMA-3, by Scintrex/Unisearch Associates Inc.); a detailed description of this instrument was given by Schiff et al.[75] and Kelly et al.[76] A further variation on the luminol chemiluminescent detector for $NO_{2(g)}$ was introduced by Mikuska and Vecera;[77] this configuration employed a continuous spray of luminol solution, immediately below the PMT. CL was generated from the stream of analyzed gas. Another detection scheme modification was made by Collins and Pehrsson[78] wherein $NO_{2(g)}$ reacted on the surface of a glass containing immobilized luminol molecules within a hydrogel or polymeric thin film positioned in front of a PMT tube. Yet another variation was developed by Robinson et al.[79] where a bundle of porous polypropylene hollow fiber membranes was used to bring the $NO_{2(g)}$ into contact with luminol solution. Chemiluminescence occurring within the translucent hollow fibers was detected using a miniature PMT tube.

The present work was adapted from the chemiluminescent aerosol detector of Mikuska and Vecera[77] for its simplicity, efficiency and high sensitivity. The aim of this work is to evaluate, assess and further improve the analytical capability of detection of $NO_{2(g)}$ with the luminol reaction.

Experimental Section

Reagents and Chemicals

Luminol powder of 98% purity (5-amino-2,3-dihydro-1,4-phthalazinedione) was obtained from Acros Organics (New Jersey, USA) and used without further purification. Potassium hydroxide, methanol, ethanol, tert-butanol, hydrogen peroxide, sodium bicarbonate, and sodium carbonate were all obtained from Fischer Science Company (Pittsburg, PA). Para-iodophenol was obtained from Sigma Aldrich Chemical Company (St. Louis, MO). Deionized water was obtained by passing distilled water through a Millipore Milli-Q deionizing system

All gases purchased were of the highest purity. A tank of 99% nitrogen gas was purchased from BOC Gases Inc. (Murray Hill, NJ). Nitrogen dioxide gas buffered with nitrogen gas was purchased from Safety Products Inc. (Lakeland, FL).

Apparatus and Methodology

Luminol-CL detector. Figure 3-4 is the instrumental set-up used for measuring and optimizing the chemiluminescence signal arising from the basic luminol solution and nitrogen dioxide gas. The three main sections are a gas delivery system, reaction chamber and measuring electronics. The gas delivery system consisted of the gas samples and mass flow controllers (Alicat Instrument Inc.,Tuczon.AZ) used for dilution. The chemiluminescence reaction set-up was adapted from the NO_2 atmospheric monitoring system developed by Mikuska and Vecera.[77] A stream of NO_2 gas passed through a concentric nebulizer (Type C-Q nebulizer manufactured by Precision Glass Blowing, Centennial, Colorado) allowing the basic luminol solution to be aspirated into the reaction chamber and dispersed to form a fine mist with a large interface area for NO_2 and luminol reaction. The aerosolized luminol solution is directed toward the bottom wall of the reaction cell with PMT orthogonal to the direction of the mist's propagation. The reaction was done in a batch mode which last for twenty seconds. The luminescent radiation

resulting from the reaction between the luminol alkaline solution aerosol and NO_2 gas is detected by a cooled R3896 photomultiplier tube (PMT).The PMT has a spectral response range from 185 to 900 nm with maximum sensitivity at 450 nm. The PMT is operated at -850 V and a temperature of 10 to 15^oC. The photocurrent signal from the PMT is amplified by Kiethley Model 6514 electrometer which is connected to a computer by a GPIB-USB-HS digital-analog converter from the National Instrument Laboratory. EXCELINK software is used to control all the data acquisition. All data are then processed using Origin 6.1 and Excel software.

The reaction cell is made of a Teflon tube with an inner diameter of 2.10 cm and a length of 4.57 cm. It is encased in an aluminum housing to completely seal the reaction from external light sources. One end of the reaction cell is open to the PMT tube, separated only by a fused silica window with the diameter of a 1.50 cm.

The concentric nebulizer is connected to the side of the reaction cell and oriented parallel with respect to the PMT detector.

CL emission spectrum set-up. A Fluorolog-Tau-3 spectrofluorometer (Jovin Yuon Inc., Edison, NJ) in chemiluminescence mode (excitation source turned off) is used to obtain the emission spectra. A block diagram of the instrument is depicted in Figure 3-5. In the first set-up, a 25 ppm NO_2 standard gas was purged into the quartz cell containing 0.01 M luminol in 1 M KOH. In the second set-up, a peristaltic pump (Rainin, Model Rabbit) was set at desired flow rate to deliver H_2O_2 solution into the quartz cell containing luminol solution.

Gas-liquid exchange module set-up. A diagram of the gas liquid exchange module is shown in Figure 3-6A. This device was provided by Dr. John W. Birks from University of Colorado. The device is made up of microporous membrane allowing the NO_2 gas to react with alkaline luminol-H_2O_2 solution. The membrane consists of a bundle of approximately fifty

polypropylene capillary fibers having an outer diameter of 380 μm, a wall thickness of 50 μm, and a pore size of 0.2 μm (Akzo Nobel, Scottsboro, AL). The fibers are encased in a polymer housing and the entire unit will be referred as the gas-liquid exchange module. The actual picture of the set-up is shown in Figure 3-6B.

The luminol solution flows through the interior of the fibers, while the NO_2 gas flows around the exterior of the fibers. The aqueous solution remains in the interior of the fibers due to the hydrophobic nature of the polypropylene. Gases diffuse through the pores of the membrane and into solution, resulting in the chemiluminescent reaction. NO_2 was detected above the background signal due to the reaction of H_2O_2 and luminol. The fibers and the polymer are translucent, allowing the transmitted light to be detected by a PMT.

Luminol/H_2O_2-CL detector. Figure 3-7 is a schematic diagram for a luminol/H_2O_2-CL detector. The gas-liquid exchange module is used as the CL reaction cell, and a miniature head-on R647 photomultiplier tube (PMT) tube is used to detect the light emitted. The PMT has a spectral response range from 300 to 650 nm with a maximum sensitivity at 420 nm. The PMT is operated at -850 V at ambient temperature. The photocurrent signal from the PMT is amplified by a Kiethley Model 6514 electrometer which is connected to a computer by GPIB-USB-HS digital-analog converter from National Instruments. EXCELINK software is used to control all the data acquisition. All data are then processed using Origin 6.1 and Excel software.

A series of peristaltic pumps is used to pump the luminol and H_2O_2 solutions into the gas-liquid exchange module. The two solutions are mixed in a tee just prior to the exchange module. The flow rate was set at 1.0 L/min for each solution. The gas outlet is connected to the exhaust fume hood.

Dilution set-up. NO_2 standards in ppb range were prepared by dynamic dilution of 5 to 25 ppm standard NO_2/N_2 mixtures. Pure N_2 gas was used as the diluent. A block diagram of the set-up is shown in Figure 3-8. Gas flow rates were controlled by mass flow controllers. An in-line gas mixer filled with 4 mm glass beads housed in a polystyrene casing was used to ensure efficient gas mixing. Mass flow controllers were calibrated electronically using a Humonics Optiflow 650 Digital flow meter and manually using a GC bubble flow meter.

Results and Discussion

In order to have a highly sensitive method for NO_2 determination based on its chemiluminescence reaction with luminol, both the physical and chemical parameters of the system were optimized. Physical parameters are related to overall design of the reaction cell/detector configuration, whereas chemical parameters are affected by the preparation of the chemical components of the basic luminol solution.

Chemical Parameters

The optimal solution composition for NO_2 detection was determined by systematically varying the concentration of potassium hydroxide (KOH) and chemiluminescent enhancer reagents such as p-iodophenol, methanol, ethanol and t-butanol. The effect of the concentration of these reagents on chemiluminescence intensity was studied by varying the concentration of one component over a range while holding the other components constant.

The effect of KOH concentration on the emission intensity is shown in Figure 3-9A. As the concentration of KOH increased, the decay rate of the reaction becomes faster, which consequently decreased the integrated chemiluminescence signal. By obtaining the integral or area of the entire peak for each corresponding signal from Figure 3-9A and plotting it against the pOH, the optimum KOH concentration of 0.2 M can be inferred which corresponds to

pH=13.1 as seen from Figure 3-9B. The result is consistent with previous studies [75; 77] verifying that excess OH^- quenches the chemiluminescence radiation.

Maeda et al.[73] obtained a maximum CL signal for luminol concentrations of 3 x 10^{-4} M to 3 x 10^{-3} M with no variation within that range. Mikuska and Vecera[77] as well as Wendel [74] agreed with this observation. Kok et al.[80] obtained peak chemiluminescence intensity at 2.4 x 10^{-4} M luminol and a 50% decrease for an order of magnitude change about this value. The result of our experiment is presented in Figure 3-10 where a peak occurs for 5 x 10^{-3} M luminol which is in agreement with previous results [73;77].

Based on the experimental results acquired by Wendel et al., the addition of water soluble alcohols such as methanol, ethanol or t-butanol to the alkaline luminol solution resulted in a two-fold increase in the chemiluminescence signal with $NO_{2(g)}$. Based on our results, addition of alcohols had negligible effect on the reaction, as can be seen in Figure 3-11.

Thorpe and et al. [81] used phenol derivatives such as p-iodophenol and p-phenyl phenol to enhance light emission for the reaction between hydrogen peroxide (H_2O_2) and luminol. They were able to observe that the light emitted in the reaction decayed slowly and its intensity was about 1000 fold greater than the unenhanced reaction. Addition of p-iodophenol to the basic luminol solution was investigated and it was found out that the presence of 0.01 M p-iodophenol significantly enhanced the integrated chemiluminescence signal up to 10 times, as shown in Figure 3-12.

The mechanism of the p-iodophenol enhancement of chemiluminescence signal is still unresolved. Here, it was shown that the emission spectra of phenol-enhanced and unenhanced reactions are remarkably similar (Figure 3-13), suggesting two plausible hypotheses that (1) p-iodophenol as a chemiluminescent enhancer reagent is neither a more efficient emitter nor

fluorescent acceptor, but exerts its action earlier in the complex reaction between luminol and the oxidant and (2) p-iodophenol enhanced the chemiluminescence signal of aerosolized luminol-$NO_{2(g)}$ system by significantly decreasing the dielectric constant of the aerosolized luminol solution, which enhances the desolvation of luminol enolate anions on the surface of the aerosol and thus, increasing the frequency of interaction of the reagents involved. This is supported by the fact that the signal enhancement using p-iodophenol can only be observed with the chemiluminescence aerosol detector and not by simply bubbling the NO_2(g) into the bulk of the basic luminol solution as seen on Figure 3-13B and 3-13C,respectively.

Physical Parameters

Gas and liquid flow rates. The gas flow rate was varied with a mass flow controller and it was noted that above 0.7 SLPM (~24 psi), the chemiluminescence signal saturates (Figure 3-14). The luminol uptake at this gas flow is 1.10 mL/min. Since the response was independent of gas flow rate, the instrument is a concentration detector rather than a mass detector. A flow rate of 0.7 SLPM was used for further studies.

Cell design. The change in chemiluminescence intensity as a function of the orientation of the concentric nebulizer with respect to the detection window was investigated. It was observed that if the NO_2-luminol mist entered parallel to the PMT window, a signal enhancement of about 8 fold occurred compared to introduction of the NO_2-luminol mist perpendicular to the detection window (Figure 3-15).

Two different sets of reaction cell were used for this experiment. The set-up described under the methodology section was used for the experiment where the orientation NO_2-luminol mist was parallel with respect to the PMT window which will be referred as Set-up A. For the set-up where the NO_2-luminol mist was oriented orthogonal to the PMT window, a completely different reaction cell of the same design and configuration as Set-up A was used except that the distance

between the nebulizer and the detection window was approximately four times farther than Set-up A and a stream of N_2 gas was allowed to blow continuously on the PMT window as the reaction was in progress. In this way, it could be argued that the significant difference in the signal was due to impaction of aerosolized solution on the surface of the PMT window.

Shelf life of the alkaline luminol solution. It was observed from previous studies [74; 80] that luminol-NO_2 chemiluminescence intensity increased with the age of the luminol solution. Hence, a controlled study of the chemiluminescence intensity as a function of time from the preparation of the solution was made. An optimized luminol solution was prepared (5×10^{-3} M luminol, 0.01 M p-iodophenol in 0.2 M KOH) and the chemiluminescence reaction from a 5 ppm standard source of NO_2 was measured. This measurement was done as soon as the solution was made and repeated periodically for at least 2 months. According to Wendel et al.[74], the chemiluminescence intensity increased by as much as 20-fold over the course of days, and after this initial "aging" period, it was found out that the signal did not change appreciably over longer storage period. However, our results (Figure 3-16) did not observe this trend. Instead, it was observed that the basic luminol solution gave a slight change in chemiluminescence readings from day 0 up to day 71.

Performance of Luminol-CL Detector

All the optimized parameters obtained were then applied to construct the calibration curve for NO_2 (Figure 3-17). A calibration working curve was generated by making three replicate measurements of the NO_2 standards. The linear range of the detector was measured using known concentrations of NO_2 from 33 ppbv to 25 ppmv. The calculated detection limit with a signal to noise ratio of 3 was 19 ppt NO_2. A calibration sensitivity of 7.08×10^{-8} C/ppb NO_2 was obtained. The non-zero intercept is a reflection of the background of the instrument.

Performance of Luminol/H_2O_2 CL Detector

The luminol/ H_2O_2 CL detector was tested for direct detection of NO_2. NO_2 reacted with H_2O_2 to form a potent oxidizer peroxynitrite ($ONOO^-$) as shown by the following reaction:

$$2NO_2 + H_2O_2 + OH^- \rightarrow 2ONO_2^- + H_2O \quad (3\text{-}8)$$

Peroxynitrite is capable of oxidizing luminol to an excited state of 3-aminophthalate, which relaxes by emitting light as can be seen in reaction 3-9.[82]

$$2ONO_2^- + \text{luminol} \rightarrow \text{3-aminophthalate} + N_2 + h\nu \quad (3\text{-}9)$$

The NO_2 signal resulting from peroxynitrite formation is detected on top of the background signal resulting from the slow oxidation of luminol by H_2O_2. Optimal conditions obtained previously were used to generate the calibration curve for NO_2. The concentrations of H_2O_2 and luminol in a bicarbonate/carbonate buffer (with pH=10.25) were 2 mM and 4 mM, respectively. Responses of the detector to NO_2 standards in the range of 33 ppb to 25 ppm are depicted in Figure 3-18. The working curve was generated by making three replicate measurements of the NO_2 standards. The calculated detection limit and the calibration sensitivity were 178 pptr NO_2 and 2.43 x 10^{-8} C/ppb, respectively.

Luminol CL Detector Compared to Other CL Set-ups

The LOD ratio of luminol CL detector to luminol/H_2O_2 CL detector is 9 which can be attributed to the following reasons: (1) in the first set-up surface interaction between the NO_2 gas and luminol solution was maximized through nebulization (2) the first set-up also had a significantly lower background signal due to the absence of H_2O_2 and the peristaltic pumps (3) the side-on PMT used for the first set-up was more sensitive compared to the head-on PMT used in the second set-up.

In general, the luminol-CL detector gave a better LOD compared to other existing CL set-ups as shown on Table 3-1.

Conclusion

The luminol-CL detector for quantifying NO_2 is based on the NO_2 CL reaction with aerosolized basic luminol solution. The aerosol is formed by continuous nebulization of reagent solutions by the stream of analyzed gas in a sealed reaction chamber. The intensity of the CL signal was detected by a PMT. The current system improved the detection limit obtained previously by others optimization of all the feasible physical and chemical parameters involved in the chemiluminescence reaction between luminol and NO_2. A detection limit of 19 ppt NO_2 at (S/N) = 3 was obtained. The optimal reagent solution from the viewpoint of sensitivity of the response to NO_2 (maximum signal/signal noise ratio) was 5 x 10^{-3} M luminol + 0.01 M p-iodophenol + 0.2 M KOH. A Luminol/H_2O_2 CL set-up was also explored where a bundle of porous polypropylene fibers was used to bring the NO_2 into contact with luminol solution. A LOD of 178 ppt NO_2 at (S/N) = 3 was obtained.

The newly developed CL instrument benefits from superior sensitivity, simplicity, and reliability, which are very attractive in chemical sensor. It is anticipated that the CL detector developed can be used as a diagnostic tool and aid in developing a better explosive detector.

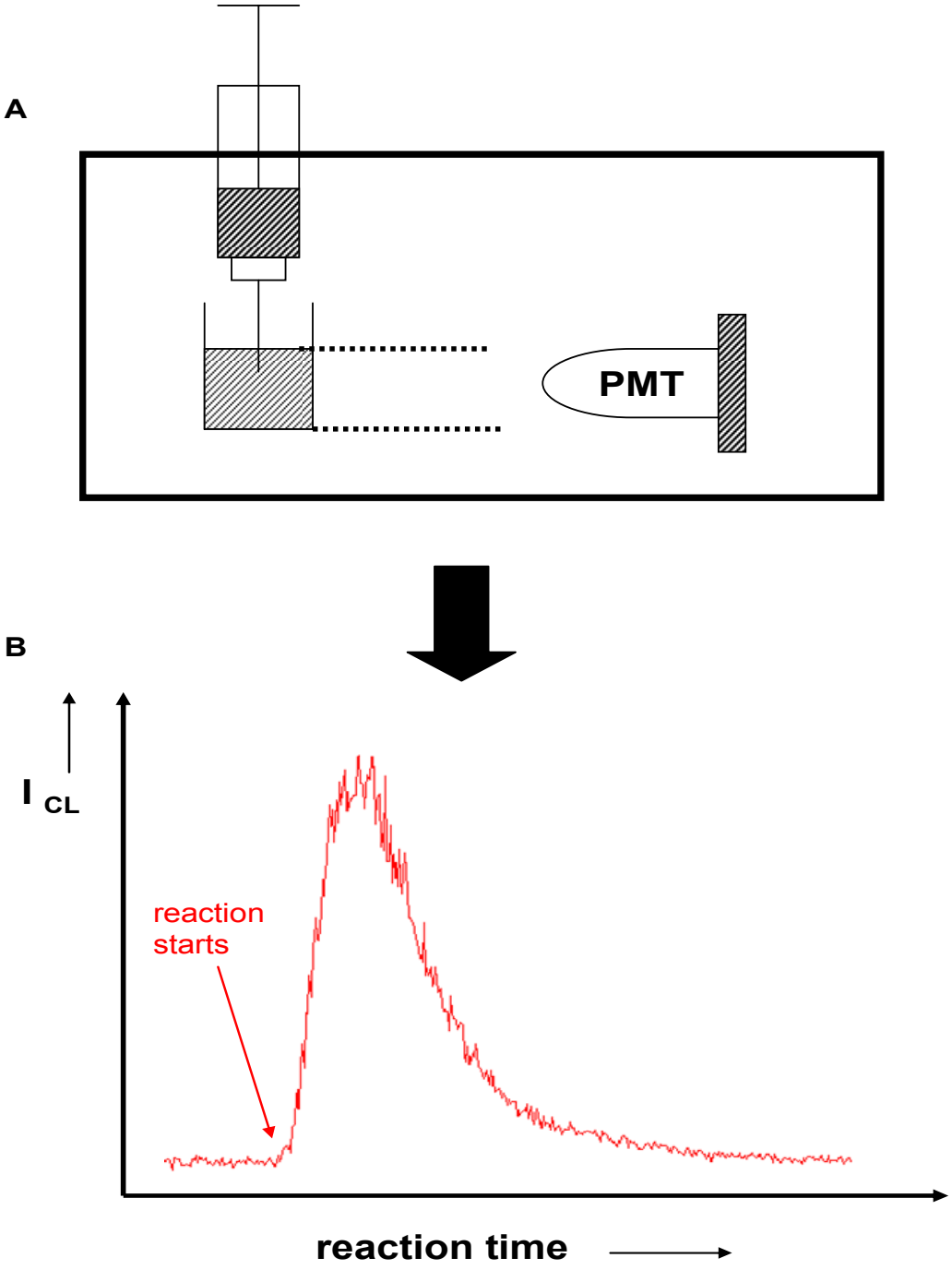

Figure 3-1. Schematic diagram for static CL device. A) the sample and the CL reagent(s) are introduced in the reaction cell and the final reagent is injected to initiate the CL emission, then light is monitored by the PMT detector B) curve showing CL intensity as a function of time after the reagents are mixed to initiate the reaction.

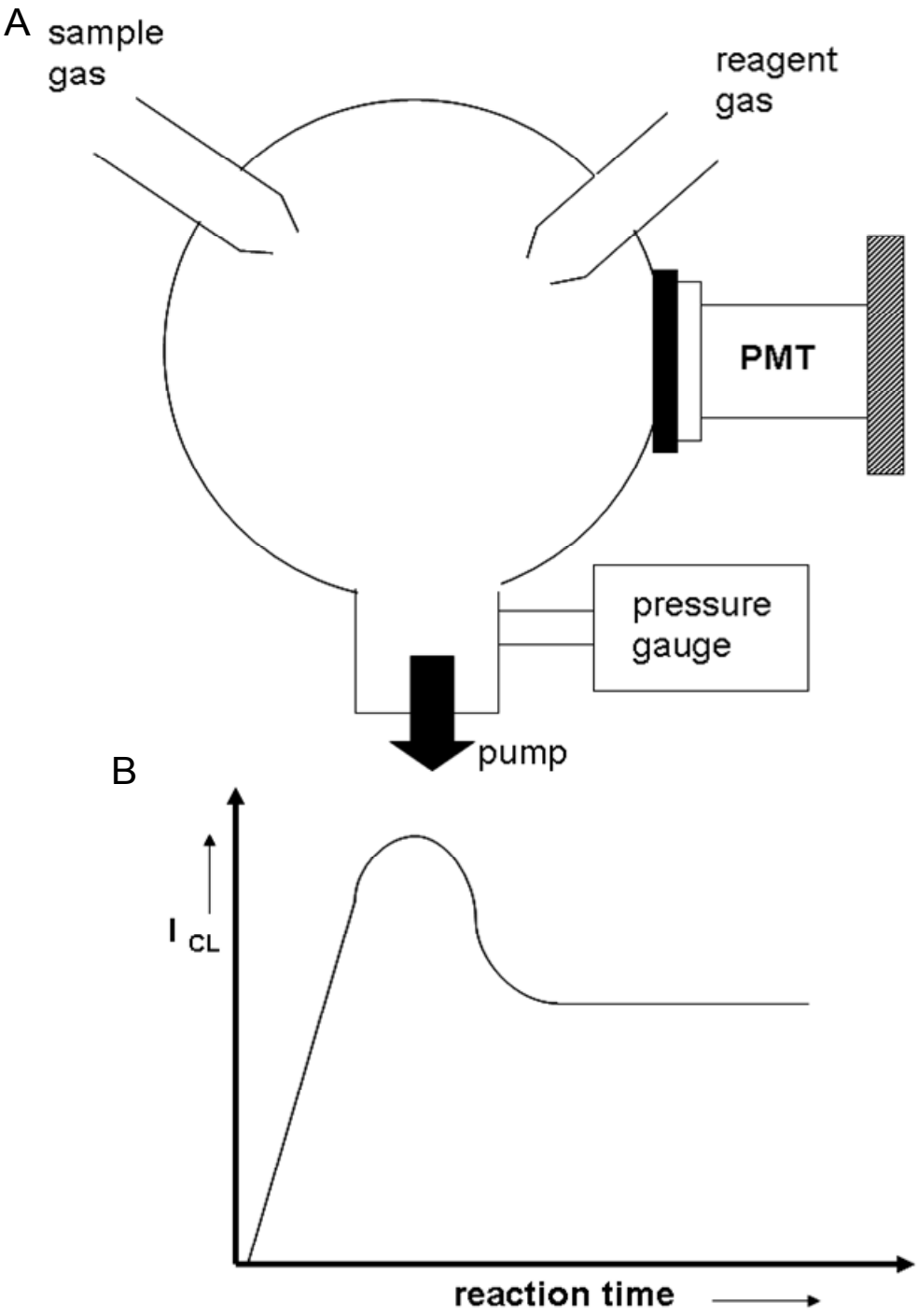

Figure 3-2. Schematic diagram for continuous CL device: A) the sample and the CL reagent(s) are introduced simultaneously and continuously into the flow cell B) a steady state signal is achieved when the cell is totally filled with the reaction mixture.

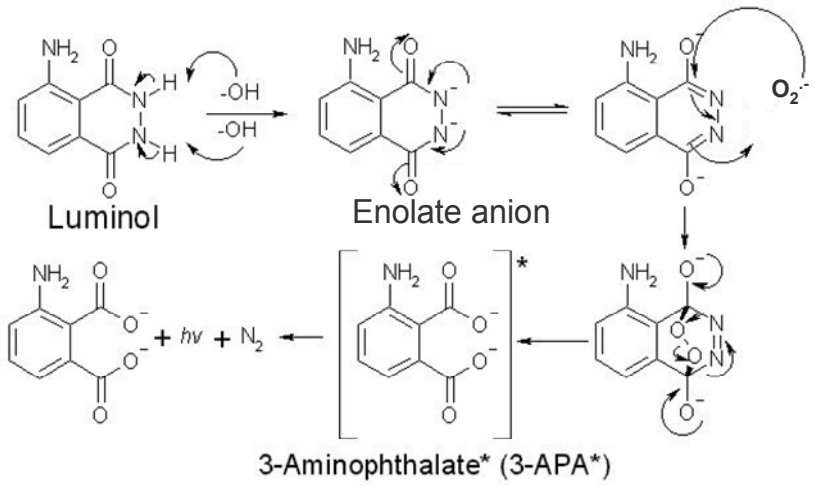

Figure 3-3. Luminol oxidation mechanism.

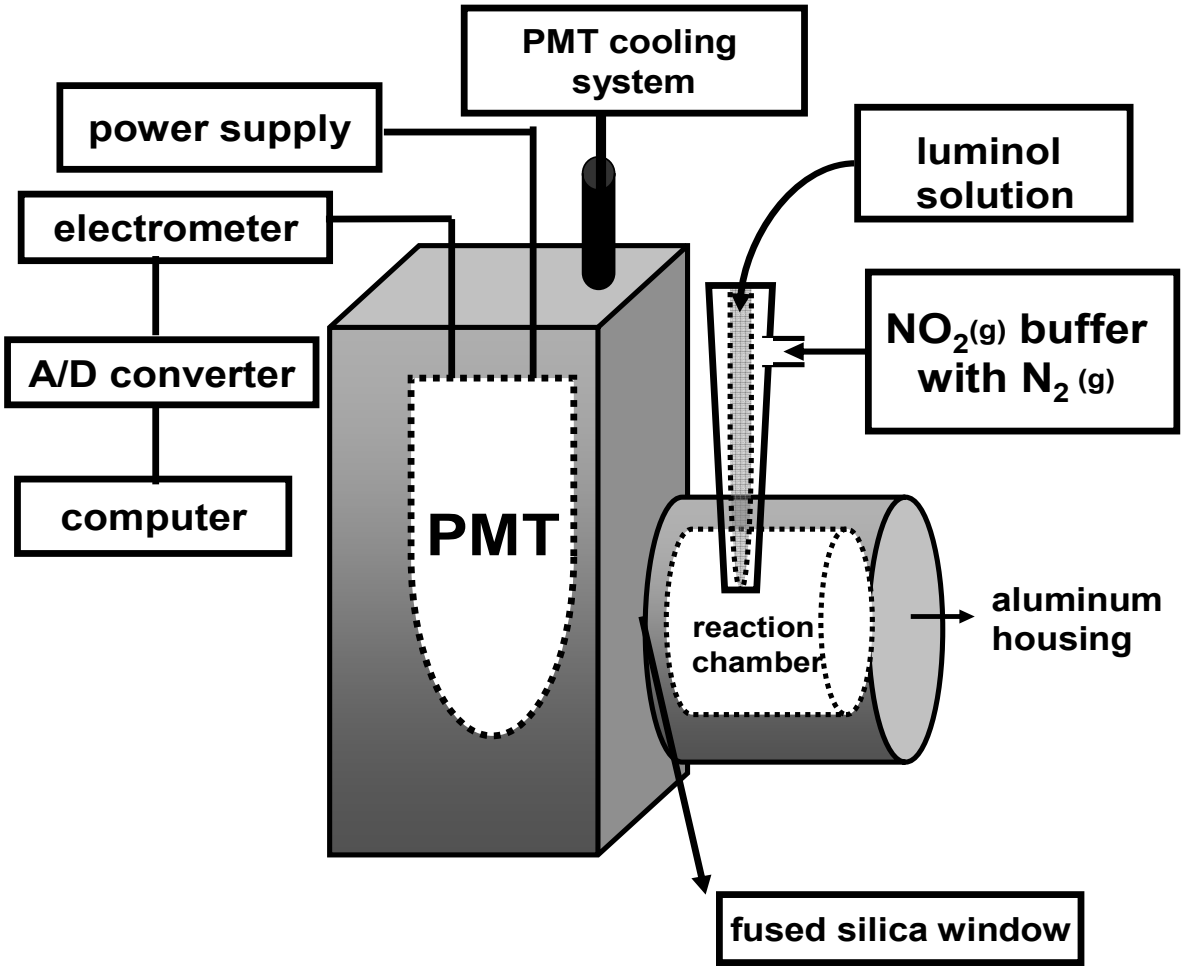

Figure 3-4. Luminol-CL detector set-up.

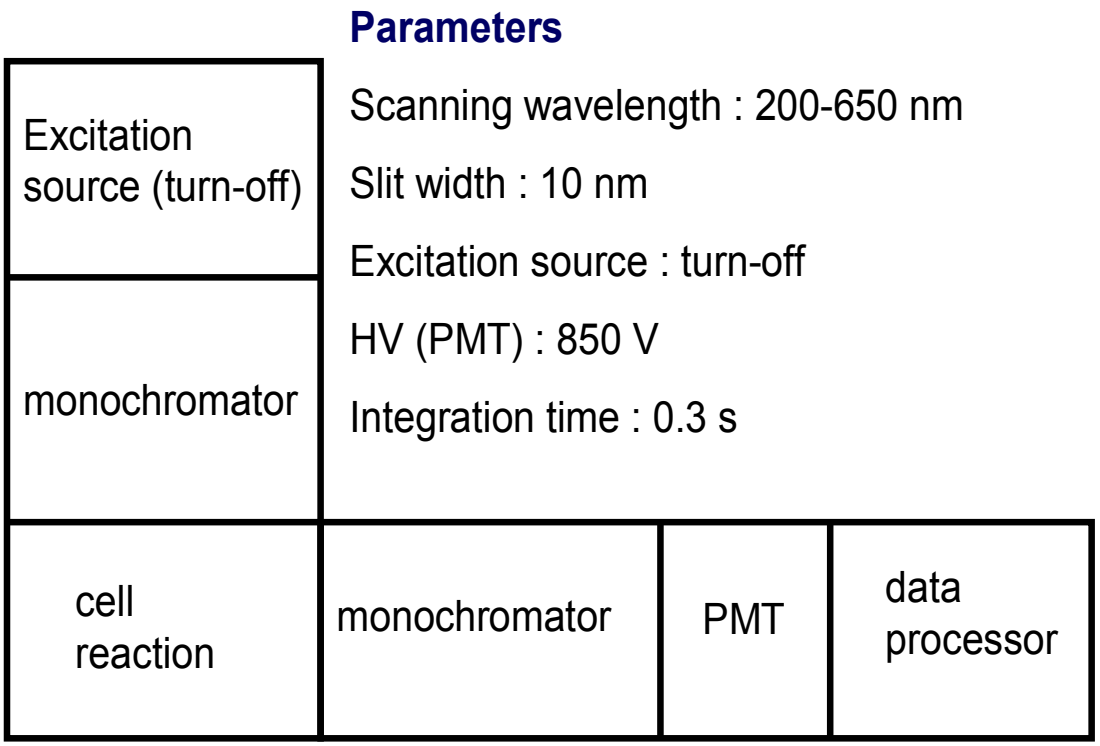

Figure 3-5. Schematic of spectrofluorometer used for acquiring luminol-NO_2 CL emission spectra.

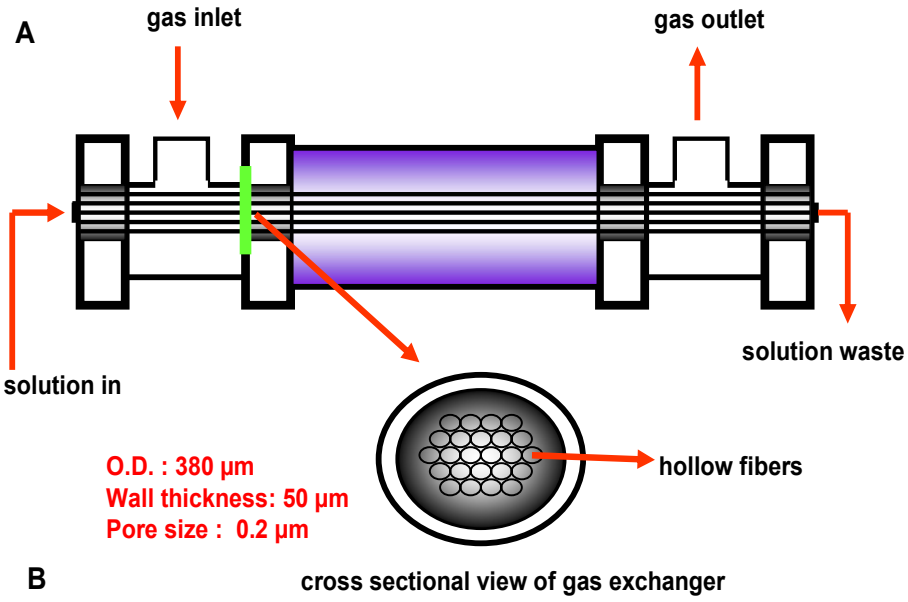

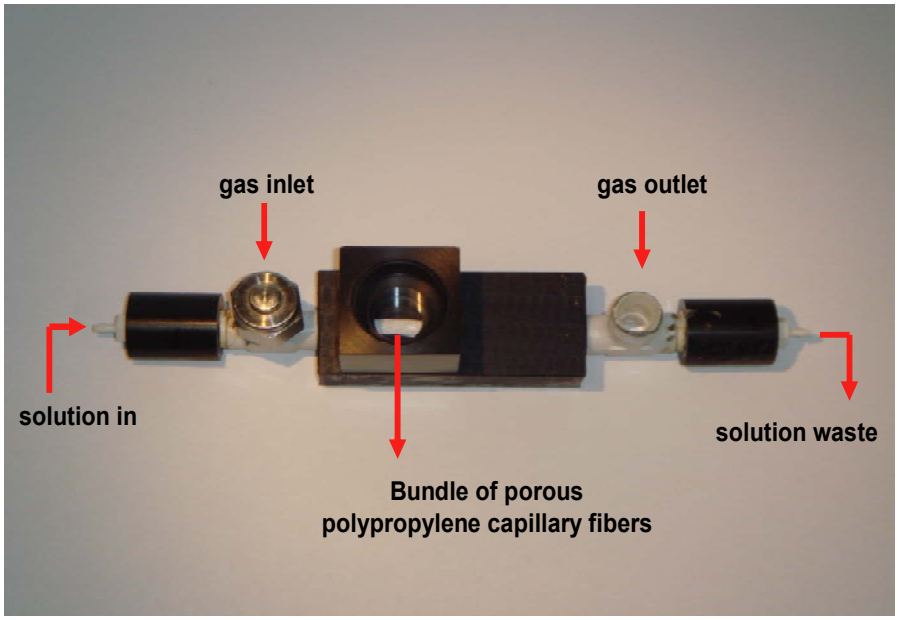

Figure 3-6. Chemiluminescence Set-up II.A) schematic of gas-liquid exchange module set-up B) the actual picture of the set-up.

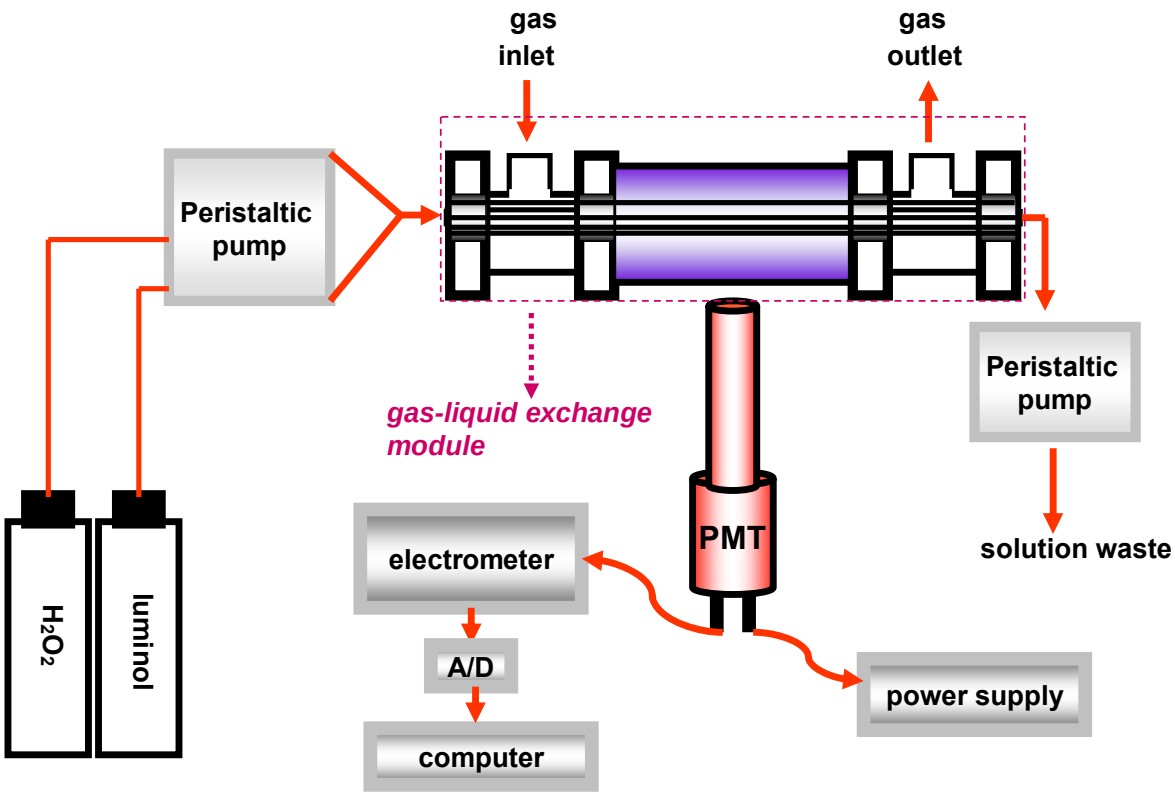

Figure 3-7. Luminol/H_2O_2-CL detector.

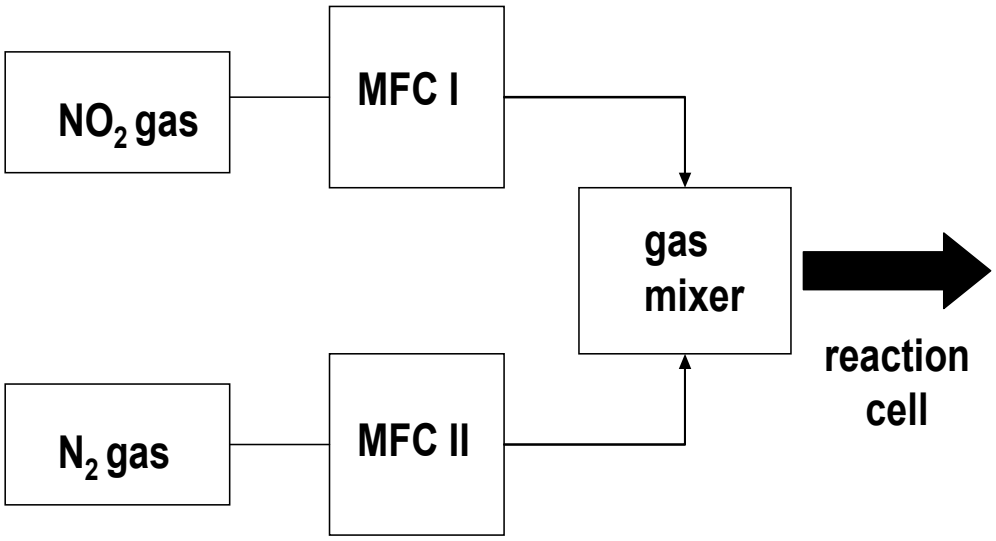

Figure 3-8. Dilution set-up.

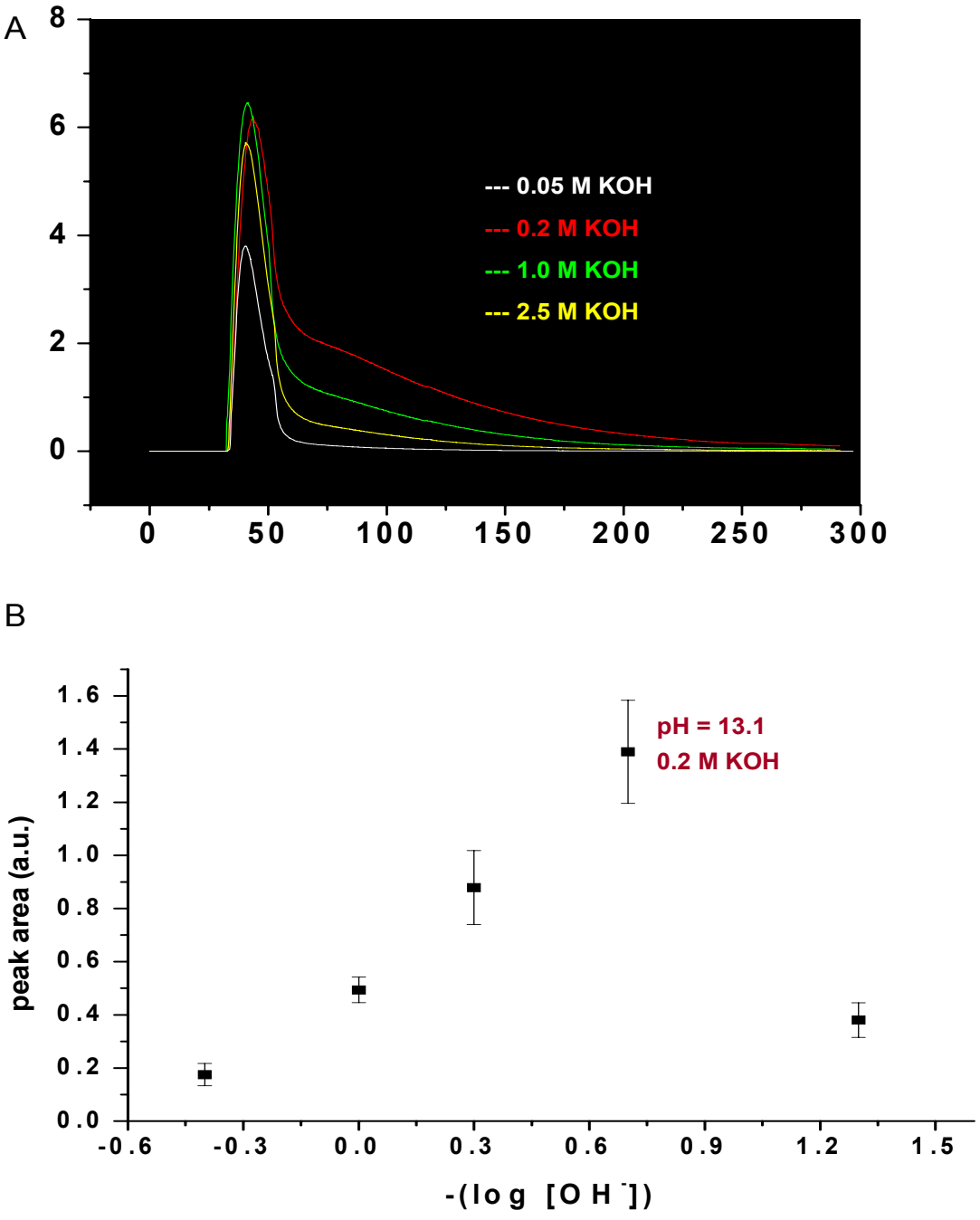

Figure 3-9. Effect of KOH concentration on A) decay rate of luminol-NO_2 reaction and B) on CL signal.

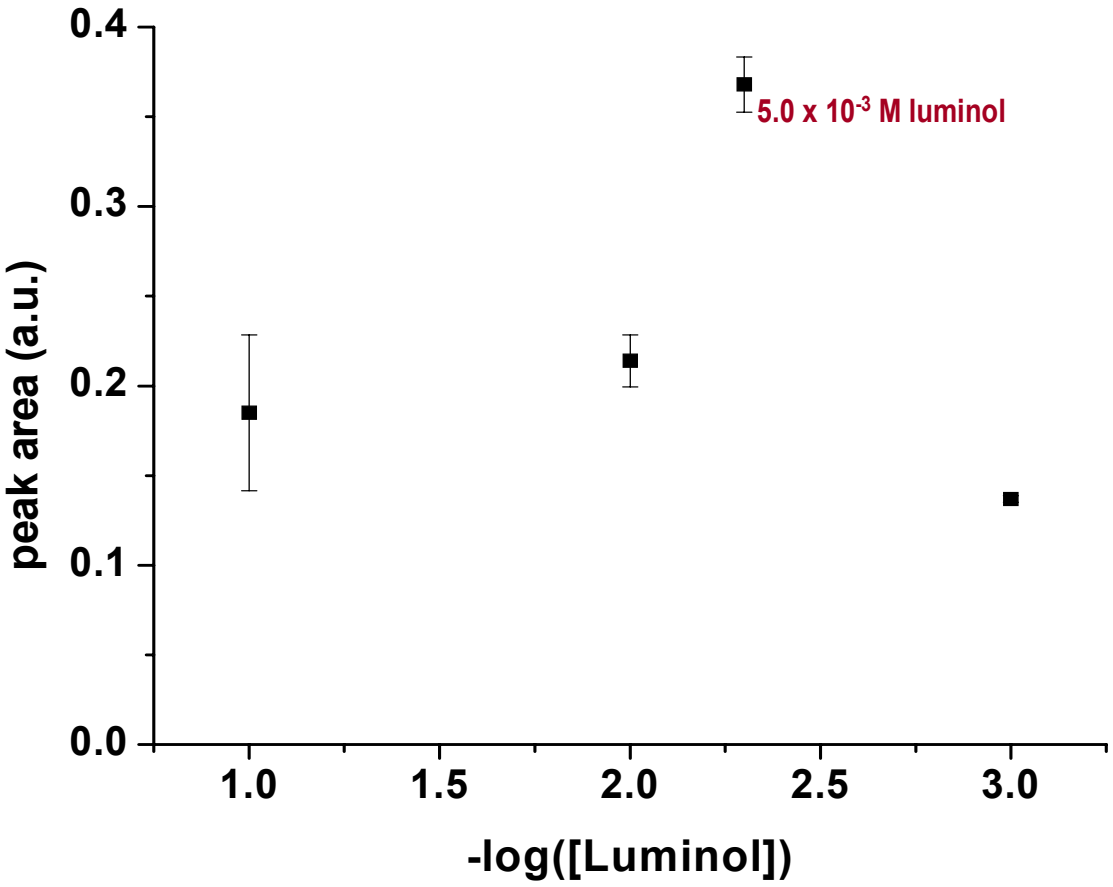

-

Figure 3-10. Effect of luminol concentration on CL signal.

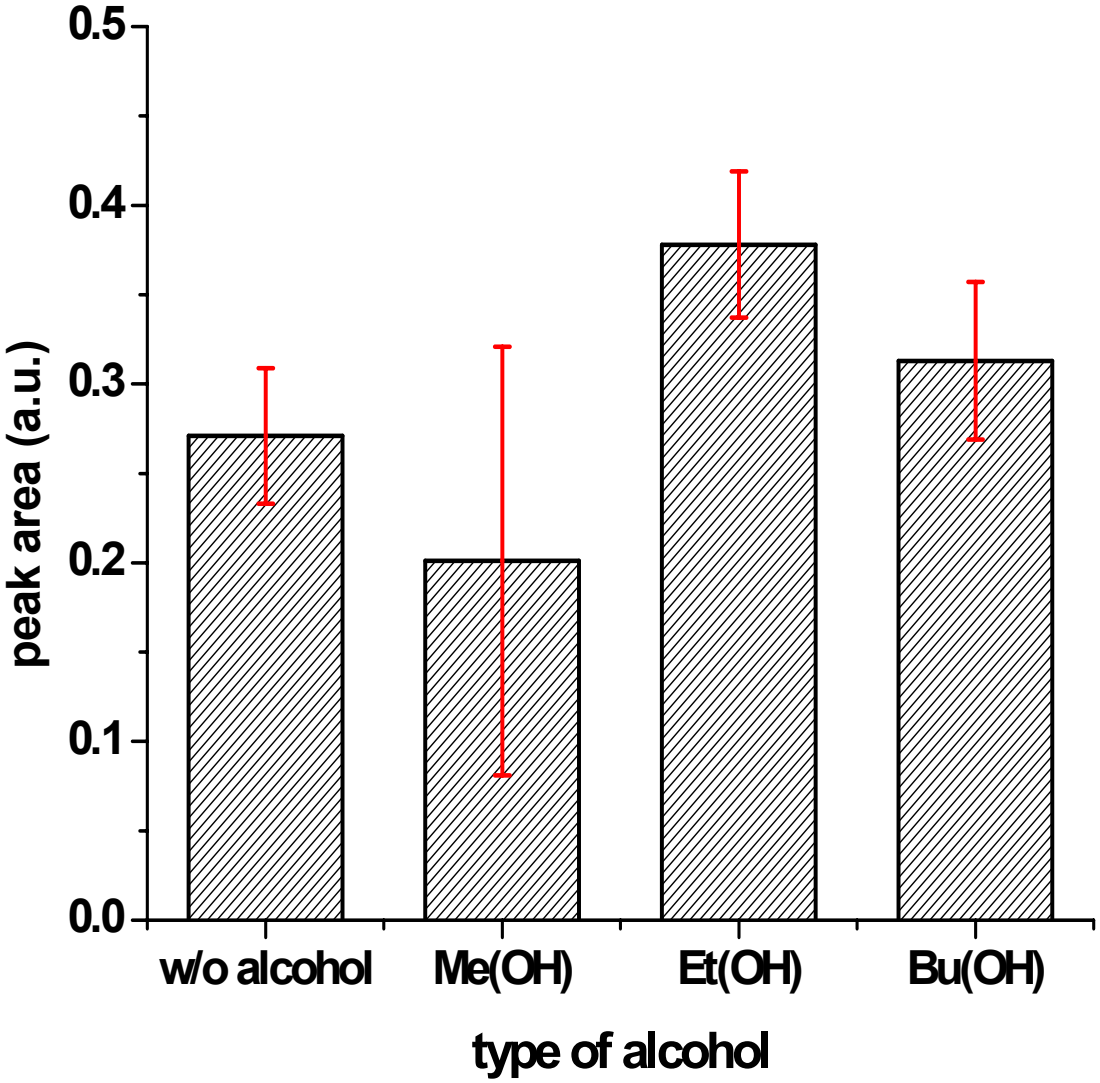

Figure 3-11. Effect of adding various type of alcohols on CL signal.

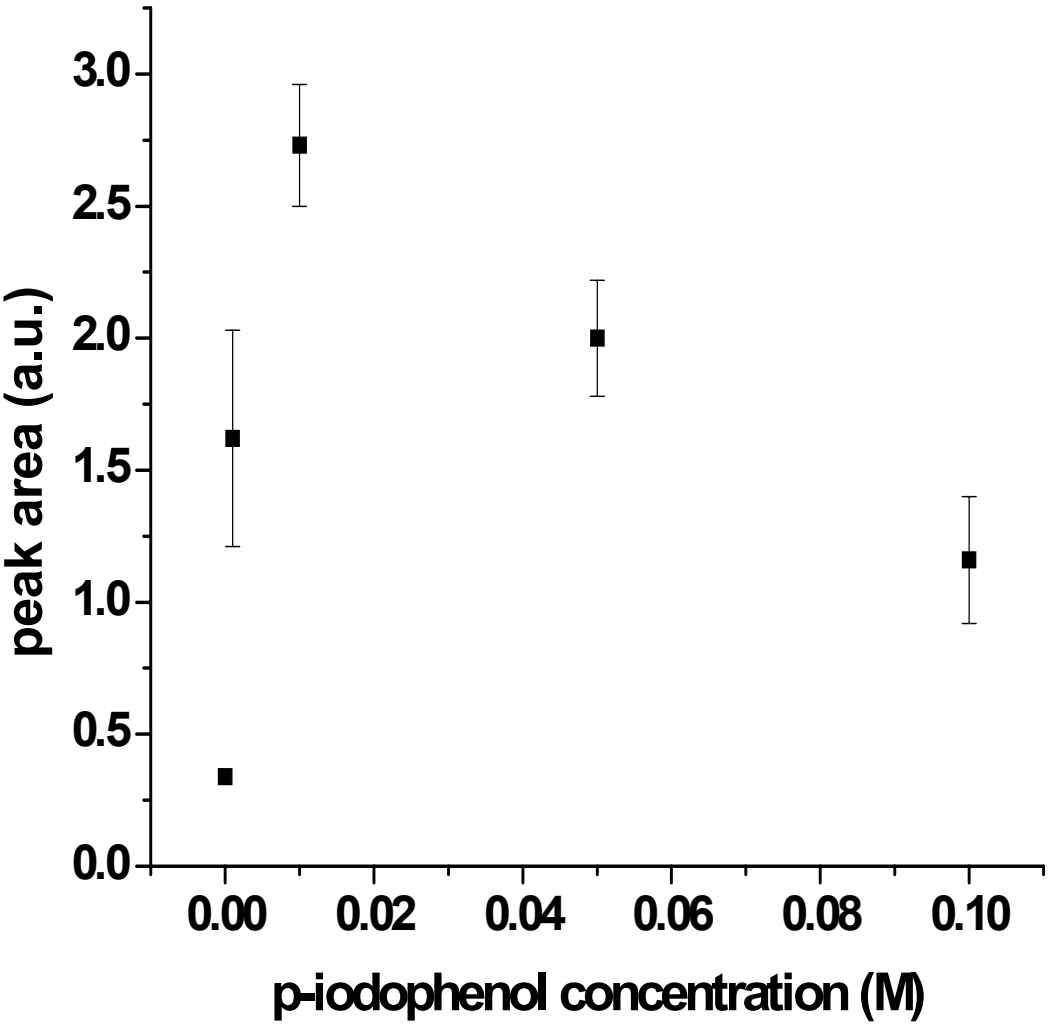

Figure 3-12. Effect of p-iodophenol concentration on CL signal.

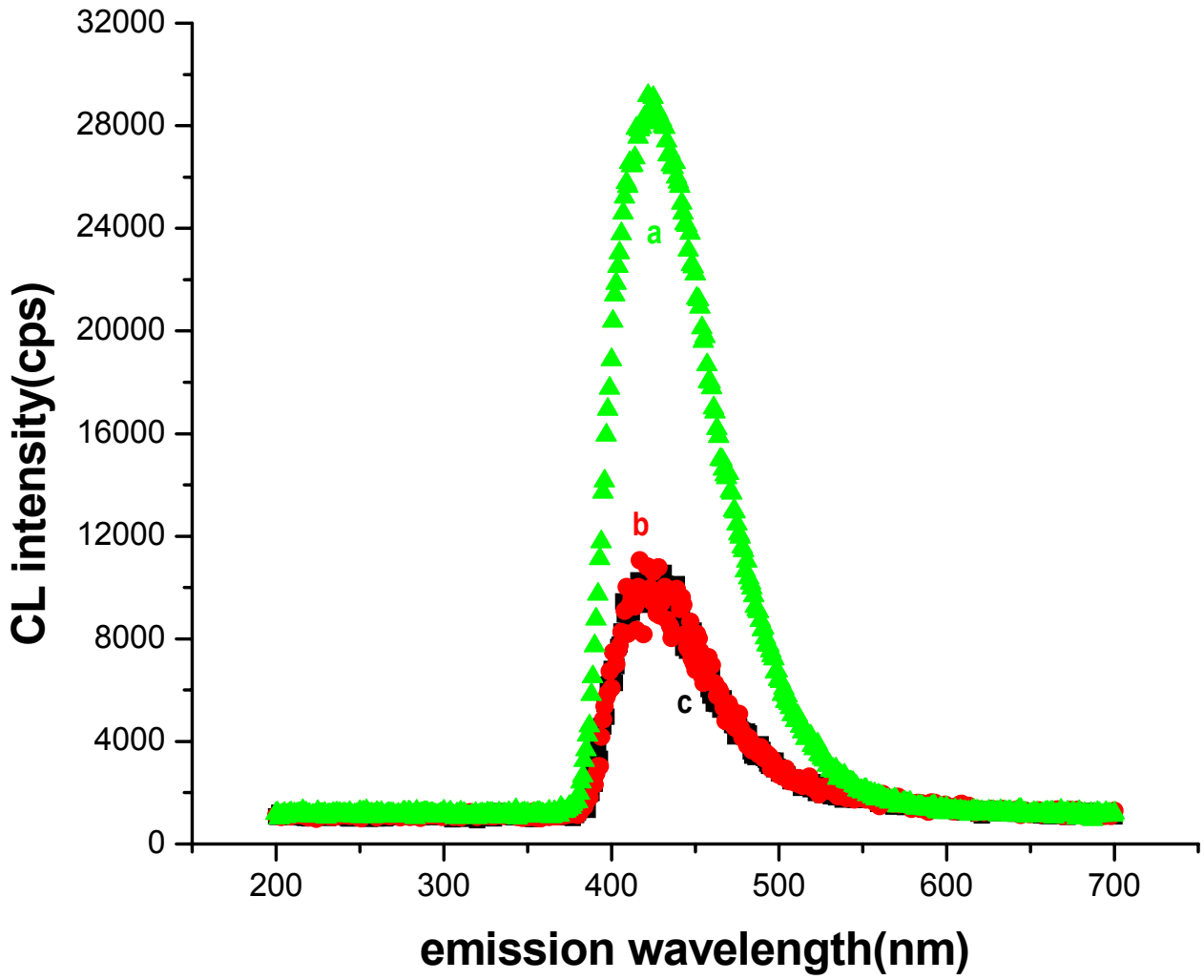

Figure 3-13. Luminol-NO_2 Emission Spectra. A) chemiluminescence spectrum obtained from reaction of luminol with H_2O_2 B) chemiluminescence spectrum obtained from reaction of luminol with NO_2 C) chemiluminescence spectrum obtained from enhanced reaction of luminol with NO2 using p-iodophenol.

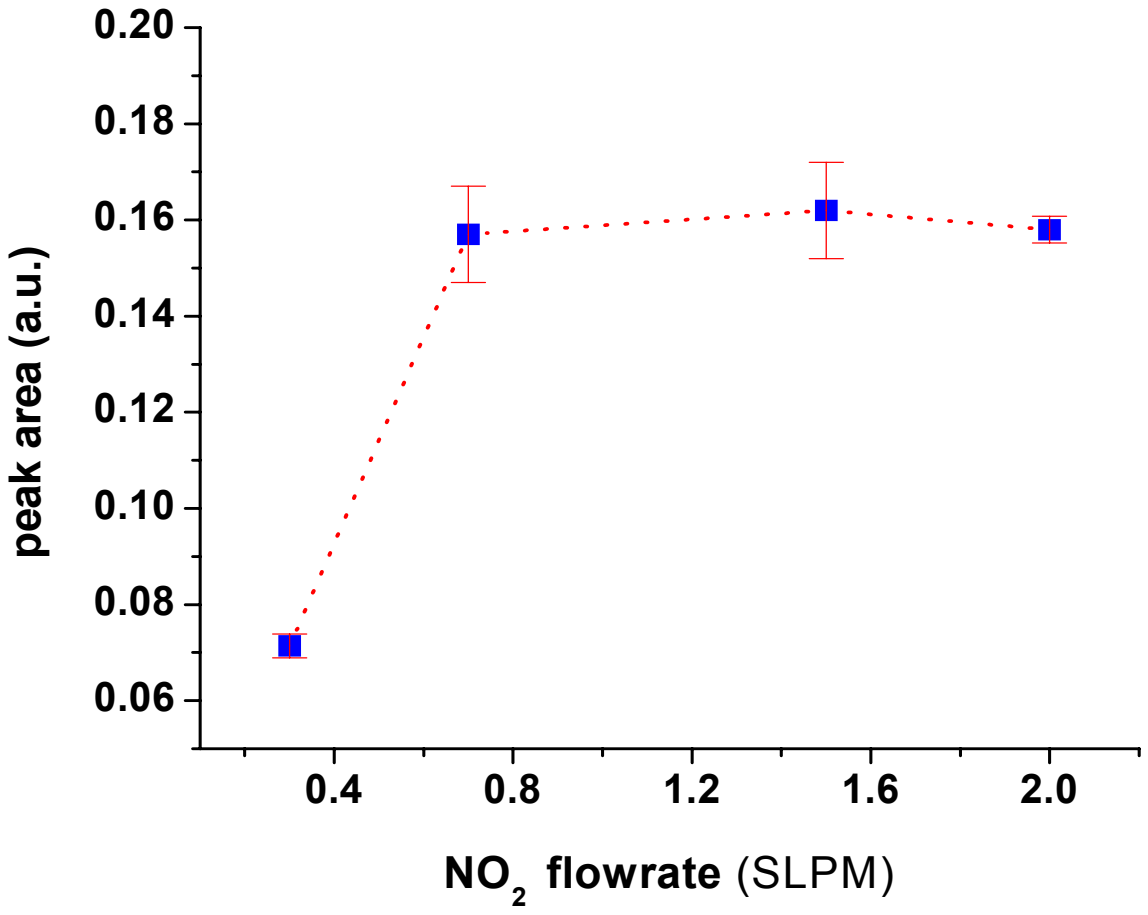

Figure 3-14. Effect of gas sample flow rate on CL signal.

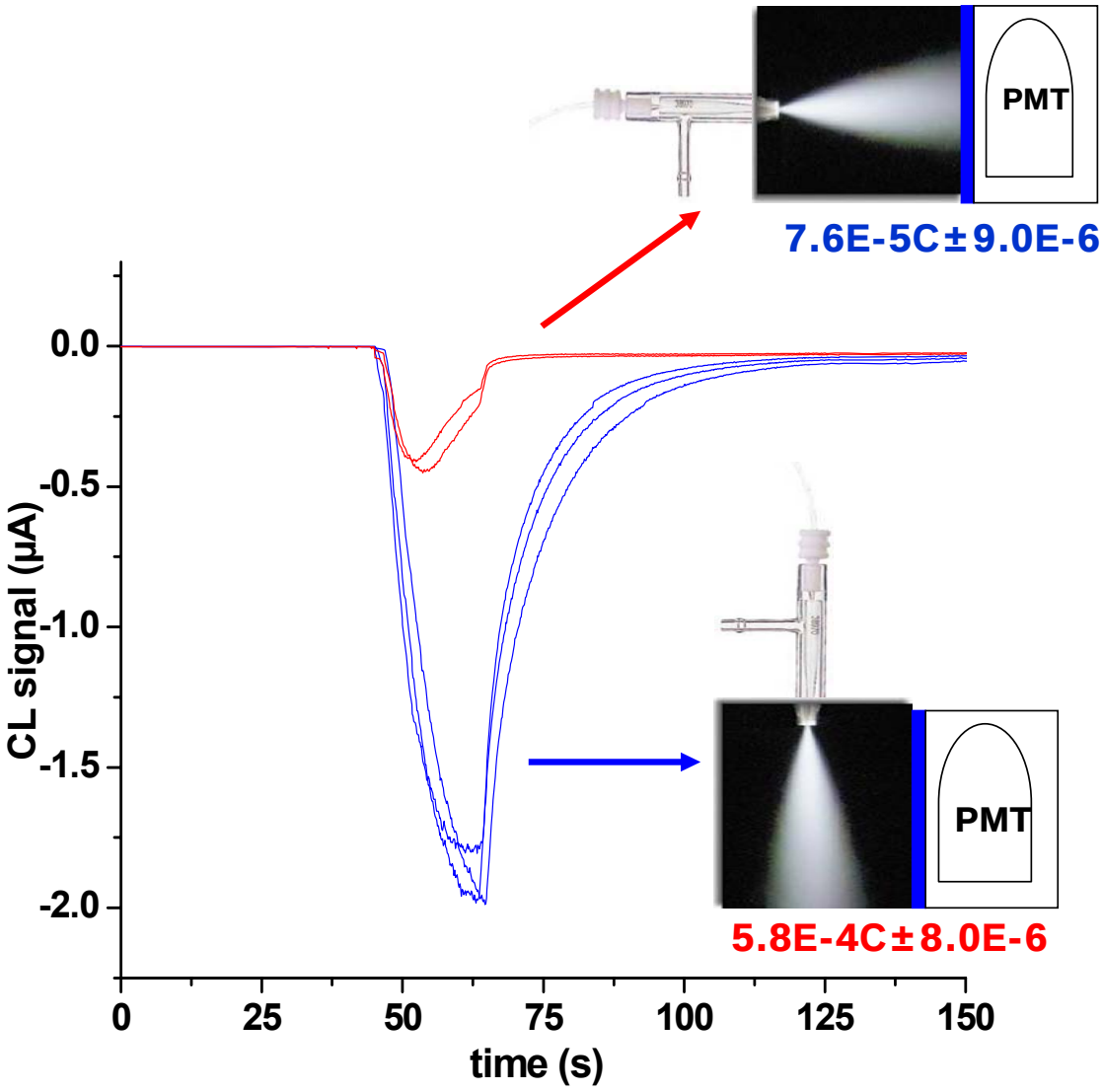

Figure 3-15. Effect of the orientation of luminol-NO_2 mist with respect to the PMT window on signal response.

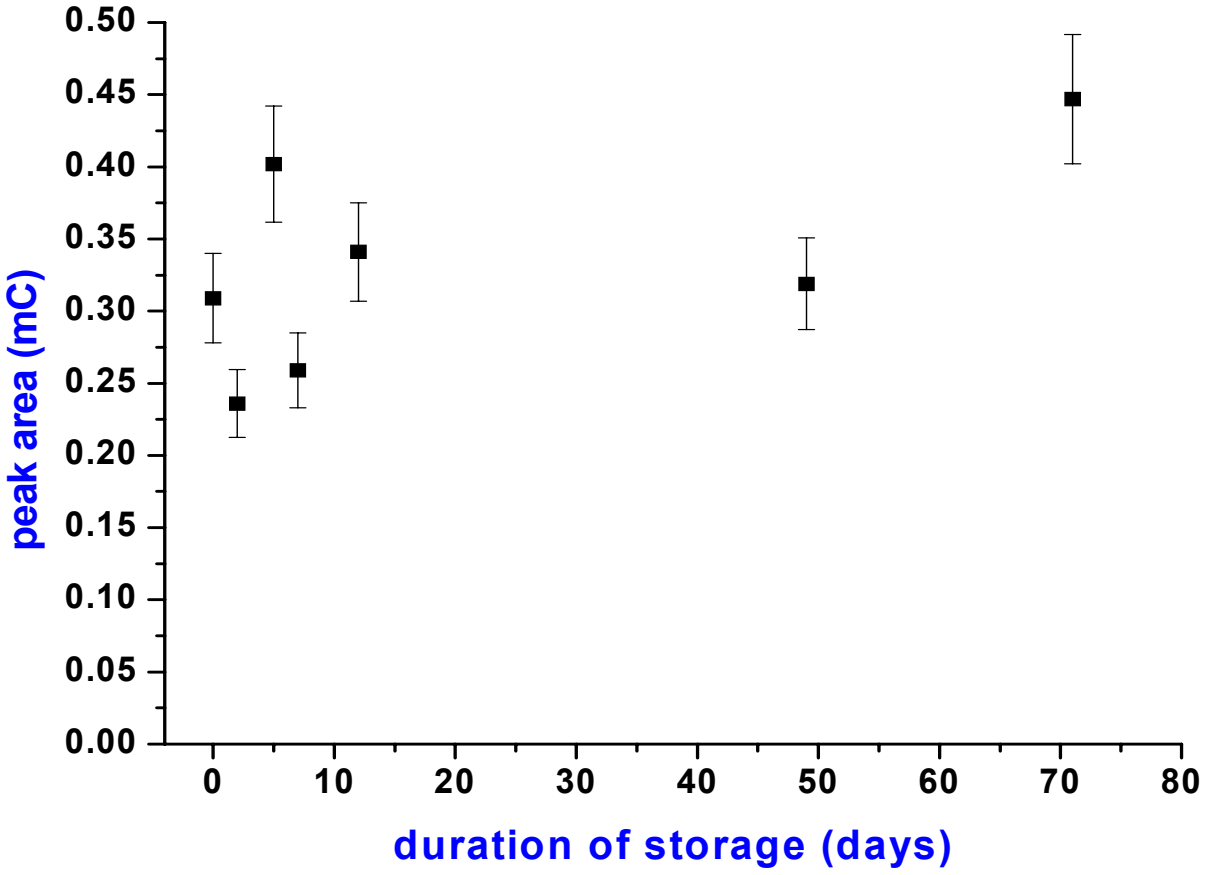

Figure 3-16. Effect of the storage time of luminol solution on CL signal.

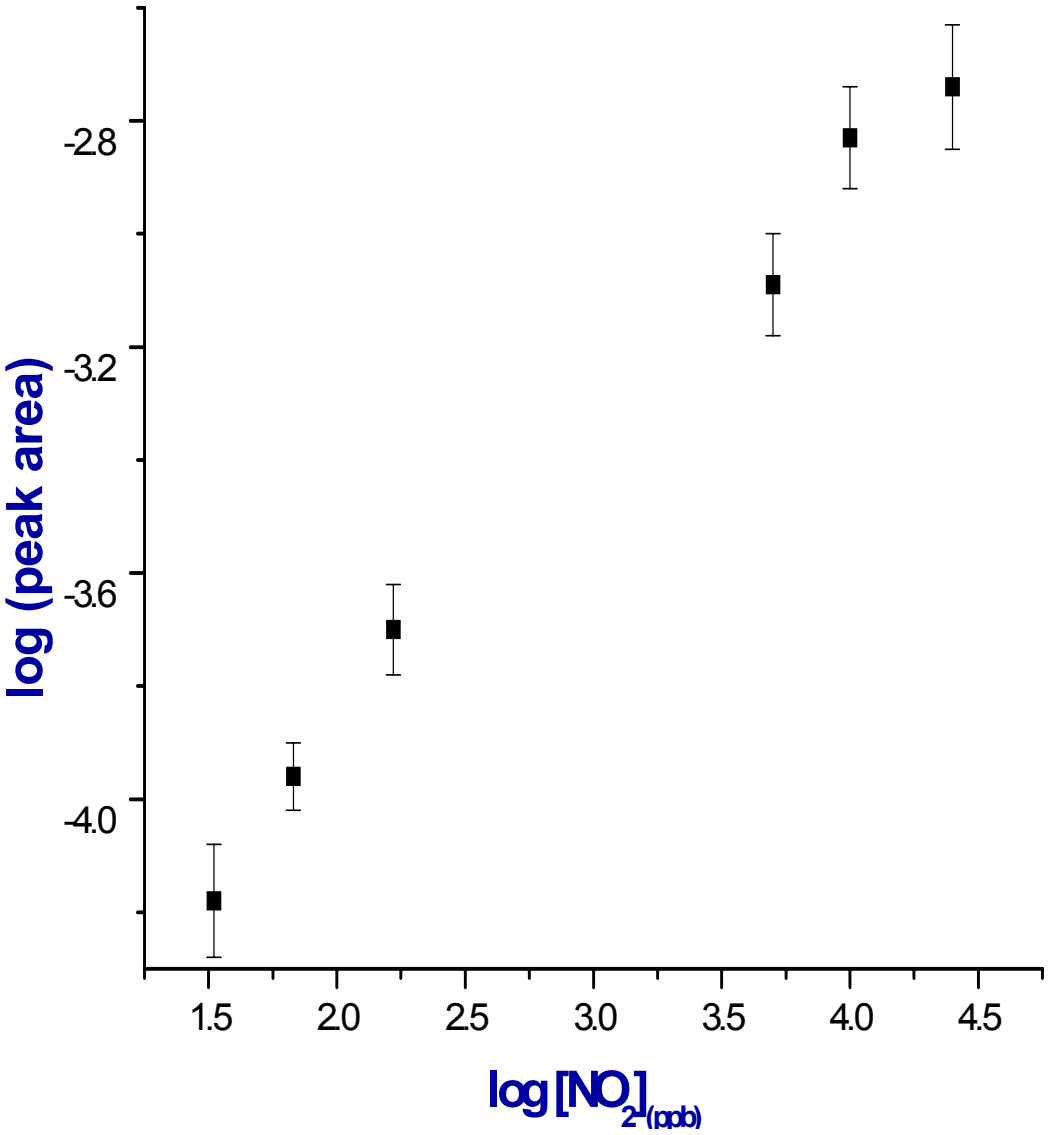

Figure 3-17. Calibration curve of NO_2 using Luminol-CL set-up.

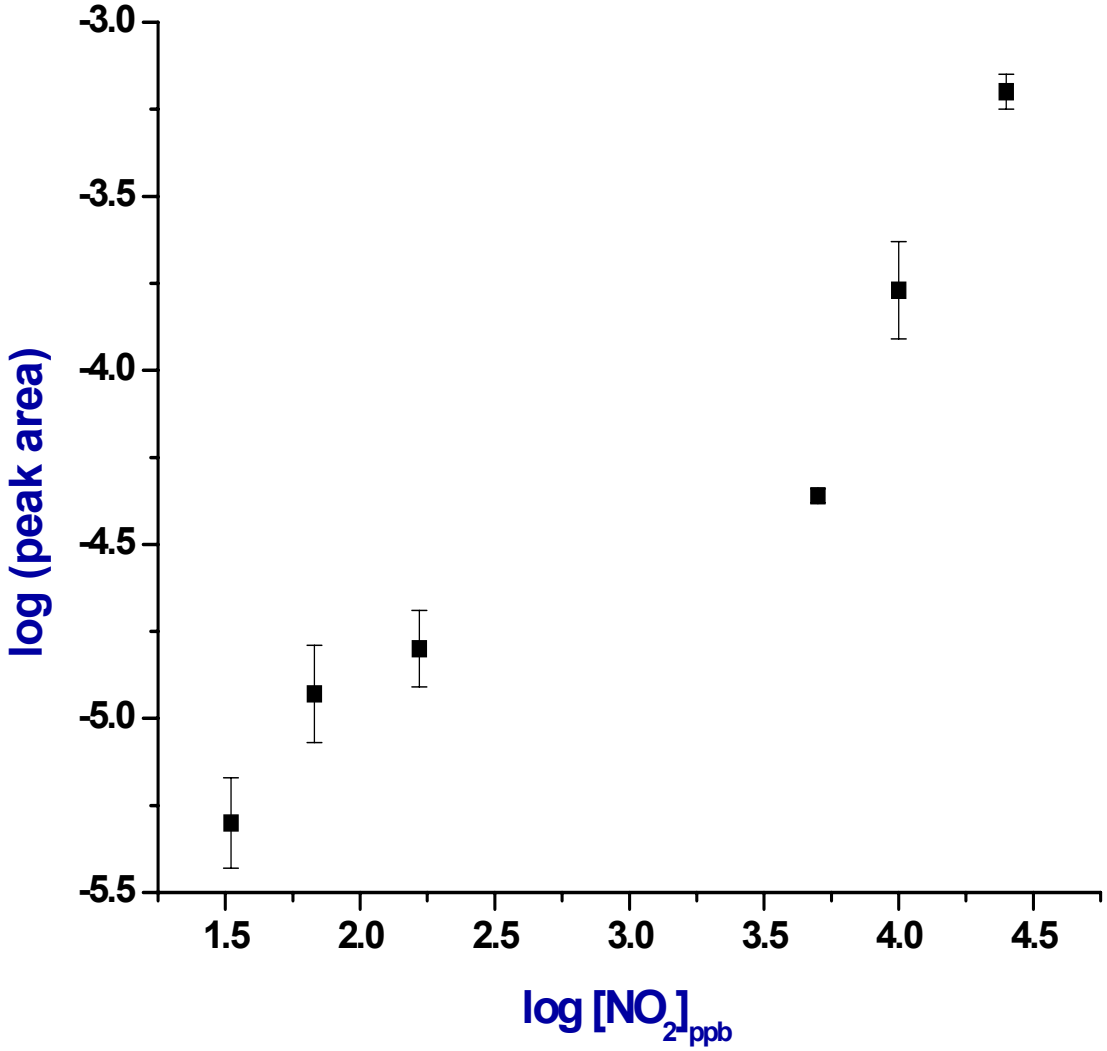

Figure 3-18. Calibration curve of NO_2 using Luminol/H_2O_2-CL set-up.

Table 3-1 Summary of the LOD obtained from different luminol-NO_2 CL set-ups.

Researchers	LMN-NO_2 reaction set-up	Detection limit
Maeda et al. (1980)[73]	Passing NO_2 gas on the surface of continuous flowing luminol solution	50 pptr
Wendell et al. (1983)[74]	Blowing NO_2 gas on the surface of filter paper on which luminol solution was allowed to flow	30 pptr
Schiff et al. (1986)[75]	Blowing NO_2 gas on the surface of fabric wick on which luminol solution was allowed to flow	5 pptr
Mikuska et al. (1992)[77]	Reacting NO_2 gas with aerosol of luminol solution	0.24 ppm (lowest concentration detected)
Collins et al. (1995)[78]	Blowing NO_2 gas on the surface of polymeric thin film of luminol	0.46 ppbv
Monterola et al. (2007)	Reacting NO_2 gas with aerosol of luminol solution	19 pptr

CHAPTER 4
CONVERSION OF NO TO NO_2

Introduction

Photofragmentation of nitro-based explosives using a UV laser produced both nitrogen dioxide (NO_2) and nitrogen oxide (NO) fragments. Detection of these fragments indicates the presence of explosives. However, NO cannot be detected by luminol chemiluminescence and hence must be converted back to NO_2 to enhance the sensitivity for explosive detection. Several methods for NO to NO_2 conversion has been reported for atmospheric monitoring purposes. This chapter begins with a review of those methods and is followed by a description of the oxidation unit used to integrate the photofragmentation and chemiluminescence set-ups into a single device for explosive detection.

Review of Methods for NO oxidation to NO_2

Several methods have been used for oxidizing NO to NO_2. Among these are potassium permanganate and sulfuric acid ($KMnO_4$/ H_2SO_4), iodine pentoxide (I_2O_5), acidified MnO_2, persulfate, ozone (O_3), heated chlorine dioxide (ClO_2), oxygen (O_2), and chromium oxide (CrO_3).[82] Each method has certain disadvantages especially during real time analysis. Persulfate and $KMnO_4$/ H_2SO_4 are not quantitative oxidizers while acidified MnO_2 is not stable.[82] An excess of O_3 will convert NO all the way to nitric acid (HNO_3) in the presence of moisture.[83] Also, O_3 cannot be used as an oxidant because it produces an interfering signal with luminol solution. A disadvantage in the use of I_2O_5 is that it is sensitive to many other reducing agents. ClO_2 has been demonstrated to yield good conversions, but must be generated in situ which is quite inconvenient. Gaseous O_2 oxidizes NO slowly and can only be used for concentrations above 100 ppm. [83]

CrO_3 coated on an inert substance has been shown to give the best results for NO to NO_2 conversion. Oxidation efficiency close to 100 % was achieved in the range of 30 to 80 % relative humidity.[82-84]

The work presented here described the fabrication of an oxidation unit for conversion of NO to NO_2 conversion that was used to integrate the photofragmentation and chemiluminescence units into an explosive detector device.

Experimental Section

Reagents and Chemicals

Reagent grade CrO_3 (~98%) was purchased for Sigma Aldrich (St. Louis, MO). Glass beads (D = 4 mm) were purchased from Fischer Scientific (Hampton, NJ). A tank of 10 ppm NO and 10 ppm NO_2 both buffered with N_2 were purchased from Airgas South Inc. (Gainesville, FL) and Safety Products Inc.(Lakeland, FL), respectively.

Apparatus and Methodology

CrO_3 Oxidation unit. The CrO_3 oxidation unit was prepared by coating CrO_3 on glass beads. Glass beads were chosen since it is an inert substance and beads were used to provide high surface area. The first step for preparing the CrO_3 converter was soaking the glass beads in a 20 %(w/v) aqueous solution of CrO_3 for about 30 minutes. After soaking, the glass beads were filtered and dried in an oven at 105^{o}C for 30 to 45 minutes. The glass beads were then packed in a 1" diameter by 8" length stainless steel tubing.

CrO_3 Oxidation Unit/Luminol-CL Detector Tandem. Figure 4-1 is the experimental set-up used for evaluating the efficiency of the CrO_3 oxidation unit. A 10 ppm NO in N_2 was used as reference sample. The gas sample flow rate was controlled by the mass flow controller which was then connected to the CrO_3 oxidation unit. Oxidized products were then introduced

into the CL unit through the side arm of the concentric nebulizer. The operating conditions of the instrument were essentially the same as those described in Chapter 3.

Results and Discussion

The CrO_3 oxidation unit was tested for efficiency in converting NO to NO_2 by passing a 10 ppm NO/N_2 sample through the converter. The sample flow rate was set to 100 mL/minute. The NO_2 produced upon oxidation was detected by the luminol-CL detector. Figure 4-2A shows the CL signal acquired with 10 ppm NO in N_2 without CrO_3 oxidation unit whereas Figure 4-2B shows the signal obtained after passing the same gas sample through the CrO_3 converter. Figure 4-2C shows the signal observed after passing 10 ppm NO_2 in N_2 through the same converter. Based on the three replicate measurements, average peak areas for 10 ppm NO and 10 ppm NO_2 after passing through the same converter were 857.1±127.5 and 1488.5±225.3, respectively. Conversion efficiency of 58% was obtained. The lower conversion efficiency can be attributed to relative humidity of the NO sample. It is well established that the efficiency of NO oxidation by CrO_3 varies with sample water content, being greatest at mid-range relative humidity (30 to 80 %) but much poorer near both extremes. [82-84]

Conclusion

CrO_3 oxidation unit has approximately 58% NO to NO_2 conversion efficiency which was anticipated to significantly enhance the sensitivity of the Photofragmentation-Chemiluminescence apparatus for explosive detection.

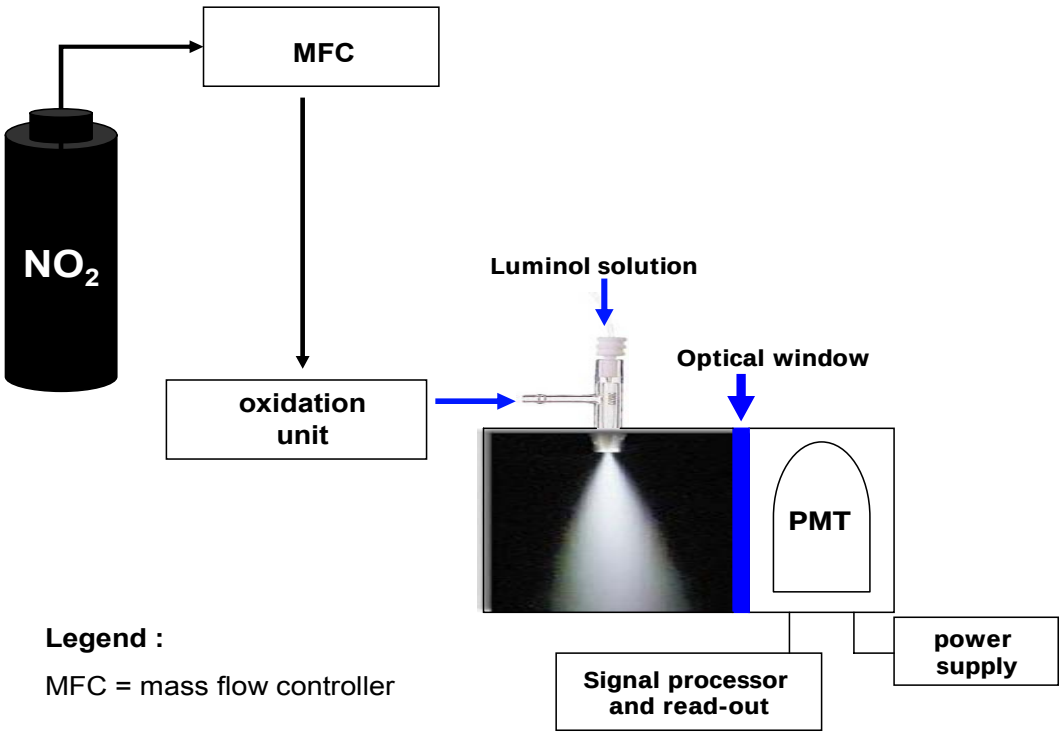

Figure 4-1. Experimental set-up used for evaluating the efficiency of CrO_3 oxidation unit.

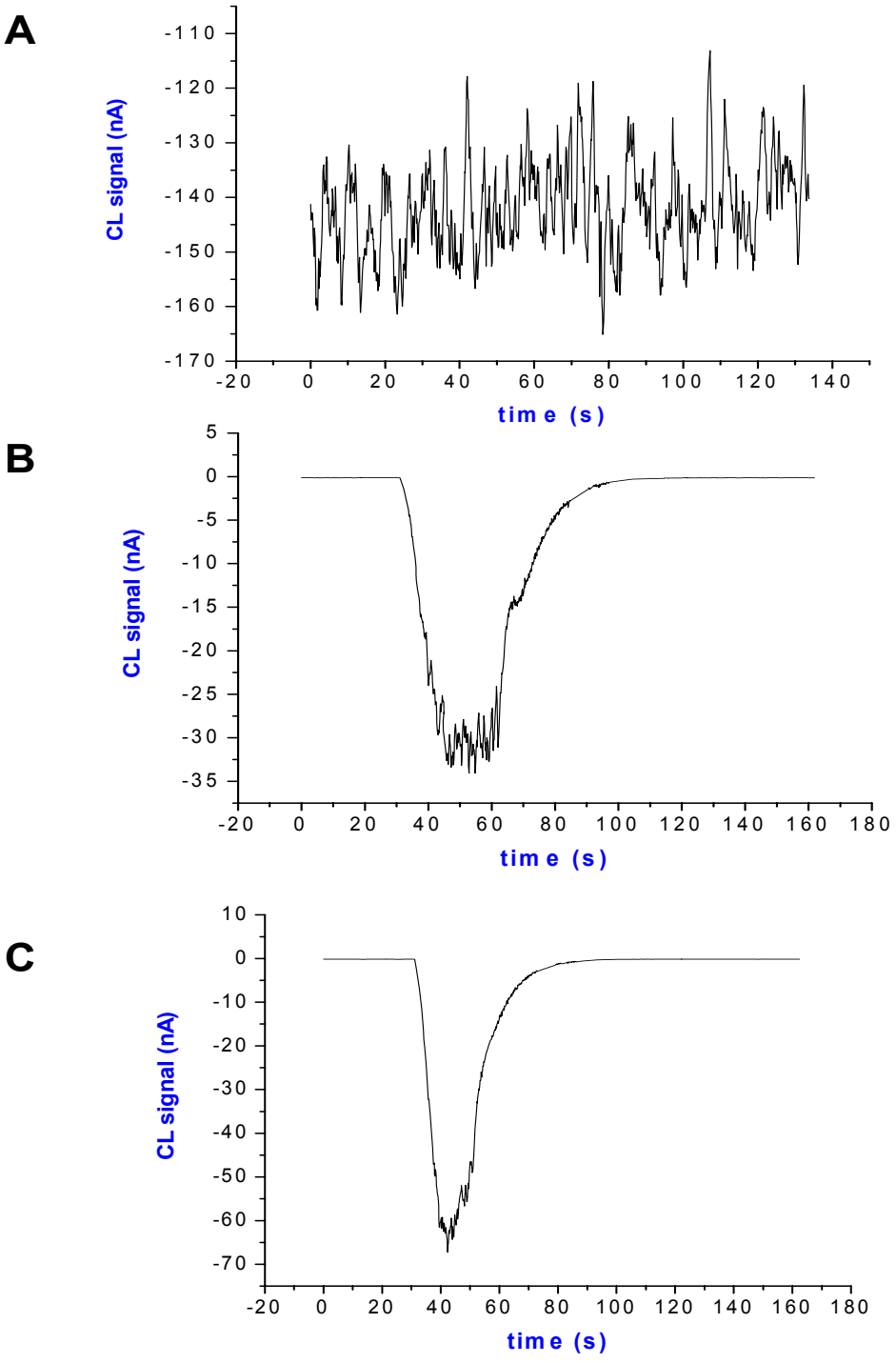

Figure 4-2. CL spectra of A) 10 ppm NO/N_2 B) 10 ppm NO/N_2 after passing through CrO_3 oxidation unit C) 10 ppm NO_2/N_2 after passing through CrO_3 oxidation unit.

CHAPTER 5
LASER PHOTOFRAGMENTATION AND CHEMILUMINESCENCE FOR NITRO-BASED EXPLOSIVE DETECTION

Introduction

Common explosives contain NO_2 functional group and since there are relatively few naturally occurring sources of nitro compounds, its presence can be used as a signature for explosive detection. Explosive detection using Photofragmentation-Fragment Detection (PF-FD) has been explored. This chapter begins with a review of those methods and is followed by a description of a new instrument based on laser photofragmentation and luminol chemiluminescence.

Review of PF-FD Methods for Explosive Detection

The PF-FD approach most often utilized when the analyte molecule does not lend itself to direct spectroscopic detection. In general, atoms and small molecules (composed of 2 to 3 atoms) can be detected directly by absorption, fluorescence, or ionization techniques.[44] This is due to a favorable combination of usually strong optical transitions and sharp, well resolved spectral features that provide effective optical activity. However, it is often the case for larger molecules such as the explosive compounds that the transitions are weaker and the spectral features are broad and poorly defined. In these cases, direct detection of the molecule by any of the above techniques is not analytically practical. While direct detection may not be feasible, the PF products of explosive such as $NO_{x\ (x=1,\ 2)}$ can be readily detected. Since $NO_{x\ (x=1,\ 2)}$ fragments are characteristic of the chemical composition of the explosive compounds, they also contribute to the selectivity of the method.

A patented instrument based on PF-FD technique for explosive compounds was reported by Nguyen et al.[85;86] The instrument is based on coupling pyrolyis with luminol chemiluminescence detector. Explosive samples were collected and pyrolyzed under

electronically heated Pt-Rh wire at 700°C. The NO_2 fragments that were generated after pyrolysis were swept into a reaction cell containing basic luminol solution. The luminol solution was separated from the remainder of the reaction cell by a semi-permeable hydrophobic PTFE membrane. The membrane was permeable to NO_2, thereby allowing diffusion to bring the NO_2 into contact with luminol solution. Light emitted from the reaction was detected by a photomultiplier tube (PMT) coupled to the reaction cell. The method claimed a detection limit of 100 ppt for DMBA.

There are several disadvantages regarding the pyrolysis method. First of all, pyrolysis produced many decomposition pathways, one of which is the detonation reaction of the explosive samples. TNT, for instance, is known to detonate at 502°C and upon detonation, TNT decomposes as follows: [3]

$$2C_7H_5N_3O_6 + \Delta \rightarrow 3N_2 + 5H_2O + 7CO + 7C \qquad (5\text{-}1)$$

Reaction 5-1 significantly diminished NO_2 fragments detectable. Secondly, pyrolysis is a time consuming method which is definitely a drawback for a fast real time analysis.

Due to limitations of the pyrolysis method, research on PF-FD techniques was pursued using laser photofragmentation. Laser photofragmentation followed by fragment detection using Resonance Enhanced Multi-photon Ionization Time-of-Flight Mass Spectrometer (REMPI-TOFMS) or Laser Induced Fluorescence (LIF) was not only performed for elucidating the photodissociation pathways of explosive compounds but for real time explosive monitoring as well.

Lemire et al.[53] and Simeonsson et al.[54] used PF-REMPI-TOFMS with a laser operating at 226 nm to photofragment the parent explosive compound and photoionize the resulting NO fragments. The NO^+ ions were subsequently detected using a TOFMS. The technique was

demonstrated using nitrocompounds such as nitromethane, DMNA, RDX, NB, *o*-NT, *m*-NT and TNT. Limit of detection for each analyte is tabulated in Table 5-1.

Wu et al.[87], Boudreax et al.[88], Parpar et al.[89], and Swayambunathan et al.[90] used PF-LIF in detecting explosives in various media including soil. Analytical figures of merit for these works are also tabulated in Table 5-1.

In 1999 and onwards, Sausa et al.[91-94] replaced TOFMS with an ion probe made up of miniature square electrodes to collect the resulting electrons and ions from PF of explosive compounds. The modification makes the device simpler and portable without trading its sensitivity for $NO_{(x = 1, 2)}$. Pertinent results regarding this technique are noted at Table 5-1.

Finally, a new prototype instrument was developed in this study by coupling the accuracy and convenience of laser photofragmentation over pyrolysis and the sensitivity for $NO_{(x =1,2)}$ detection of luminol-chemiluminescence (CL) detector over TOFMS and LIF.

Experimental Section

Reagents and Chemicals

All of the reagents and chemicals were essentially the same as those described in Chapters II, III, and IV. Basic luminol solution was prepared by dissolving luminol and p-iodophenol in 0.2 M KOH to make 5 x 10^{-3} M luminol and 0.01 M p-iodophenol, respectively. Para-iodophenol served as the chemiluminescent enhancer reagent and was added after dissolving the luminol into the KOH solution.

Standard solutions of aromatic compounds such as NT, TNT, and 2,4 NT were purchased from Accustandards (New Haven, CT).

Apparatus and Methodology

Photofragmenation-Chemiluminescence Detector (PF-CL). Figure 5-1 is a schematic of the experimental set-up for explosive detection using PF followed by CL. It consists of three main sections: (1) PF unit (2) Oxidation unit (3) CL unit.

The PF unit is essentially the same as described in Chapter II except for an additional heating system allowing the generation of the explosive vapor. After PF, the products were swept into the oxidation unit where NO fragments were converted back to NO_2. The NO_2 fragments were then subsequently detected by the CL unit. The complete description of the CL and oxidation units was discussed in Chapter III and IV, respectively.

Varying explosive vapor concentration can be generated as a function of temperature based on Clausius-Clapeyron Equation. The following equations were used to calculate the explosive vapor concentration: [91; 95]

$$\log [\text{PETN}]\ \text{ppt} = -7243/T(K) + 25.56 \qquad (5\text{-}2)$$

$$\log [\text{RDX}]\ \text{ppt} = -6473/T(K) + 22.50 \qquad (5\text{-}3)$$

$$\log [\text{TNT}]\ \text{ppt} = -5481/T(K) + 19.37 \qquad (5\text{-}4)$$

The temperature of the vapor was assumed to be the same as the temperature of the PF cell. The temperature was monitored using a thermocouple thermometer.

The sample preparation for solid explosive was the same as described in Chapter II. The total mass ablated for each experimental run was determined using Sartorious micro balance.

PF efficiency of Nitro-aromatic compounds. Uniform thin films of NT, TNT, and 2-4 NT were prepared by depositing 40 μL of solution of the target compound dissolved in acetone in a small aluminum cylindrical cup container (O.D. = 1.9 mm; Depth = 4.5 mm).The solvent was then allowed to evaporate at room temperature overnight. For each measurement, five different containers containing uniform thin film of selected explosive were used.

PF of NO_2 with luminol-CL detector. Figure 5-2 shows the PF set-up for verifying the further photodissociation of NO_2 to NO and O* upon absorption of a photon in 193 nm wavelength. The set-up consists of the analyte-transport system and luminol-CL detector. The experiment was performed by generating the NO_2 gas through reacting Cu and concentrated HNO_3 in a reaction vessel **A**. The NO_2 generated from the reaction was swept into the quartz reaction cell **B** by opening solenoid valves 1 and 2 simultaneously. This step allowed the reaction cell **B** to be filled up by NO_2 gas. After quite sometime, solenoid valves 1 and 2 were closed and the laser was fired into reaction cell **B**. A total of 1000 pulses were used for each experimental run with pulse energy of 5 mJ/pulse and a repetition rate of 50 Hz. After PF, solenoid valves number 2 and 3 were opened to sweep all the PF products into the CL unit. Then, the luminol-CL detector measured the remaining NO_2 left in the cell. Then, a reference signal was acquired by repeating the whole process without turning the laser on.

Results and Discussion

Relative PF Efficiency of Nitro-aromatic Compounds

PF of solid explosive samples can be described in the following stepwise manner. The first step involved the absorption of sufficient laser radiation by the solid explosive sample. Upon absorption, a plume of explosive will form and expand away from the sample surface as a result of pressure difference between the rapidly vaporized sample and the surrounding atmosphere. The subsequent photon absorption of the explosive vapor will produce PF products, such as NO and NO_2.

Photolysis of solid structurally similar compounds such as NT, 2,4 NT, and TNT were performed. The parent molecules of these compounds contained one, two, and three NO_2 moieties, respectively. Figure 5-3 shows the luminol-CL signal obtained from the $NOx_{(x = 1,2)}$ fragments of these compounds at varying laser energy. The slopes acquired from these sets of

data (Table 5-2) suggest non-linearity in the PF efficiency of these compounds where PF efficiency is defined as follows:

$$\% \text{ PF efficiency} = (\text{moles of } NO_2 \text{ detected by CL})/(\text{moles of } NO_2 \text{ available}) \times 100\% \quad (5\text{-}5)$$

The non-linear behavior in the PF efficiency can be attributed to the difference in the latent heat of sublimation (ΔH_s) for each compound. As ΔH_s increases, the more energy is required for a substance to vaporize. In the PF process for a solid explosive sample, this will consequently result in less explosive vapor for photolysis. Actual numerical values of ΔH_s for these nitrocompounds were not available, however, their vapor pressure at ambient condition have been well studied and are given in Table 5-2. The vapor pressure is linearly related to ΔH_s. From Table 5-2, NT has the lowest molecular mass implying that it has the weakest intermolecular force of attraction resulting in the highest vapor pressure at ambient condition. As a consequence, the laser irradiated spot of NT produced a plume with the highest concentration of explosive vapor favoring the most efficient photolysis. The higher slope value of TNT compared to 2,4 NT can be explained by a single photon absorption capable of simultaneous multi-NO_2 scission. This process defies the higher vapor pressure of 2,4 NT compared to TNT.

NO_2 Photolysis with Luminol-CL Detector

Results obtained from the time resolved absorption experiment in Chapter 2 on photolysis of NO_2 into NO and O* using ArF laser was further confirmed by using the luminol-CL detector. Figure 5-4 shows the CL signal of the NO_2 gas before and after photodissociation. Significantly lower CL signal was observed after the PF of NO_2 gas sample.

Analytical Capability of PF-CL Detector

The interaction of laser photons with both solid and vapor phase PETN was investigated by the quantity of $NO_{x\ (x=1,2)}$ fragments generated after photolysis. Figure 5-5 presented the effect of varying laser pulse energy on CL signal obtained from the $NOx_{\ (x=1,2)}$ generated. In the

absence of CrO_3 converter, it can be assumed that the CL signal is due to NO_2 fragments alone. The amount of NO_2 released for both solid and vapor phase of PETN increased linearly within lower fluence range (e.g., a range of 2.5 to 5 mJ/pulse for solid PETN and 2.5 to 7.5 mJ/pulse for PETN vapor). However, at higher laser fluence, the quantity of NO_2 fragments produced does not significantly changed. The pattern signifies that higher laser fluences yield faster photon deposition on the sample which favorably induced the sequential two-step PF process (Reactions 5-4 and 5-5) to take place.

$$C(CH_2)_4O_4(NO_2)_4 + h\upsilon \rightarrow C(CH_2)_4O_4(NO_2)_3 + NO_2; \quad h\upsilon = 193 \text{ nm} \qquad (5\text{-}4)$$

$$NO_2 + h\upsilon \rightarrow NO + O^*; \quad h\upsilon = 193 \text{ nm} \qquad (5\text{-}5)$$

The presence of CrO_3 oxidizer for NO to NO_2 conversion yielded an increasing plot of NO_2 fragments within the entire range of laser fluence for both solid and vapor phase of PETN indicating that higher photon intensity per pulse consequently produced more $NOx_{(x=1,2)}$ fragments.

Figure 5-6 shows the effect of varying total number of laser pulses at constant pulse energy for both solid and vapor phase of PETN. The trend shows that the detected $NOx_{(x=1,2)}$ fragments increase with increasing pulse number as long as there is an available sample to photolyze.

The analytical capability of the method for trace explosive detection was obtained. In trace explosive detection, the explosive residue can be present in two forms: vapor and particulate. Vapor detection examines the vapor emanating from concealed explosive sample and particulate detection refers to the microscopic residues of explosives that would be present on individuals or material which have been through contamination.

Figure 5-7 and 5-8 show the effect of laser parameters such as the total number of pulses and energy on the amount of solid PETN ablated which directly affects the corresponding CL signal obtained. The dependence of the CL signal on the amount of PETN ablated was projected on x,y axis for both graphs (solid points). Both sets of data best fitted into exponential equations of $y = (4x10^{-6})\ m^{1.5021}$ and $y = (2x10^{-5})\ m^{1.6266}$ for the total number of pulses and laser energy dependent graphs, respectively. The y and m variables correspond to the CL signal and the amount of the ablated PETN, respectively. Both of these equations were used to estimate the amount of PETN residue that can be positively confirmed by the method. A positive confirmation is defined as the amount of PETN residue that provides a signal to background ratio of 10. A surface concentration range of 61 to 186 ng/cm^2 of PETN was calculated.

By using identical laser parameter conditions, calibration curves for the vapor of RDX, PETN, and TNT were obtained (Figure 5-9). Rough limits of detection (LOD) as well as the calibration sensitivity for each analyte were determined. The LOD is defined as $(3 \cdot \sigma_{Blk})/m$ where σ_{Blk} is the standard deviation of the background signal and m is the calibration sensitivity or the slope of the CL peak area versus the explosive concentration (in ppb) plot. Table 5-3 gives the LOD values of 3.45 ppb for PETN, 1.73 ppb for RDX and 34.5 ppb for TNT.

Ranking the compounds by LOD yields RDX<PETN<TNT. The analytical detection limit is dependent on a number of parameters including (1) the PF cross section or absorption coefficient of the parent molecule at 193 nm, and (2) the PF efficiency of the parent molecule at 193 nm to yield $NOx_{(x=1,2)}$ fragments. Ordering the compounds by absorbance at 193 nm yields TNT>RDX≈PETN. A priori, the anticipated result should be that the order of compound's LOD is parallel with their absorbance order. Surprisingly, this is not the case: The TNT's

absorption coefficient is higher than that of RDX and PETN, yet its LOD is poorer. Clearly, the molecule's absorption coefficient plays less of a role in its LOD.

The LOD ratio of TNT to PETN is ~ 10 which is similar to the value reported previously[92]. A plausible argument for TNT's LOD being higher than PETN and RDX might be due to TNT's several alternative decomposition pathways that compete with R-NO_2 bond scission. These include the oxidation of $-CH_3$ to form anthranil, [96; 97] nitro-nitrite isomerization[98] and possibly rearrangement of the ring substituents.[99] These pathways decrease the initial production of $NO_{x(x= 1,2)}$ and contribute to TNT's lower sensitivity relative to RDX and PETN.

PETN has a LOD that is a factor of nearly 2 times greater than that of RDX. This suggest that the process of NO_2 release in RDX molecules is more complicated than the simple cleavage of a single nitro functional group and may involve the loss of more than one nitro group for each molecule. The energy for the ring's N-N bond cleavage is lowered after the removal of a nitro group, and further decomposition generating additional NO_2 is feasible even without photon absorption.[51]

Conclusion

PF efficiency of nitro compounds is not linearly related to the quantity of NO_2 moieties of the parent molecule which was proven by photo dissociation of NT, TNT, and 2,4 NT.

Photolysis of NO_2 fragments into NO and O* was verified using luminol-CL detector.

The interaction of laser photons with solid and vapor phase of PETN was investigated. At lower laser fluence, a linear increase on the quantity of NO_2 fragments produced was observed for both solid and vapor phase of PETN. However, at higher laser fluences, saturation of NO_2 production occurred which implies that at higher photon intensities, the proposed sequential two-step PF mechanism as shown below took place.

$$R{-}NO_2 + h\upsilon \rightarrow R + NO_2; \quad h\upsilon = 193 \text{ nm} \qquad (5\text{-}6)$$

$$NO_2 + h\upsilon \rightarrow NO + O^*; \quad h\upsilon = 193 \text{ nm} \qquad (5\text{-}7)$$

The presence of CrO_3 oxidizer for NO to NO_2 conversion significantly enhanced the sensitivity of the detector in analyzing both the solid and vapor phase of PETN.

By using laser PF followed by NO_2 detection with luminol-CL technique, it is feasible to detect energetic materials in real time at ambient conditions. Detection limits of 3.4 ppb for PETN, 1.7 ppb for RDX, and 34.5 ppb for TNT were obtained. It was also demonstrated that the presence of PETN residue within the range of 61 ng/cm^2 to 186 ng/cm^2 can be detected at a signal to background ratio of 10 using a few micro joules of laser energy.

Table 5-1. Summary of the performance of various explosive detectors based on PF-FD technique.

Research group/ Year	Method/Comments	LOD	
GW Lemire, JB Simeonsson, RC Sausa (1993)[53]	PF-REMPI-TOFMS	CH_3NO_2 1000 ppb DMNA 450 ppb RDX 8 ppb TNT 24 ppb NB 2400 ppb	
JB Simeonsson, GW Lemire, RC Sausa (1993)[54]	PF-REMPI-TOFMS	LOD (ppm) at λ=193nm CH_3NO_2 0.18 DMNA 0.51 NB 0.49 o-NT 0.12 m-NT 0.10 TNT 0.21	LOD (ppm) at λ=226nm 1.0 0.45 2.4 15 36 1.7
D Wu, J Singh, F. Yuch, D. Monts (1996)[87]	PF-LIF TNT in soil	TNT = 40 ppb at 373 K	
G Boudreax, T. Miller, A. Kurefke, J Singh, F. Yuch, D Monts (1999)[88]	PF-LIF	TNT H_2O 500 ppm TNT soil 100 ppm	
T. Arusi-Parpar, D. Heflinger, R. Laui (2001)[89]	PF-LIF at 1atm, 24°C	TNT 8 ppb at (S/N) = 10	
V.Swayambunathan, G. Singh, RC Sausa (1999)[90]	PF-LIF both CH_3NO_2 and TNT are not detected at 454 nm and (355 + 450)nm	LOD at 227 nm CH_3NO_2 4.3 ppm TNT 37 ppm	LOD at (355+227) 3.3 ppm 2.6 ppm
V.Swayambunathan, G Singh, RC Sausa (1999)[91]	PF-REMPI with ion probe detector PF-LIF	LOD with REMPI TNT 70 ppb RDX 7 ppb PETN 2 ppb	LOD with LIF 37 ppm NOT DETECTED NOT DETECTED

Table 5-1. (Continued)

Research group/ Year	Method/Comments	LOD	Research group/ Year
V.Swayambunathan, G Singh, RC Sausa (1999)[92]	PF-REMPI with ion probe detector PF-LIF	LOD with PF-REMPI at 227 and 454 nm (ppm), respectively PETN 0.5;20.4 RDX 0.4;not detected TNT 4.4 ppm;not detected	LOD with PF-LIF at 227 and 454 nm (ppm), respectively 2.2;140 1.6 ppm;not detected 3.8 ppm;not detected
J. Cabalo, R Sausa, (2003)[93]	Laser Surface PF-Fragment Detection Spectroscopy (REMPI-ion probe detector)	RDX 1.4 ng/cm^2	
J. Cabalo, R Sausa, (2005)[94]	Laser Surface PF-Fragment Detection Spectroscopy (REMPI-ion probe detector)	RDX 1.4 ng/cm^2 HMX 2.0 ng/cm^2 CL20 7.1 ng/cm^2 TNT 15.4 ng/cm^2	
Monterola, M.P.P., Smith,B.W.,Omenetto, N.,Wineforner,J.W. (2007)	Photofragmentation-Luminol-NO_2 Chemiluminescence Method	RDX 1.7 ppbv PETN 3.4 ppbv TNT 34.5 ppbv (S/N) = 3	PETN 61 to 186 ng/cm^2

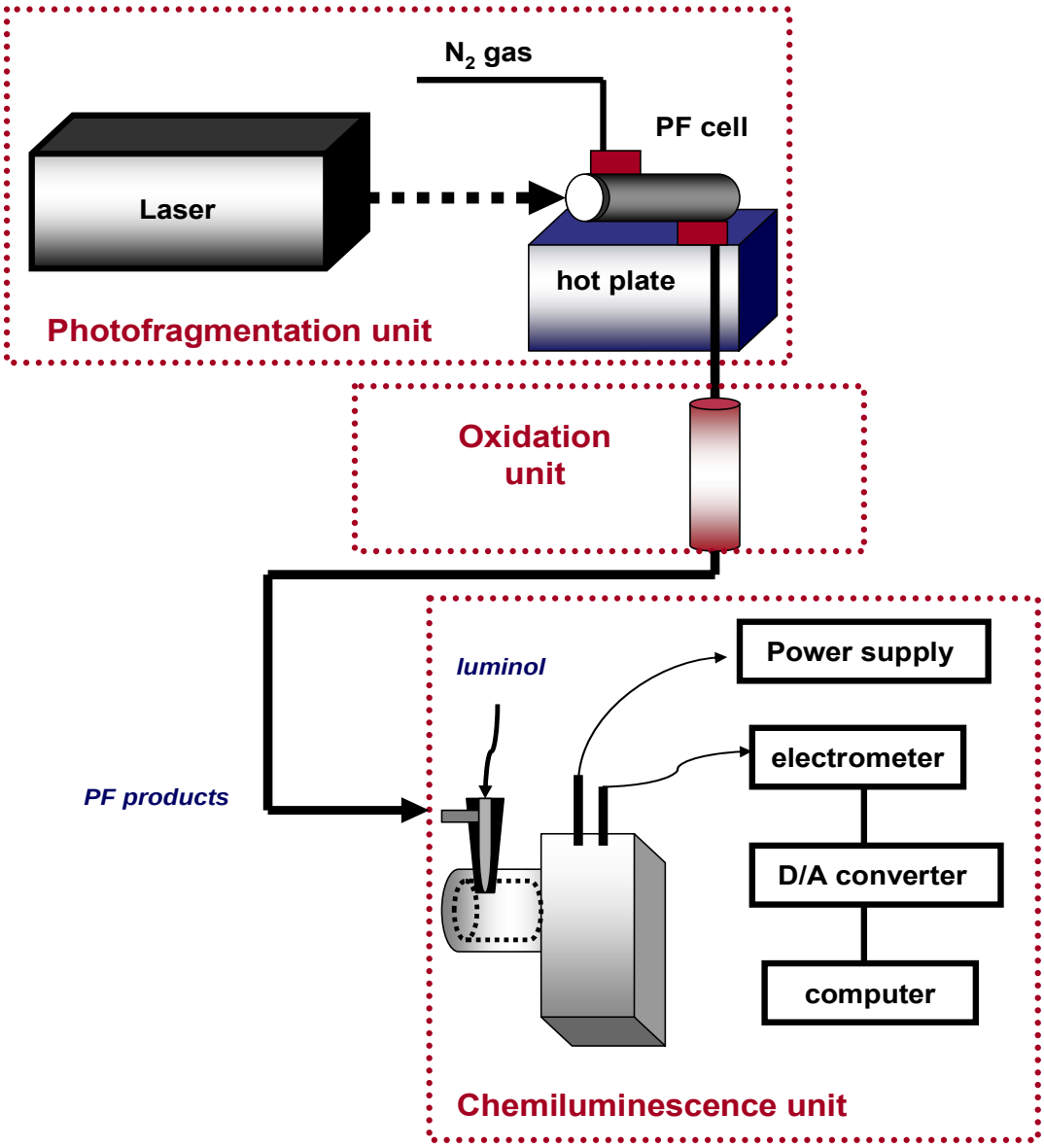

Figure 5-1. Photofragmentation-Chemiluminescence detector.

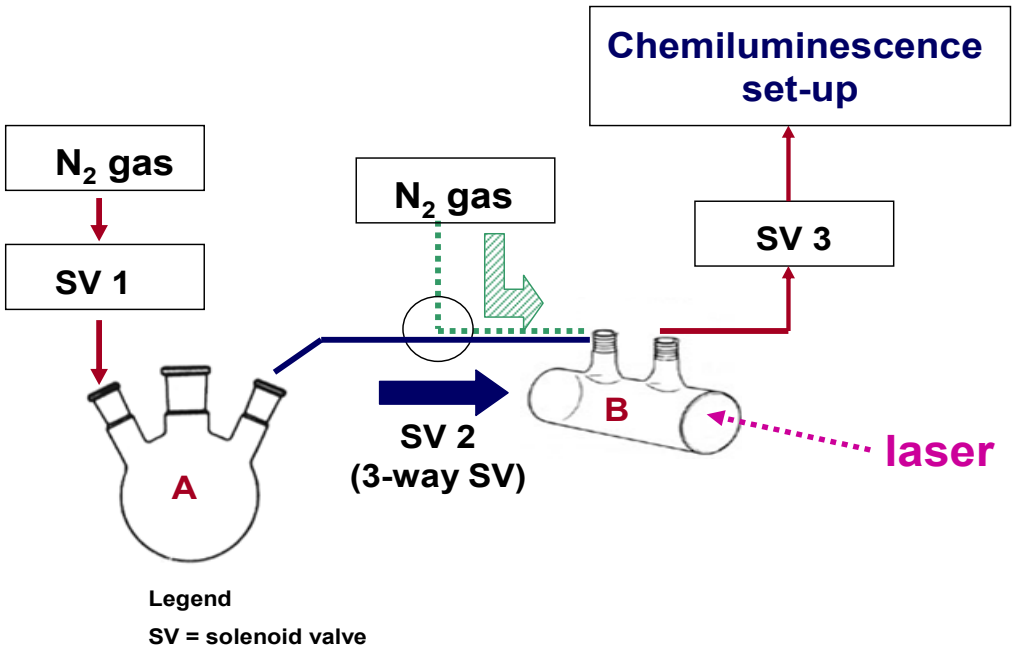

Figure 5-2. Photofragmentation set-up used for NO_2 photolysis.

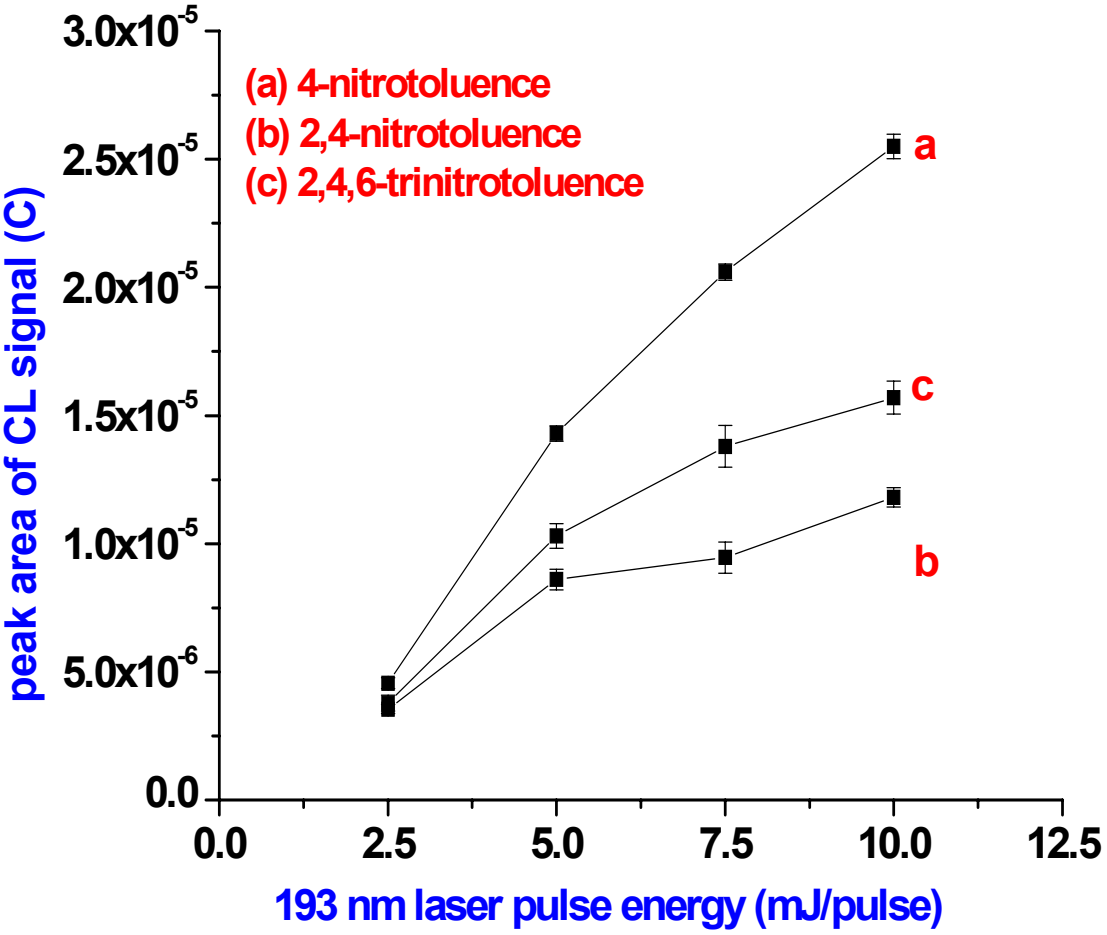

Figure 5-3. Chemiluminescence signals obtained for nitro-aromatic compounds at varying laser energy.

Table 5-2. Determination of PF efficiency of nitro-aromatic compounds.

Explosive sample [a]	MM (amu)	VP at 25°C (torr)	Slope of the CL signal vs. Energy plot (C mJ^{-1})
NT	137.14	1.5×10^{-1} (199.1 ppm)	$3.0 \times 10^{-6} \pm 5.7 \times 10^{-8}$
2-4 NT	182.14	2.1×10^{-4} (0.28 ppm)	$1.1 \times 10^{-6} \pm 5.2 \times 10^{-8}$
TNT	227.13	5.8×10^{-6} (7.7 ppb)	$1.7 \times 10^{-6} \pm 8.7 \times 10^{-8}$

[a] Abbreviations: NT, nitrotoluene; 2,4-NT, 2,4 dinitrotoluene; TNT, 2,4,6 trinitrotoluene

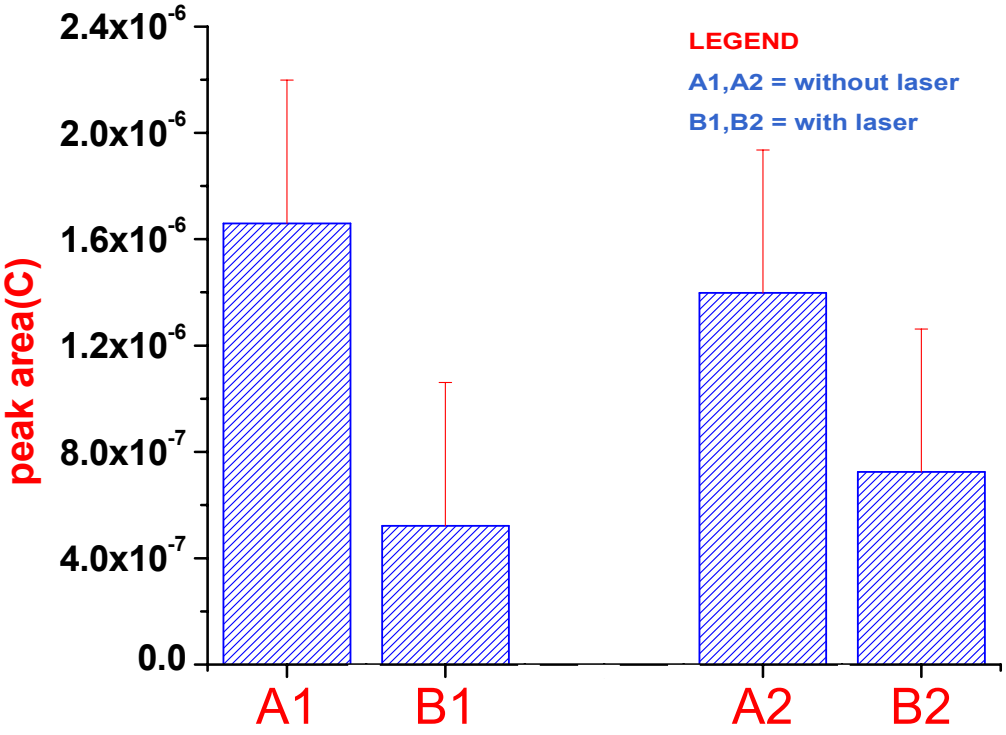

Figure 5-4. Chemiluminescence signals obtained before and after PF of NO_2.

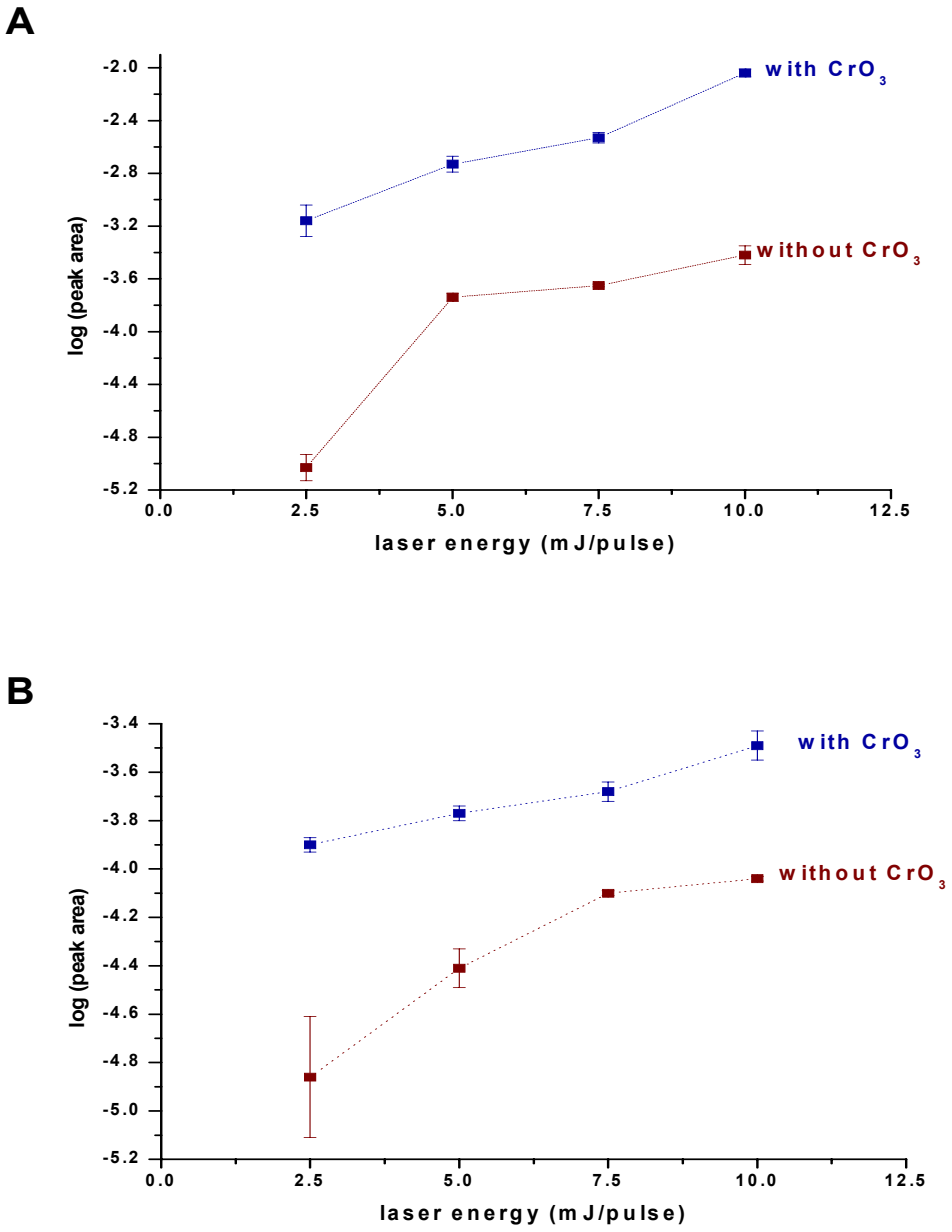

Figure 5-5. Effect of varying laser energy on the CL signal of $NO_{x(x=1,2)}$ fragments obtained after photofragmentation of A) solid and B) vapor phase of PETN.

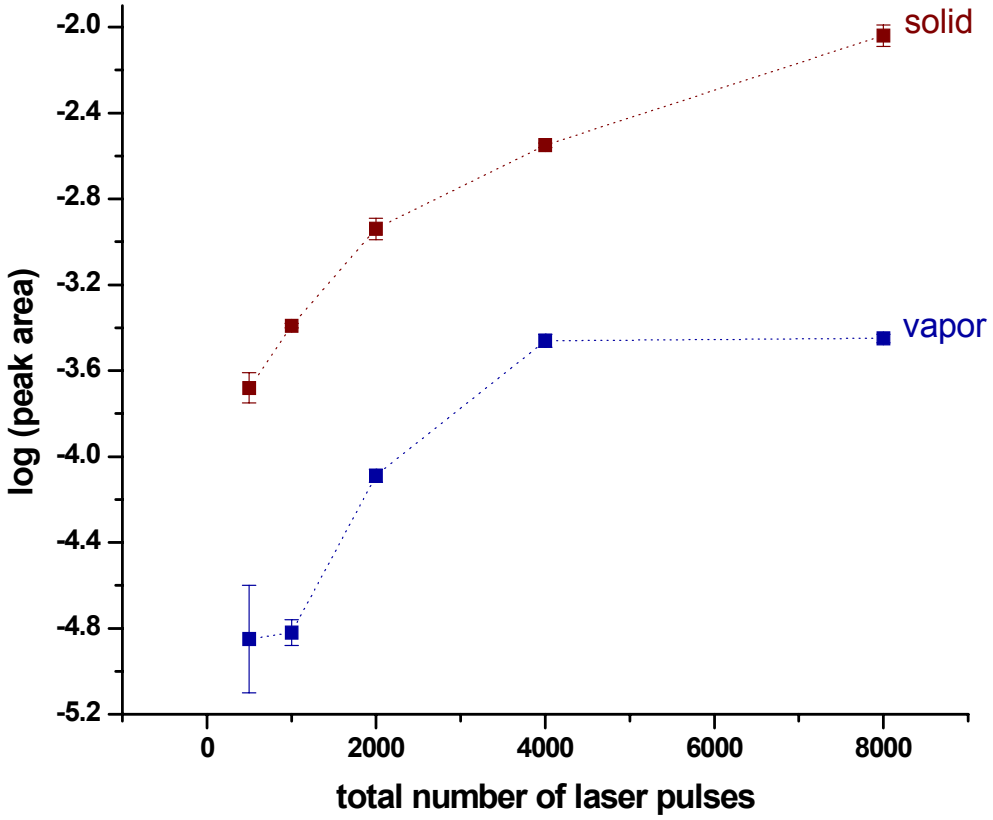

Figure 5-6. Effect of varying total number of laser pulses on the CL signal of $NO_{x(x=1,2)}$ fragments obtained after PF of solid and vapor phase of PETN.

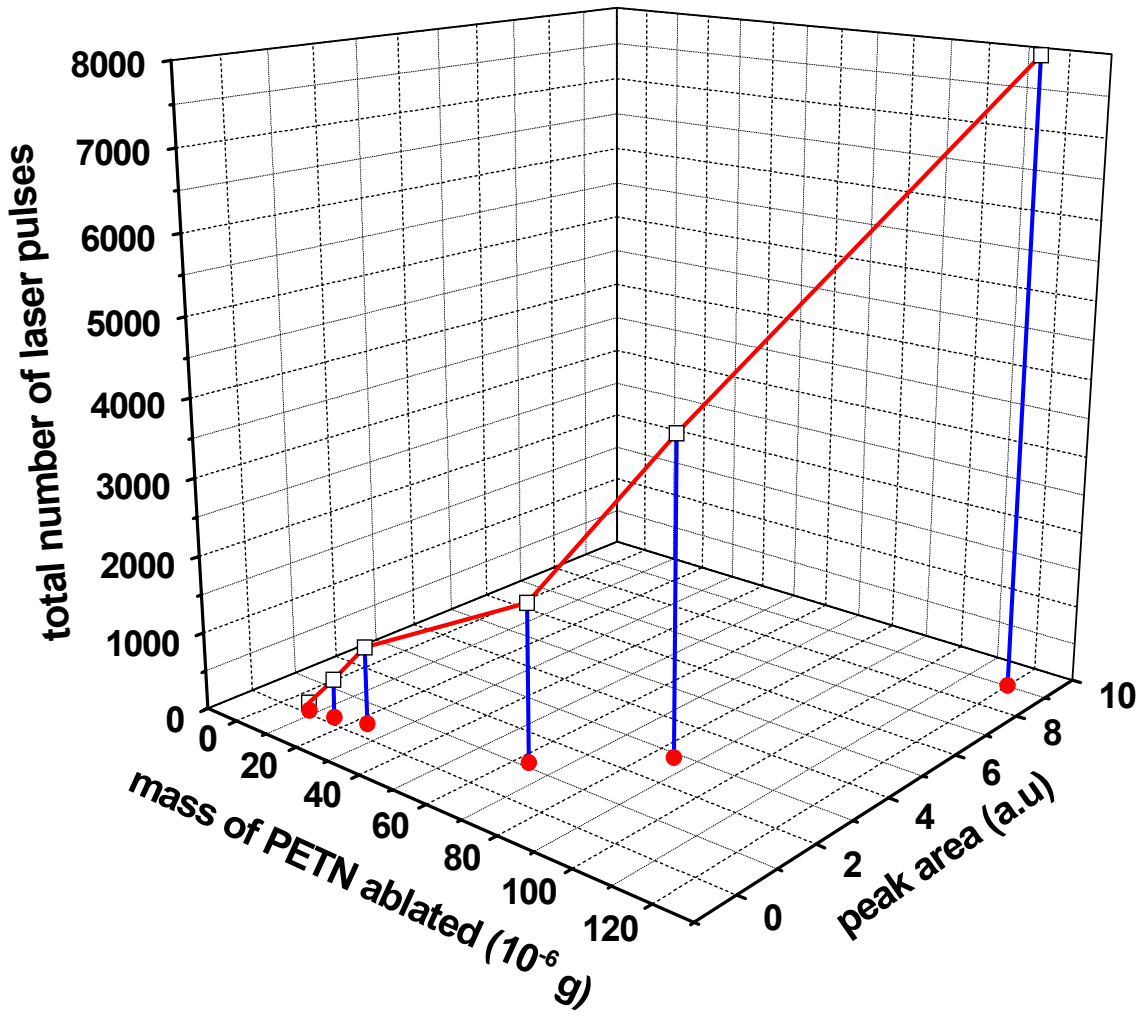

Figure 5-7. Effect of varying total number of laser pulses on the mass of PETN ablated and on the CL signal of $NOx_{(x=1,2)}$ fragments obtained after PF of solid PETN.

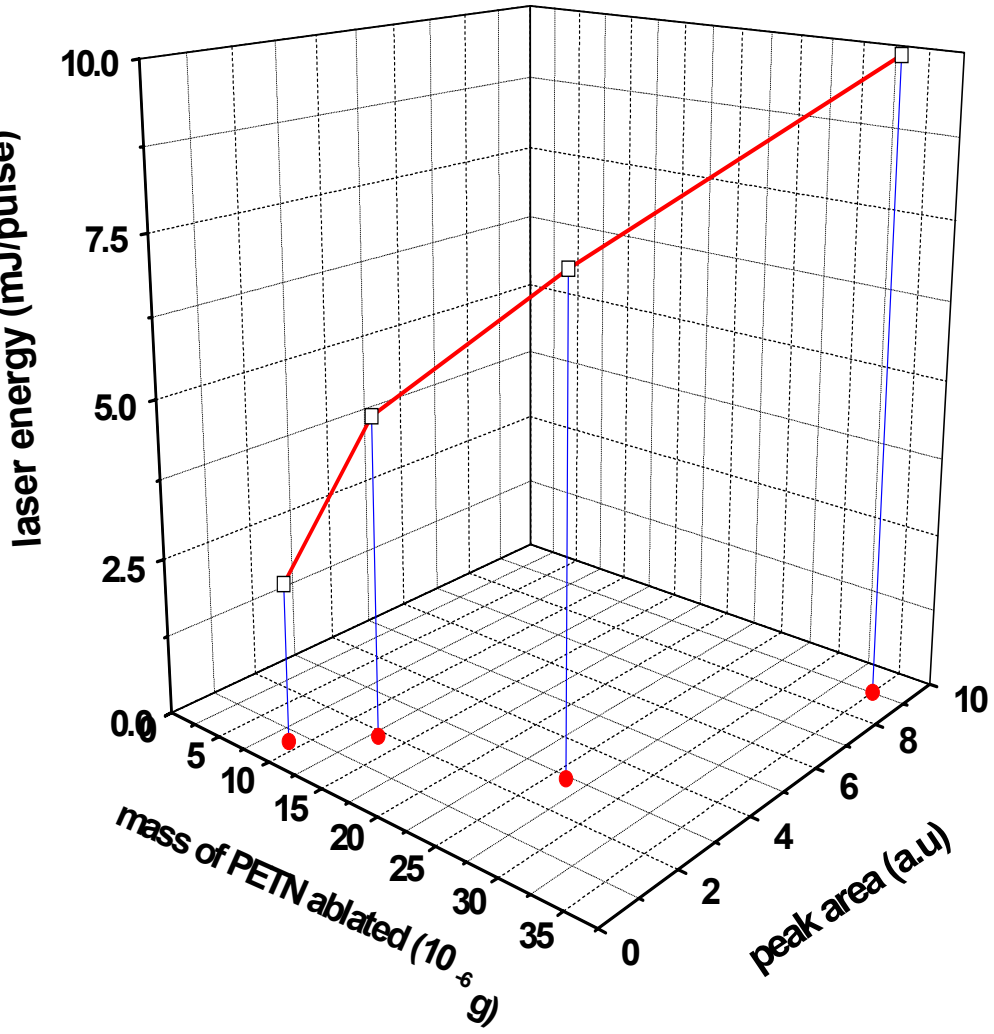

Figure 5-8. Effect of varying laser energy on the mass of PETN ablated and on the CL signal of $NO_{x(x=1,2)}$ fragments obtained after PF of solid PETN.

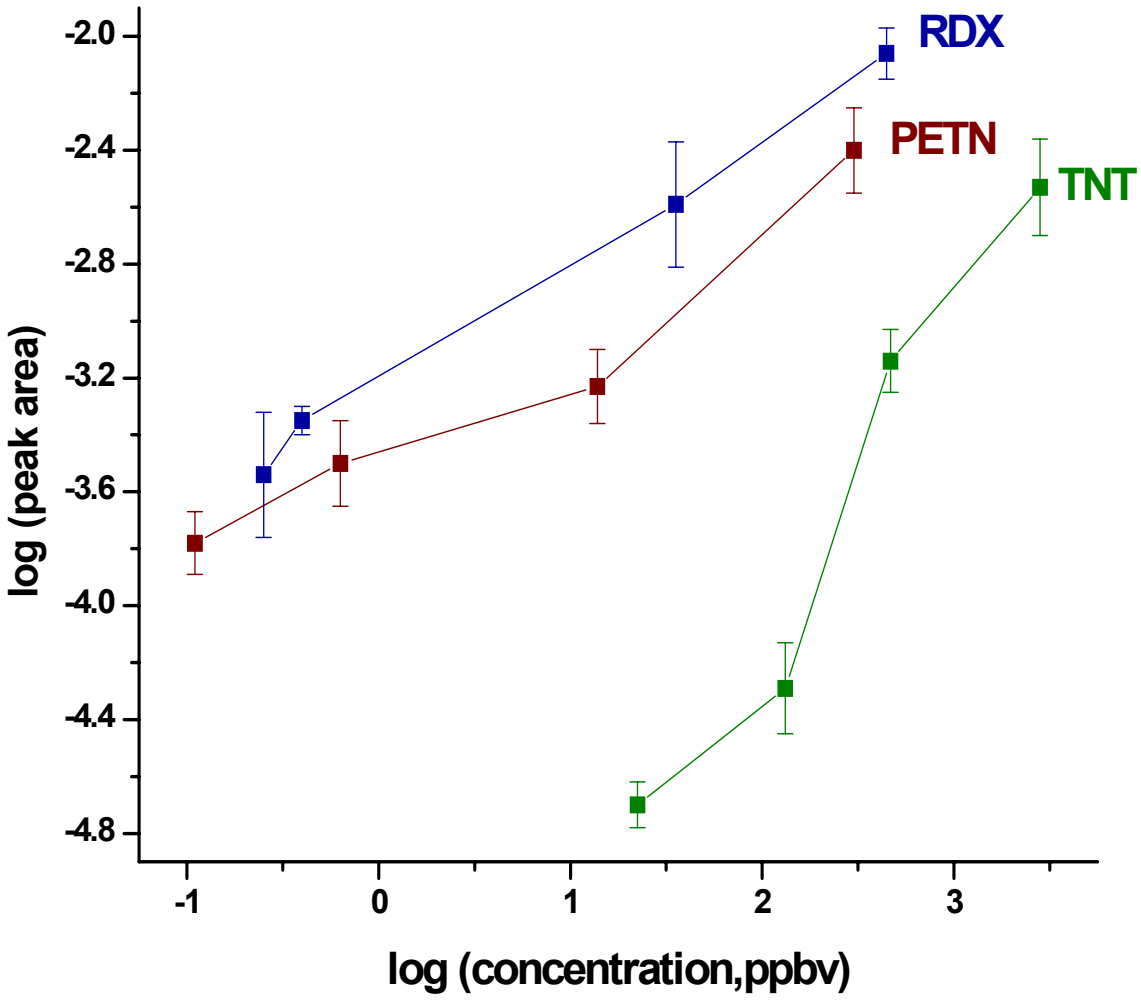

Figure 5-9. Calibration curves of PETN, RDX, and TNT.

Table 5-3 Analytical figures of merit of PF-luminol CL detector for some nitro-based explosives.

Explosive sample [a]	LOD at (S/N) = 3	Calibration sensitivity (CL signal/ppb)
PETN	3	1×10^{-5}
RDX	2	2×10^{-5}
TNT	34	1×10^{-6}

[a] Abbreviations:PETN, 1,3-dinitro-2,2-bis(nitramethylpropane); RDX, 1,3,5-trinitro-1,3,5-triazacyclohexane; TNT, 2,4,6 trinitrotoluene

CHAPTER 6
DIRECT DETECTION OF EXPLOSIVE IN SOIL

Introduction

Rapid and on-site detection of nitro-based explosives in a complex matrix such as soil is essential in providing an appropriate feedback during the characterization or remediation of contaminated sites. This chapter begins with the discussion of explosives as an environmental pollutant followed by a review of current monitoring explosive techniques, and finally an evaluation of the analytical capability of PF-luminol CL detector for PETN analysis in soil.

Environmental Hazards of Explosive Contaminated Soil

Soil contamination of nitro compounds is a problem because of the scale on which explosives have been manufactured, used, and tested. Contamination occurred during the manufacturing of explosives which required large amounts of water for purification. The waste water from this process is usually placed in lagoons or sedimentation basins.[100] Many sites also became contaminated through open detonation and burning of explosives at army depots, evaluation facilities, artillery ranges, and ordinance disposal sites.

The United States Department of Defense has identified more than 1 000 sites with explosive contamination of which 87% exceeded permissible contaminant levels.[101] Most contamination exists in near surface soils and in the vicinity of firing range targets. A primary concern is that soil contaminants may eventually migrate to groundwater and contaminate drinking water supplies of nearby communities. TNT, RDX, HMX, and PETN are weakly to moderately soluble in water with solubility of 130, 40, 5, and 43 mg/L, respectively at 25^{o}C.[102]

Nitro-based explosives are toxic and present harmful effects to all of life forms. TNT is on the list of US EPA priority pollutants: it's a known mutagen and can cause pancytopenia as a result of bone marrow failure.[103] TNT also causes the formation of methemoglobin on acute

exposures and anemia on chronic exposures. It also causes toxic hepatitis, leukocytosis, peripheral neuritis, muscular pains, cardiac irregularities, renal irritation, and bladder tumors.[1] On the other hand, RDX is considered as a possible human carcinogen (Class C) of EPA. RDX caused liver tumors in mice that were exposed to it in the diet. RDX also produced smaller offspring in rats. Clinical findings in low level long term exposures may include tachycardia, hematuria, proteinuria, mild anemia, neutrophilic leukocytosis, and electroencephalogram (EEG) abnormalities.[2] In general, nitro compounds are generally recalcitrant to the biosphere, where they constitute a source of pollution due to both toxic and mutagenic effects on human, fish, algae, and microorganisms.

Review of Explosive Detection in Soil

Various analytical methods for detection of nitro-based explosive present in soil have been reported. These are mostly spectrometric such as Electron Capture Detector (ECD) [11; 104], Thermal Energy Analyzer (TEA) [12; 105], Ion Mobility Spectrometry [15; 16] and UV Absorption coupled with several different separation methods such as extractions, gas and liquid chromatography, and electrophoresis. Voltammetric and amperometry [106; 107] methods were also commonly used in determination of trace levels of explosive substances in soil. The basic principles of these methods were discussed in Chapter I.

The current techniques mentioned above are often cost prohibitive, time consuming, and labor intensive. To characterize a site for explosive detection using these methods, it is necessary to follow a standard protocol starting from sample collection. Then, the analyte from the soil is extracted from the soil sample using organic solvent such as acetonitrile under at least 18 hour of sonication in cooled ultrasonic water bath before the actual analysis. Indeed, these traditional methods are laborious, time consuming, impractical and ineffective for field analysis.

Explosive field analysis is valuable due to extremely heterogeneous distribution of explosives in contaminated soils requiring enormous sampling sites. With such enormous sampling sites, a cost effective tool is necessary. Since cost per sample is lower, more samples can be analyzed producing more reliable results. Also, the availability of near-real time results permits re-design of the sampling scheme while in the field which facilitates more effective use of off site laboratory facilities with more robust analytical methods.

Currently, field methods for detection of explosives in soil include colorimetric[108] and immunosensors methods.[109] Both methods have several drawbacks. A colorimetric technique is used only for rugged qualitative analysis and often gives unreliable results. Immunosensors suffer because antibodies of all explosive materials likely to be encountered are needed, i.e., specific antibody is required for each compound of interest. This adds to the cost of an immunosensors. Also, when multi-analyte sensors are used, there is poor signal discrimination and as a result sensitivity is lost.

PF-Luminol CL detector is a promising technique for both on-site and off-site explosive detection in soil. The newly developed method has the following attributes: (1) it is simple and straightforward technique (2) it requires no sample preparation; (3) it is fast and provides a real time response; (4) all components including CL sensors can be made rugged and field portable.

An actual analysis of PETN contaminated soil was demonstrated and the analytical capability of the method was discussed.

Experimental Section

Chemical and Reagents

All the reagents and chemicals used for this experiment were exactly the same as Chapter V. The soil matrix used was a standard reference material (SRM-2704) prepared by the National Institute of Standards and Technology (NIST). SRM-2704 is freeze dried river sediment that was

sieved and blended to achieve a high degree of homogeneity. It is intended primarily for use in the analysis of sediments, soils, or material of similar matrix.

Apparatus and Methodology

The experimental set-up is the same as Chapter V except for the CL cell reaction. During the course of the dissertation, the geometry of the CL cell reaction underwent several revisions. The final reaction cell was designed with several goals in mind. First, the area of the PMT window was maximized. It was hoped that this would increase the detector sensitivity. A second expectation was this configuration prevented condensing of the luminol solution on the surface of the PMT window. Finally, by providing a compartment waste for the luminol solution, necessary maintenance such as periodically cleaning the cell was no longer necessary. The cross section of the CL cell reaction is shown in Figure 6-1.

The method of analysis is the same as described in Chapter V except for the laser parameters. In each experimental run, 8 000 laser pulses with average laser energy of 8 mJ/pulse was used. The laser repetition rate was set to 50 pulses per second.

Sample preparation. A known mass of soil was accurately weighed on a small piece of weighing paper. The soil sample was quantitatively transferred and tightly packed into a small aluminum cylindrical cup container (O.D. = 1.9 mm; Depth = 4.5 mm). Exactly 40 μL of the standard PETN solution in acetone was deposited on the top of the soil sample. Then the sample was dried in the oven at 60^{o}C for an hour to evaporate the solvent. To achieve varying concentration of PETN in soil, different standard PETN solutions ranging from 0.4 to 0.16 mg/mL were prepared. The explosive concentration in soil (mg/g) was calculated by using the following equation:

$$\text{Explosive contamination (mg/g)} = \frac{\text{[PETN] (mg/mL)} \cdot (40\ \mu\text{L})\ (10^{-3})}{\text{Weight of soil (g)}} \qquad (5\text{-}1)$$

Results and Discussion

The analysis was done by imaging an ArF laser beam on the explosive contaminated soil. The photofragmented products were then measured using Luminol-CL detector. Each experimental run was at least repeated eight times on the same sample spot. A calibration curve was generated by plotting peak area against concentration ranging from 0.4 to 9.0 parts per thousand PETN. Figure 6-2 best fitted a polynomial equation of $y = 2.4x^2 + 3.9x + 2.8$ where y equal to the CL peak area and x is the concentration of PETN in soil in parts per thousand. The curve has a correlation coefficient value (R^2) equal to 0.9996. Based on this curve, a detection limit was established. The limit of detection (LOD) is defined as ($3\sigma_{Blk}/m$) where σ_{blk} is the standard deviation of the blank and m is the calibration sensitivity or the slope of the line. This definition is restricted for the cases of a calibration line where the slope is constant, however, the calibration curve obtained for this analysis is curvilinear (slope is variable) and the definition provided is not useful without modification. The above equation can be redefined as follows:

$$LOD = 3\sigma_{blk}/\{dy/dx[f(x)]\} \qquad (5\text{-}2)$$

where the slope is replaced as a differential coefficient of function x, which in this case is the PETN concentration in soil. The equation of the slope is then given by:

$$m = 2(2.4x) + 3.9 \qquad (5\text{-}3)$$

LOD range of 0.5 to 4.3 ppm of PETN was obtained with x values equal to 0.4 and 9.0 parts per thousand of PETN. The precision of the method has been established at the lowest concentration of PETN which gave a relative standard deviation (RSD) of 30 % where n = 10. Larger variations obtained in the signal especially in the lower concentration range, is due to the decreasing surface concentration of the contaminant as the laser ablates deeper into the soil matrix.

The LOD was also estimated by considering only the linear plot obtained from the first four data points. A linear equation of $y = 15.662x - 4.2364$ was obtained where y is the peak area of the signal and x is the PETN concentration in ppth. An LOD of 1.6 ppm was calculated from this plot.

The LOD of the method is comparable to other current techniques as can be seen in Table 1-1 and 5-1.The analytical capability of this method can be applied in analysis of any typical explosive contaminated soil given in Table 6-1. Based on the data tabulated in Table 6-1, the TNT concentration in the soil ranges from 4 000 to 1 200 ppm whereas the concentration of other explosive contaminants is less than 300 ppm. The nitrogen content of the soil was 7.5 ppm as ammonium ion and nitrate concentrations vary from 6 to 12 ppm.[102; 110]

Pure $NaNO_2$ and $NaNO_3$ were photolyzed and analyzed with the same method in order to investigate the potential interferent during the analysis but both compounds did not give a significant CL signals as can be seen in Figure 6-3.

Conclusion

PF-Luminol-CL detector is a promising method for analysis of trace explosive in soil. The LOD range of 0.5 to 4.3 ppm for PETN was established. The PF-luminol CL detector is comparable to current techniques available. The most advantageous characteristic of the PF-luminol CL detector compared to other traditional methods is its simplicity and reliability. The technique also requires no sample preparation and provides fast real-time responses.

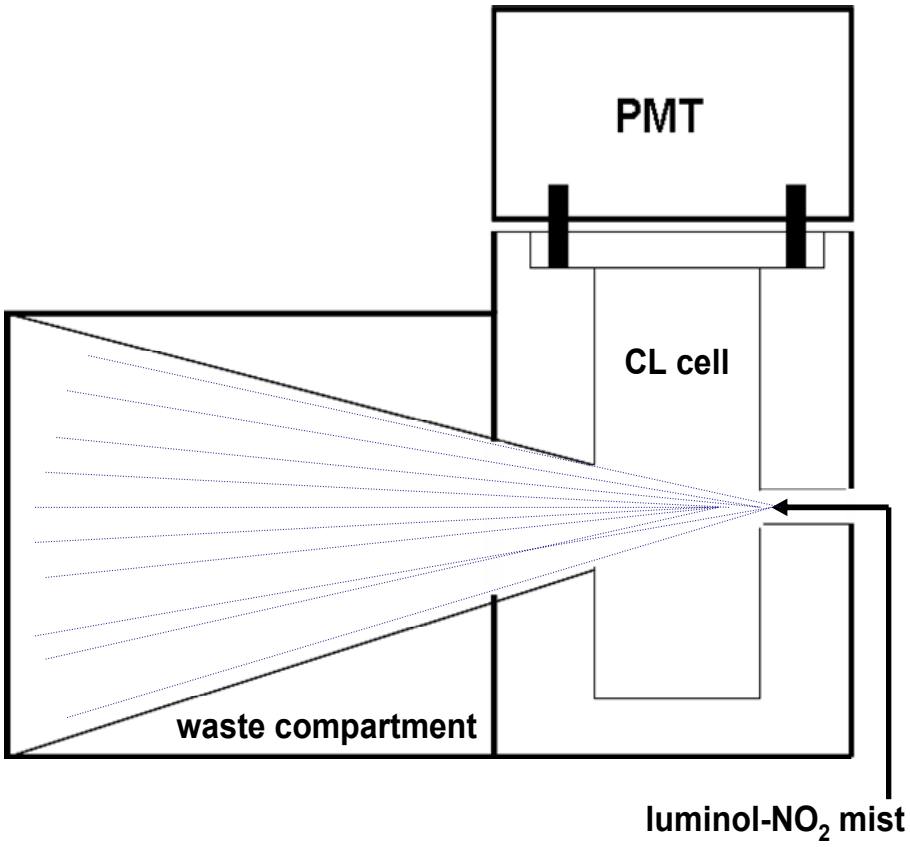

Figure 6-1. Cross section of the CL cell.

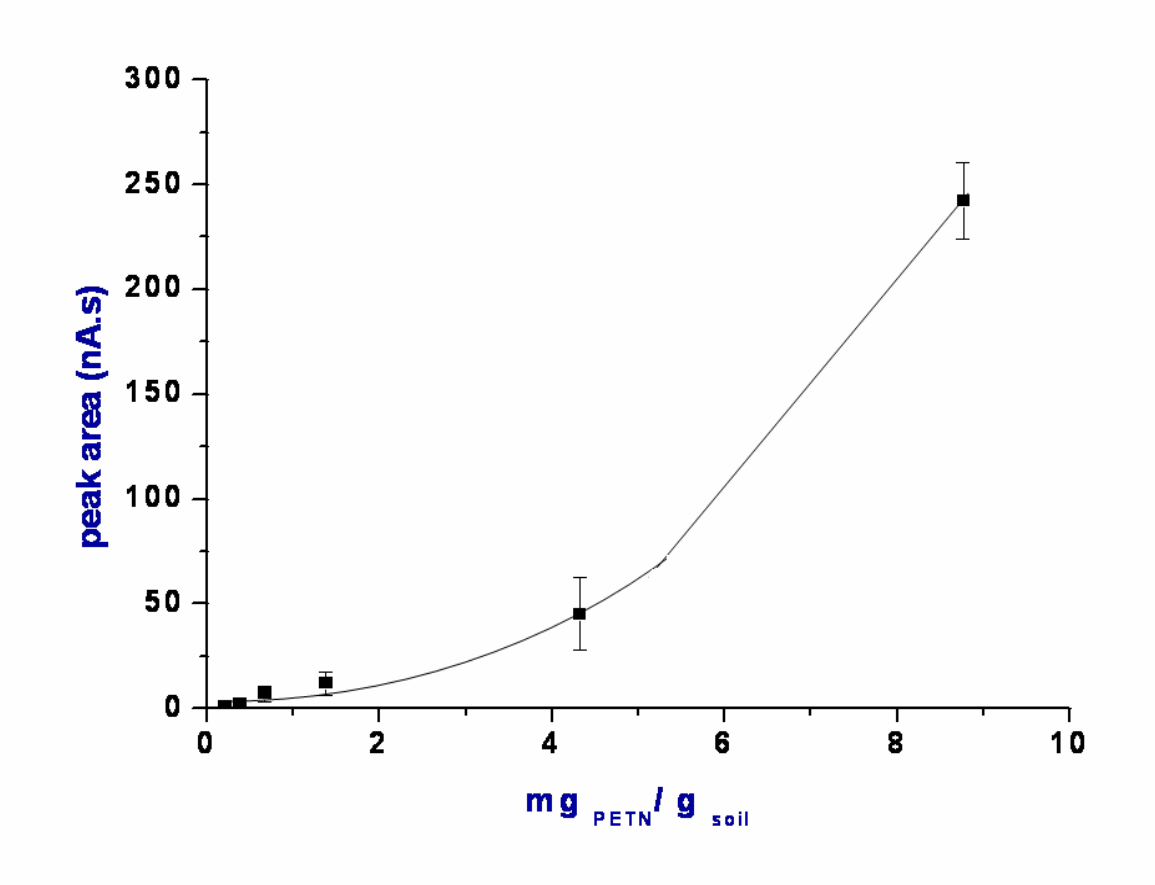

Figure 6-2. Calibration curve for PETN contaminated soil.

Table 6-1. Explosives concentration in the contaminated soil [102; 110]

Explosive [a]	Concentration range (mg explosive/kg of soil)
TNT	4 000-12 000
TNB	175-300
2,4-DNT	50-200
RDX	50-125
HMX	50-100

[a] Abbreviations: TNT, 2,4,6-trinitrotoluene; TNB, trinitrobenzene; 2,4 DNT, 2,4-dinitrotoluene; RDX, hexahydro-1,3,5-trinitro-1,3.5-triazine; HMX, octahydro-1,3,5,7-tetranitro-1,3,5,7-tetraazocine

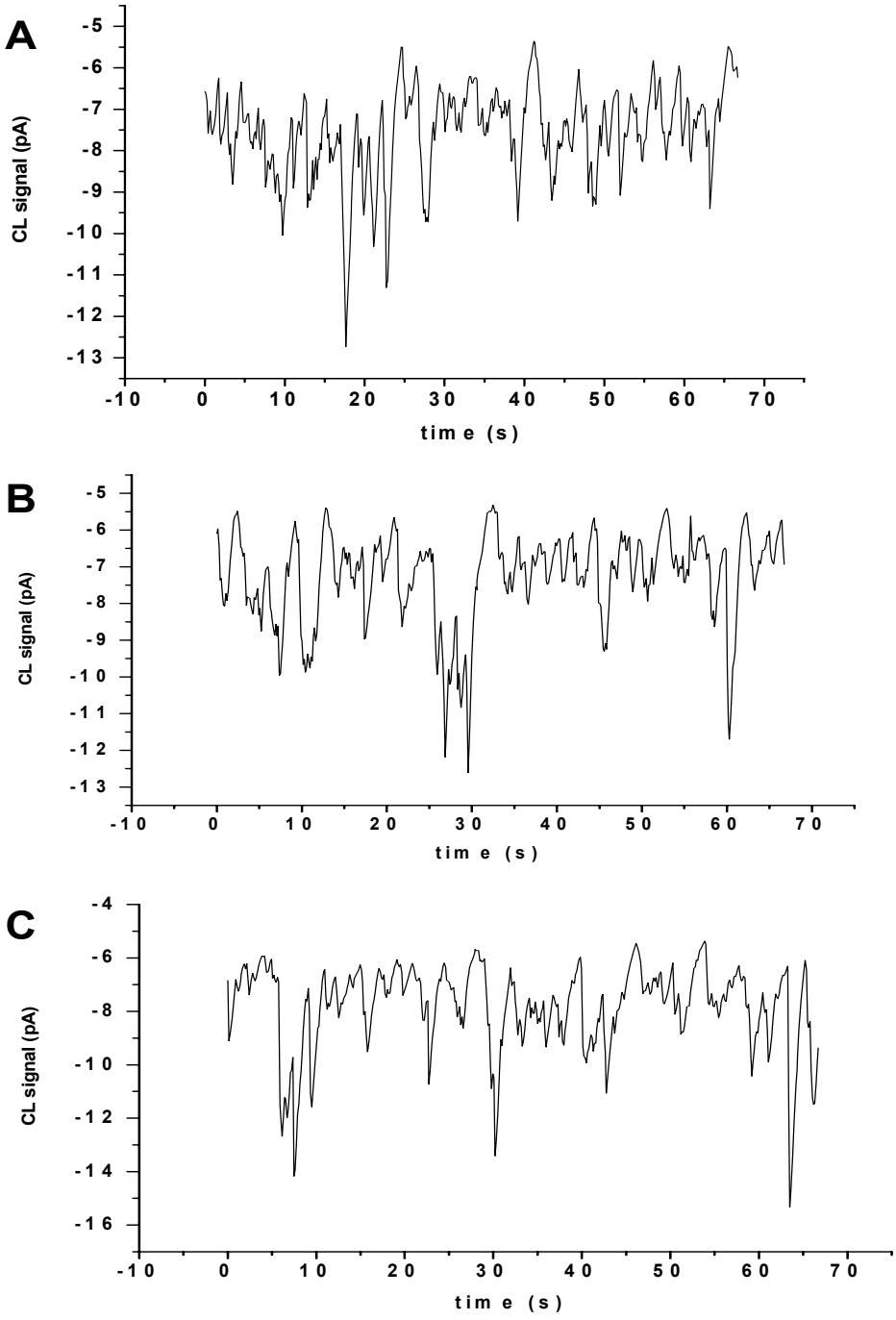

Figure 6-3. CL Spectra after PF of A) empty sample holder B) pure $NaNO_2$ C) pure $NaNO_3$.

CHAPTER 7
CONCLUSIONS AND FUTURE WORKS

Summary and Conclusions

The purpose of this research was to develop a simple, fast, reliable, sensitive and potentially portable explosive detection device employing laser photofragmentation (PF) followed by heterogeneous chemiluminescence (CL) detection. The work was divided into four stages: (1) discerning the PF pathways of nitro-based explosives (2) luminol-CL method development and optimization for improving NO_2 sensitivity (3) construction of CrO_3 oxidizer for NO to NO_2 conversion (4) evaluation of the device in detecting nitro-based explosives in various media such as air and soil.

In the first stage of the research, the following PF pathways were verified using classical colorimetric analysis and fast time resolved absorbance method.

$$R{-}NO_2 + h\nu \rightarrow R + NO_2; \quad h\nu = 193 \text{ nm} \qquad (7\text{-}1)$$

$$NO_2 + h\nu \rightarrow NO + O^*; \quad h\nu = 193 \text{ nm} \qquad (7\text{-}2)$$

Confirmation of $NO_{x(x=1,2)}$ generation after photolysis of nitro-based explosives was the basis for developing an explosive detector based on PF-Fragment detection scheme.

The second stage involved the development and optimization for NO_2 detection using luminol CL. In this system, a stream of NO_2 gas passed through a concentric nebulizer and used to aspirate a spray of luminol solution. The aspiration process maximized NO_2/luminol contact area, thereby, enhancing the CL signal. The current system was able to improve the detection limit attained so far through optimization of all the feasible physical and chemical parameters involved in the chemiluminescence reaction between luminol and NO_2. Detection limit of 19 ppt NO_2 at (S/N) = 3 was reported. The optimal reagent solution from the viewpoint of sensitivity of the response to NO_2 (maximum signal/signal noise ratio) is 5×10^{-3} M luminol + 0.01 M p-

iodophenol + 0.2 M KOH. Luminol/H_2O_2 CL set-up was also explored where a bundle of porous polypropylene fibers was used to bring the NO_2 into contact with luminol solution. LOD of 178 ppt NO_2 at (S/N) = 3 was obtained.

In the third stage, a CrO_3 oxidizer was constructed for NO to NO_2 conversion. Photolysis of nitro compounds produced NO (reaction 7-2) which is not detectable by luminol-CL system. To further increase the sensitivity of the device for NO_2 fragments, NO must be converted back to NO_2.

Finally, the fourth stage was integration of PF and CL units by a CrO_3 oxidizer into an explosive detection device. The system was able to detect energetic materials in real time at ambient conditions. Detection limits of 3.4 ppbv for PETN, 1.7 ppbv for RDX, and 34.5 ppbv for TNT were obtained. It was also demonstrated that the presence of PETN residue within the range of 61 ng/cm^2 to 186 ng/cm^2 can be detected at a given signal to background ratio of 10 using a few micro joules of laser energy. The technique also demonstrated its potential for direct analysis of trace explosive in soil. LOD range of 0.5 to 4.3 ppm for PETN was established, an analytical capability comparable to current techniques available. The technique most advantageous characteristic compared to other traditional methods is its simplicity and reliability. The technique also requires no sample preparation and provides fast real-time response.

Future Research Directions

Based on the results presented in this dissertation, several paths can be followed for future research studies. The future work can be grouped into (1) extending the systems applicability towards peroxide-based explosives (2) instrument's field adaptability and finally (3) instrument's performance in actual scenario.

Liquid peroxide explosives such as triacetoneperoxide (TATP) and hexamethylene triperoxide diamine (HMTD) were home-made explosives recently used in Madrid and London

subway attacks of 2004 and 2005, respectively. TATP was also been used by suicide bombers in Israel, and was chosen as a detonator in 2001 by the thwarted "shoe bomber" Richard Reid.[2]

Current analytical methods used for peroxide-based explosives include Infrared spectroscopy (IR), Raman spectroscopy, Chemical Ionization-Mass Spectrometry (CI-MS), Ion Mobility Spectroscopy (IMS), ^{1}H and ^{13}C NMR, and High Performance Liquid Chromatography (HPLC) with post column UV irradiation and fluorescence detection. Most of these techniques are applied in laboratory environment and usually not applicable to field screening scenarios. So far, the only detection method used in field analysis involved UV irradiation (λ = 254-415 nm) of the liquid explosive samples followed by hydrogen peroxide (H_2O_2) fragment detection using colorimetric technique.[111] However, this particular method involves a lot of sample preparation, used a lot of expensive reagents, time-consuming and relatively has poor sensitivity. Furthermore, the technique is only limited to liquid samples. An alternative way to overcome these issues is through direct photofragmentatation (PF) of peroxide-based explosive vapor and subsequent H_2O_2 detection using luminol-CL detector (Figure 7-1). The high volatility of these compounds is a very promising premise for developing the first known air analysis for peroxide-based explosive using our method.

After extending the chemistry of the system with peroxide-based explosives, the second direction to be considered is its portability for field adaptability. The over-all set-up including the detection system can be readily miniaturized. The most challenging task is the replacement of ArF laser but this can be feasibly done using commercially available excilamps which only weigh about 2.2 kg.[112] Excilamps provide narrow band light around a single wavelength by radiative decomposition of excimer states created by a barrier discharge. Lamps operating at wavelengths of 126, 146, 172, 193, 222, 282, and 308 are already available. Studies on

excilamps show a powerful radiation in UV and vacuum UV spectral range that allows photochemical processes that were not previously possible with lamps.[113] These lamps also operate at low temperature, generate minimal IR radiation, and allow processing of temperature sensitive substrates such as explosives. Furthermore, these equipments are highly efficient source converting power into light effectively and therefore, reducing power requirements and heat load. The system is also robust, inexpensive, and ecologically beneficial.[113]

After achieving the portability requirement, actual field testing of the instrument should be evaluated. Foreseeable problem that can be encountered during the actual testing will be the sensitivity issue of the device especially when dealing with direct explosive vapor detection with an exemption for peroxide-based explosives. As mentioned in Chapter I, nitro-based explosives significantly have low vapor pressures and the method that is suitable for its detection should be able to detect concentrations down to less than 1 ng/L (ppb level). Our current method has a LOD of 3.4, 1.7, and 34.5 ppbv for PETN, RDX, and TNT, respectively.

Improving the sensitivity of the device can be done by the following suggestions: (1) replacing the PMT detector with another PMT system which has the least dark count rate and highest photon gain and (2) eliminating the background noise due to interferences present in air such as native $NO_{x(x=1,2)}$, O_3, and SO_2.

Previous works [73-80] with atmospheric monitoring of NO_2 were able to eliminate almost 100 % of O_3 and SO_2 from air by adding Na_2SO_3 in the basic luminol solution. O_3 and SO_2 preferred and readily react with a stronger reducing agent such as Na_2SO_3 rather than basic luminol solution.

Interferences from native $NO_{x(x=1,2)}$ can be compensated in several ways. The first one involved $NO_{x(x=1,2)}$ removal prior to sample analysis. This must be done without removing the

explosive vapor or the analyte. One feasible way to do this is through chemical adsorption of NO_2 on a surface of titanium dioxide (TiO_2) photo catalyst and hygroxyapatite ($Ca_{10}(PO_4)_6(OH)_2$.[114] In this method, NO was oxidized to HNO_3 which is efficiently adsorbed on the surface of TiO_2. Removal efficiency of 98 % was achieved for this method. Another alternative option is to purge the air sample with solutions of either triethanolamine (TEA) or sodium arsenite prior to photofragmentation. Both solutions are known for their ability to pre-concentrate NO_2 in air by trapping and converting NO_2 gas to nitrite ions in the bulk solution. These absorber solutions have absorption efficiencies of 95 and 82 percent, respectively.[59] The stoichiometric factor of TEA for NO_2 to NO_2^- is 0.85 while that of sodium arsenite is unity.[115] The main concern of using these $NO_{x(x=1,2)}$ removal methods is that the feasibility of removing some of the analyte as well. Explosive vapor is prone to get easily lost to wall adsorption during transport.

The second way to compensate for the presence of native $NO_{x(x=1,2)}$ in air is to divide the volume of the air sample pumped into the instrument each time. The first sample (sample A) collected will be diverted to PF cell while the second sample (sample B) will be diverted to another cell. Both samples will undergo the same reactions of oxidation and luminol-CL except for photolysis part. The presence of explosive vapor can be confirmed by a significantly higher CL signal of the air sample that undergoes photolysis than the air sample that was not treated with UV irradiation. A positive explosive alarm will be based on the statistically established differential value between sample A and B.

In conclusion, the main drawback of PF-CL detector is its relatively high background noise due to interferents present in the air sample specifically the native $NO_{x(x=1,2)}$, thus, solid residue analysis of nitro-based explosive is preferred and more compatible for this technique.

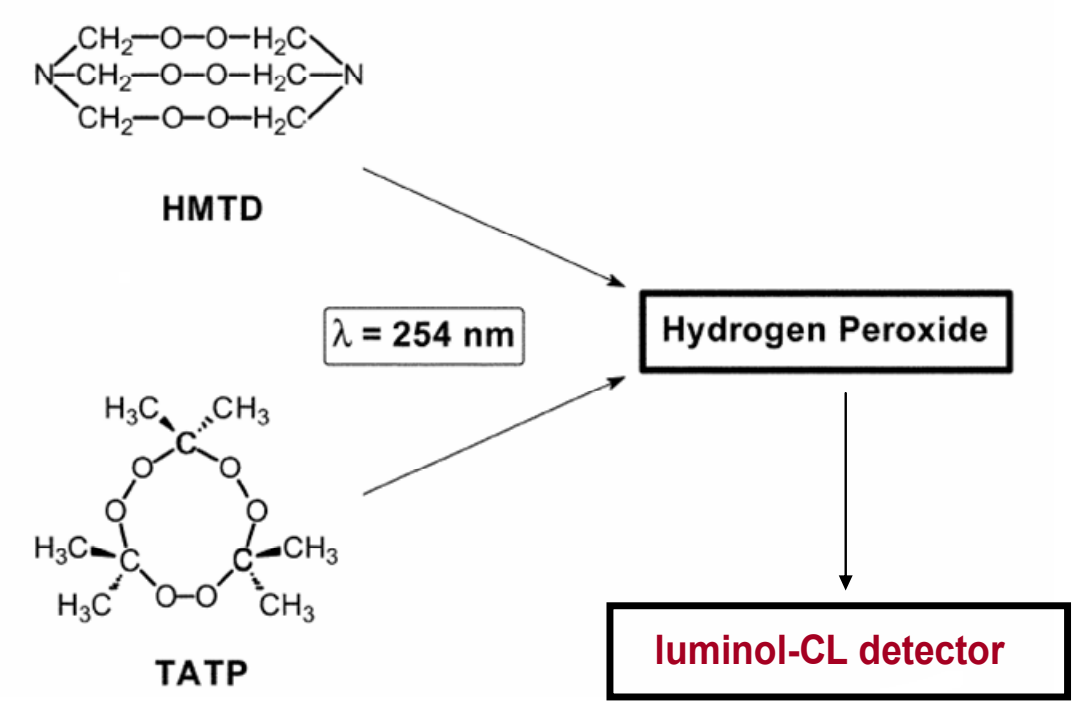

Figure 7-1. Alternative scheme for detecting peroxide-based explosives.

LIST OF REFERENCES

1. Singh, S. *J. Hazard. Mater.* **2007**, in press.

2. Mahoney, C.M.; Gillen, G.; Fahey, A.J. *Forensic Science International* **2006,** *158*, 39-51.

3. Vila, M.; Lorber-Pascal, S.; Laurent, F. *Environmental Pollution* **2007,** *148*, 148-154.

4. Ahmad, F.; Schnitker, S.P.; Journal *of Contaminant Hydrology*, **2007,** *90, 1-20*.

5. Agrawal,; J.P., Surve,; R.N.; Mehilal,; S. H.; Sonawane,; A.L. *Journal of Hazardous Materials* **2000,** *77,* 11-31.

6. Hallowell, S. F. *Talanta* **2001**, *54*, 447-458.

7. Yinon, J. *Trends Anal. Chem.* **2002**, *21*, 292-301.

8. Hilmi, A.; Luong, J.T.; *Environ. Sci. Technol*. **2000**, *34*, 3046-3050.

9. Lu, Q.; Collins, G.E.; Smith, M.; Wang, *J. Analytica Chimica Acta* **2002**, *469*, 253-260.

10. Mullen, C.; Irwin, A.; Pond, B.; Huestis, D.L.; Coggiola, M.J.; Oser, H. *Anal. Che*m. **2006**, *78*, 3807-3814.

11. Walsh, M.E. *Talanta* **2001**, *54*, 427-438.

12. Lafleur, A.L.; Mills, K.M.; *Anal. Chem.* **1981**, *53*, 1202-1205.

13. Asbury, G.R.; Klasmier, J.; Hill, H.H. *Talanta* **2000**, *50*, 1291-1298.

14. Ewing, R.G.; Atkinson, D.A.; Eiceman, G.A.; Ewing, G.J. *Talanta* **2001**, *54*, 515-529.

15. Buryakov, I.A. *J of Chromatogr*. **2004**, *800*, 75-82.

16. Khayamian, T.; Tabrizchi, M.; Jafari, M.T. *Talanta* **2003**, *59*, 327-333.

17. Matz, L.M.; Tornatore, P.S.; Hill, H.H. *Talanta* **2001**, *54*, 171-179.

18. Kanu, A.B.; Haigh, P.E.; Hill, H.H. *Analytica Chimica Acta* **2005**, *553*, 148-159.

19. Otto, J.; Brown, M.F.; Long, W. *Applied Animal Behaviour Science* **2002,** *77,* 217-232.

20. Harper, R.J.; Almirall, J.R.; Furton, K.G. *Talanta* **2005**, *67*, 313-327.

21. Harvey, S.D.; Clauss, T.W. *J. Chromatogr*. A **1996**, *753*, 81-86.

22. Pnnaduwage, L.A.; Boiadjiev, V.; Hawk, J.E.; Thundat, T. *Appl. Phys. Letter* **2003**, *83*, 1471-1475.

23. Datskos, P.G.; Lavrik, N.V.; Sepaniak, M.J. *Sens. Letters* **2003**, 25-37.

24. Ly, S.Y.; Kim, D.H. *Talanta* **2002**, *58*, 919-926.

25. Hilmi, A.; Luong, J.T.; *Environ. Sci. Technol*. **2000**, *34*, 3046-3050.

26. Wang, J.; Thongngadee, S. *Analytica Chemica Acta* **2003**, *485*, 139-143.

27. Albert, K.J.; Myrick, M.L.; Brown, S.B.; James, D.L.; Milanovich, F.P.; Watt, D.R. *Environ. Sci. Technol*. **2001**, *35*, 3193-3200.

28. Charles, P.T.; Kustebeck, A.W. *Biosens. Bioelectron*. **1999**, *14*, 391-400.

29. Dorozhkin, L.M.; Nefedov, V.A.; Sobelnikov, A.G.; Sevastjanov, V.G. *Sensors and Actuators B* **2004**, *99*, 568-570.

30. Sohn, H.; Calhoun, R.M.; Sailor, M.J.; Tragler, W.C. *Angew. Chem*. **2001**, *13*, 2162-2165.

31. Wallenburg, S.R.; Bailey, C.G. *Anal. Chem*. **2000**, *72*, 1872-1875.

32. Wang, X.; Zeng, H.; Zhao, L.; Lin, J.M. *Talanta* **2006**, *70*, 160-164.

33. De Lucia, F.C.; Harmoun, R.S.; McNesby, K.L.; Winkel R.J.; Misiolek A.W. *Applied Optics* **2003**, *42*, 6148-6150.

34. Lin, H.; Chen, Y. *Optics Express* **2006**, *14*, 415-424.

35. Shen, Y.C.; Lo, T.; Taday, P.F.; Cole, B.E.; Tribe, W.R.; Kemp, M.C. *Applied Physics Letters* **2005**, *86*, 241116-1 to 241116-3.

36. Sylvia, J.M.; Janni. J.A.; Klein, K.D.; Spencer, K.M. *Anal. Chem.* **2000**, *72*, 5834-5840.

37. Hayward, I.P.; Kirkbride, T.E.; Batchelder, D.N.; Lacey, R.J. *J. of Forensic Sciences* **1995**, *40*, 883-884.

38. Janni, J,; Gilbert, B.D.; Field, R.W.; Steinfeld, J.I. *Spectromica Acta Part A* **1997**, *73*, 255-258.

39. Xu, S.; Sha, G.; Xie, *J. Rev. Sci. Instrum*. **2002**, *73*, 255-258.

40. Balint-kurti,;G.G., Shapiro, M. *Chemical Physics* **1981,** *61,*137-155.

41. Turro, N.J. *Molecular Photochemistry*. Amsterdam, **1967**.

42. Mc Donnell L.; Heck, A.J. *J. of Mass Spectrometry* **1998**, *33*, 415-428.

43. Cabalo, J.; Sausa, R.C. *Applied Optics* **2005**, 44, 1084-1091.

44. Simeonsson, J.B.; Sausa, R.C. *Trends in Analytical Chemistry* **1998**, *17*, 542-550.

45. Monts, D.L.; Singh, J.P.; Boudreaux, G.M. *Encyclopedia of Analytical Chemist*ry, John Wiley and Sons Ltd., Chichester, **2000**, 2148-2171.

46. Ledingham, K.W.D.; Singhal, R.P. *International Journal of Mass Spectrometry and Ion Processes* **1997**, *163*, 149-168.

47. Östmark, H.; Carlson, M.; Ekvall, K. *Combustion and Flame*, **1996,** *105*, 381-390.

48. Butler, L.J.; Krajrovich, P.; Lee, Y.T. *J. Chem. Phys.* **1983**, *79*, 1708-1722.

49. Blais N. *Journal of Chem. Phys*. **1983**, *79*, 1708-1722.

50. Renlund, A.M.; Trott, W.M. *Chemical Physics Letters* **1984**, *107*, 555-560.

51. Capellos,C.; Papagrannakopoulos, P.; Liang, Y. *Chemical Physics Letters* **1989**, *164*, 533-538.

52. Galloway, D.B.; Bartz, J.A.; Huey, G.L.; Crim, F.F. *J. Chem. Phys*. **1993**, *98*, 2107-2114.

53. Lemire,G.W.; Simeonsson, J.B.; Sausa, R.C. *Anal. Chem*. **1993**, *65*, 529-533.

54. Simeonsson, J.B.; Lemire,G.W.; Sausa, R.C. *Applied Spectroscopy* **1993**, *47*, 1907-1912.

55. Marshall A.; Clark, A.; Ledingham, K.W.; Sanders, J.; Singhal, R.P.; Kosmidis, C.; Deas R.M. *Rapid Communications in Mass Spectrometry* **1994**, *8*, 521-526.

56. Ledingham, K.W. *Physica Scripta* **1995**, *158*, 100-103.

57. Simeonsson, J.B.; Lemire,G.W.; Sausa, R.C. Army *Research Laboratory Aberdeen Ground, MD, USA Available NTIS Report* **1994**. 30 Rep. Announce. Index 95(19) Abstract no. 5429519.

58. Yang, Mo; Ramsey, J.M.; Kim, B. *Journal of Rapid Communications in Mass Spectrometry* **1996**, *10*, 311-315.

59. Gayathri, N.; Balasubramanian, N. *Analusis* **1999**, 27, 174-181.

60. Finlayson, B.J.; Pitts J.N. *Atmospheric Chemistry: Fundamentals and Experimental Techniques*. John Wiley and Sons Inc. Canada, **1986**, 151-153.

61. Sun, F.; Glass, G.P.; Curl, R.F. *Chemical Physics Letters* **2001**, *337*, 72-78

62. Campana, A.G.; Baeyens, W.R. *Chemiluminescence in Analytical Chemistry*, Markel Dekker Inc., Basel, Swizerland, **2001**; Chapter 1.

63. Ingle, J.D.; Crouch, S.R. *Spectrochemical Analysis*, Prentice-Hall Inc., New Jersey, **1988**; Chapter 15.

64. Li, Y.; Qi, H.; Fang, F.; Zhang,; C. *Talanta*, **2007**, *72*, 1704-1709.

65. Isacsson, U.; Wettermark, G. *Analytica Chimica Acta* **1974**, *68*, 339-362.

66. Wendel, G.J. *Development and Application of a Luminol-based NO_2 Detector*, University of Michigan, **1985**.

67. Tahirović, A.; Čopra, A.; Mikličanin, E.O.; Kalcher, K. *Talanta*, **2007,** *72*, 1378-1385.

68. Su, Y.; Li, X.; Chen, X.; Lu, Y.; Hou, X. *Microchemical Journal*, **2007**, *In Press, Corrected Proof.*

69. White, E.H.; Zafriou, H.H.; Hill J.H.M. *J. Am. Chem. Soc.* **1964**, *86*, 940-941.

70. Shevlin,P.B.; Neufeld, H.A. *J. Org. Chem.* **1970**, *35*, 2178-2182.

71. Hersh, B.B.; Wesely, M.L. *J. Photochem.* **1974**, *10*, 409-423.

72. Roswell, D.F.; White, E.H. *Meth. Enzynol*. **1978**, *57*, 409-423.

73. Maeda, Y.; Aoki, K.; Munemori, M. *Anal.Chem*.1980, *52*, 307-11.

74. Wendel, G.J.; Stedman, H.; Cantrell, C.A. *Anal.Chem*. **1983**, *55*, 937-40.

75. Schiff, H.I.; Mackay, G.I.; Castledine, C.; Harns, G.W. *Trans Q. Water, Air and Soil Pollution.***1986**.*30*, 105-114.

76. Kelly T.J., Spicer C.W., Ward G.F. *Atmospheric Environment A* **1990**, *24*, 2397-2403.

77. Mikuska, P.; Vecera, Z. *Anal. Chem*.**1992**, *64*, 2187-91.

78. Collins, G.; Rose-Phersson, S.L. *Anal. Chem*. **1995**, *67*, 2224-30.

79. Robinson, J.K.; Bollinger, M.J.; Birks, J.W. *Anal. Chem*. **1999**, *71*, 5131-5136.

80. Kok, G.L.; Hoiler, T.P.; Lopez, M.B.; Nachitrieb, H.A.; Yuan, M. *Environmental Science and Technology* **1978**, *12*, 1072-1076.

81. Thorpe, G.H.; Kricka, L.J.; Moseley, S.B.; Whitehead T.P. *Clinical Chemistry* **1985**, *31*, 1335-1341.

82. Robinson, J.K. *Luminol-Hydrogen peroxide Detector for the Analysis of NO in Exhaled Breath*, University of Colorado, **1994**.

83. Hutchinson, G.L.; Yang, W.X.; Andre, C.E. *Atmospheric Environment* **1999**, *33*, 141-145.

84. Levaggi, P.; Kothny, E.L.; Belsky, T.; de Vera E.; Mueller, P.K. *Environmental Science and Technology* **1974**, *8*, 348-350.

85. Nguyen Dao Hinh. US Patent no. 20040169495, **1994.**

86. Nguyen Dao Hinh. US Patent no. 20040053421, **1994**.

87. Wu, D.; Singh, J.; Yueh, F.; Monts, D. *Applied Optics* **1996**, *35*, 3998-4003.

88. Boudreax, G.M.; Miller, T.S.; Kunefke, A.J.; Singh, J.; Fang-Yu, Y.; Months D. *Applied Optics.* **1999**. *38*, 1411-1417.

89. Arusi-Parpar, T.; Heflinger, D.; Lavi, R. *Applied Optics* **2001,** *46*, 6677-81.

90. Swayambunathan, V.; Singh, G.; Sausa, R.C. *Applied Spectroscopy* **2000**, *54*, 651-657.

91. Swayambunathan, V.; Singh, G.; Sausa, R.C. *Applied Optics* **1999**, *40*, 6447-6454.

92. Swayambunathan, V.; Singh, G.; Sausa, R.C. *Proceedings of International Society for Optical Engineering* **1999**, 176-184.

93. Cabalo, J.; Sausa, R.C. *Applied Spectroscopy* **2003**, *57*, 1196-1199.

94. Cabalo, J.; Sausa, R.C. *Applied Optics* **2005**, *44*, 1084-1091.

95. Lucero, D.P.; Boncyk, E.M. *Journal of Energetic Materials* **1986**, *4*, 473-510.

96. Chakraborty, D.; Muller, R.P.; Dasdupta, S.; Goddard, W.A. *J. Phys. Chem*. **2001**, *105*, 1302-1314.

97. Gonzalez, A.C.; Larson, C.W.; McMillen, D.F.; Golden, D.M. J. *Phys. Chem.* **1985**, *89*, 4809-4814.

98. He, Y.Z.; Cui, J.D.; Mallard, W.G.; Tsang, W. *J. Am. Chem. Soc.* **1988**, *110*, 3754-3759.

99. Kallman, H.P.; Spruch, G.M. *Luminescence of Organic and Inorganic Materials*. John Wiley and Sons, Inc., NY, **1969**.

100. Pennington, J.C.; Brannon, J.M. *Themochimica Acta* **2002**, *384*, 163-172.

101. Rodgers, J.D.; Nigel, J.B. *Water Research* **2001**, *35*, 2101-2111.

102. Halasz, J.D.; Groom, C.; Zhou E.; Paquet, L.; Ampleman, G.; Dubas, C.; Hawari, J. *Journal of Chromatog. A* **2002**, *963*, 411-418.

103. Morley, M.C,; Yamamoto, H.; Speitel, G.; Clausen, J.; *Journal of Contaminant Hydrology* **2006**, *85*, 141-158.

104. Jenkins, T.F.; Leggett, D.C.; Miyares, P.H.; Walsh, M.E.; Ranney, T.A.; Cragin, J.H.; George V. *Talanta* **2001**, *54*, 501-513.

105. Bowerbank, C.R.; Smith, P.A.; Futterrolf, D.D.; Lee, M.L. *Journal of Chromatog. A* **2000**, *902*, 413-419.

106. Buttner, W.J.; Findlay, M.; Vickers, W.; Davis, W.M.; Cespedes, E.R.; Cooper, S.I.; Adams, J.W. *Analytica Chimica Acta* **1997**, *341*, 63-71.

107. Hilmi, A.; Laong, J.H.; Nguyen, A. *Journal of Chromatog. A* **1999**, *844*, 97-110.

108. Uzer, A.; Ercag, E.; Apak, R. *Analytical Chimica Acta* **2005**, *534*, 307-317.

109. Gauger P.R.; Hoh D.B.; Patterson, C.H.; Charles, P.T.; Shriver-Lake L.; Kusterbeck, A.W. *Journal of Hazardous Materials* **2001**, *83*, 51-63.

110. Boopathy R. *International Biodeterioration and Biodegradation* **2000**, *46*, 29-36.

111. Schutte-Ladbeck, R.; Karst, U. *Analytica Chimica Acta* **2003**, *482*, 183-188.

112. Li, Q.; Gu, C.; Di, Y.; Yin, H.; Zhang, J. *Journal of Hazardous Materials* **2006**, *133,* 68-74.

113. Elsner, C.; Lenk, M.; Prager, L.; Mehner, R. *Applied Surface Science* **2006**, 2*52,* 3616-3624.

114. Komazaki, Y.; Shimizu, H.; Tanaka, S. *Atmos. Environ*. **1999**, *33*, 4363-4371.

115. Yuen, W.K.; Horlick, G. *Analytical Chemistry* **1977**, *49*, 1448-1450.

BIOGRAPHICAL SKETCH

Maria Pamela Pineda Monterola was born on September 18, 1977, in San Pablo City, Philippines. She is the third child of Nora Dizon Pineda and Conrado Cachero Monterola. She graduated *cum laude* with bachelor's degree in chemistry in 1998 from the University of the Philippines. She was immediately hired as a junior faculty in the same university while completing her master's degree in computational chemistry and minor degree in mathematics. In 2000, she took and topped the Philippine Licensure Examination in chemistry. In 2001, she was accepted as a research scholar in University of Tsukuba, Japan for a year. In 2007, she earned her Ph.D. degree in analytical chemistry under the research supervision of Prof. James D. Winefordner at the University of Florida.